Efficient Automotive Electromagnetic Modelling

by

James Alan Flint, M. Eng.

A Doctoral Thesis submitted in partial fulfilment of the requirements for the award of Doctor of Philosophy of Loughborough University

August 2000

To my grandparents Elsie and Ernest

ABSTRACT

THE Transmission Line Modelling (TLM) method is applied to the electromagnetic modelling of vehicles. Implications of increasing frequencies in computer models of electromagnetic compatibility (EMC) studies are discussed. Efficient algorithms and resource management strategies are developed with a view to producing accurate results in a realistic computational run time.

Theoretical aspects covered are.

- The development and accuracy of the TLM method

- An improved Partial Huygens' surface for plane wave excitation

- An evaluation of high-performance local and global absorbing boundary conditions

Implementation aspects of TLM addressed include

- The effects of arithmetic precision on link line voltage and stub impedance calculations

- The development of an object-oriented computer code using the Object Modelling Technique

- Methods for estimating and managing the memory requirement and run time of simulations

It is shown that by optimising algorithms and carefully managing resources, sufficient improvement can be made to allow relatively sophisticated models to be run on a modest desktop computer

ACKNOWLEDGEMENTS

CONTENTS

LIST OF ABBREVIATIONS AND SYMBOLS

ABBREVIATIONS

Abbreviation	Expansion
ABC	Absorbing Boundary Condition
ACN	Asymmetrical Condensed Node
CAD	Computer-Aided Design
EM	Electromagnetic
EMC	Electromagnetic Compatibility
FDFEM	Frequency Domain Finite Element Method
FDTD	Finite Difference Time Domain method
GTD	Geometrical Theory of Diffraction
HSCN	Hybrid Symmetrical Condensed Node
MoM	Method of Moments
MTBC	Matched Termination Boundary Condition
OATS	Open Area Test Site
o/c	Open circuit
OML	Object Modelling Language
PEC	Perfect Electrically Conducting
RF	Radio Frequency
RFI	Radio Frequency Interference
s/c	Short circuit
SCN	Symmetrical Condensed Node
SSCN	Symmetrical Supercondensed Node
TDFEM	Time Domain Finite Element Method
TE	Transverse Electric
TEM	Transverse Electromagnetic
TLM	Transmission Line Modelling Method
TM	Transverse Magnetic
VCBC	Variable Coefficient Boundary Condition
VIBC	Variable Impedance Boundary Condition
2-D	Two-dimensional
3-D	Three-dimensional

CIRCUIT THEORY AND TLM NOTATION

Symbol	Denotes
$A_{ij}, A_{ik}, B_{ij}, B_{ik}$	PML node scattering coefficients
C	Capacitance (F)
D_i	Node density (node s^3 m^{-3})
f_c	TLM mesh cutoff frequency (Hz)
G	Conductance (S)
I	Total current (A)
Δl	Node dimension for a cubic cell (m)
L	Inductance (H)
R	Resistance (Ω)
$\mathbf{S}$	Scattering matrix
Δt	Time step (s)
T	TLM transmission coefficient
u_{TL}	Pulse propagation velocity (m s^{-1})
u_{TLM}	Wave velocity in the TLM mesh (m s^{-1})
V	Total voltage (V)
$\Delta x, \Delta y, \Delta z$	Node dimensions for a general rectangular cell (m)
Y	Transmission line characteristic admittance (S)
$\hat{Y}$	Normalised admittance $= \frac{Y}{Y_0}$
Z, Z_{TL}	Transmission line characteristic impedance (Ω)
Γ	TLM reflection coefficient
ζ	Stub coefficient
ξ	Evanescent wave damping term

ELECTROMAGNETICS, THE PHYSICAL PROPERTIES OF MATERIALS, AND WAVES

Symbol	Denotes
c	Speed of light in vacuo $\approx 2\,997925 \times 10^8$ (m s^{-1})
$\mathbf{E}, E_x, E_y, E_z$	Electric field strength (V m^{-1})
f	Frequency (Hz)
$\mathbf{H}, H_x, H_y, H_z$	Magnetic field strength (A m^{-1})
$\mathbf{J}$	Current density (A m^{-2})
t	Time (s)
u	Wave velocity (m s^{-1})
Y_0	Intrinsic admittance of free space $= \frac{1}{Z_0}$ (S)
Z_0	Intrinsic impedance of free space $\approx 376\,7303$ (Ω)
$\delta_1, \quad, \delta_m$	Damping factors
ϵ	Permittivity (dielectric constant) (F m^{-1})
ϵ_r	Relative permittivity
ϵ_0	Permittivity of free space $\approx 8\,854187 \times 10^{-12}$ (F m^{-1})
$\theta_1, \quad, \theta_p$	Absorption angles for order p Higdon method
λ	Wavelength (m)
μ	Permeability (H m^{-1})
μ_r	Relative permeability
μ_0	Permeability of free space $= 4\pi \times 10^{-7} \approx 1\,256637 \times 10^{-6}$ (H m^{-1})
ν	Volume (m^3)
ρ	Reflection coefficient
ρ_T	Theoretical reflection coefficient
σ_e	Electric conductivity (S m^{-1})
σ_m	Magnetic conductivity (S m^{-1})
ϕ	Wave incident angle
ϕ_e	Estimate of wave incident angle
ω	Angular frequency (rad s^{-1})

MATHEMATICS

Symbol	Denotes
a, b	Finite difference parameters
$a_n(x, y, z)$	Binary array at time step n
B_m	Boundary operator of order m
D	Spatial shift operator
I	Identity shift operator
i, j, k	Dummy indices
j	$\sqrt{-1}$
K	Time shift operator
dl	Element of length
$\hat{n}$	Unit length normal vector
$\hat{x}, \hat{y}, \hat{z}$	Unit vectors in x-, y- and z-directions
$\left.\begin{array}{l} \alpha_1, \quad , \alpha_p \\ \beta_1, \quad , \beta_p \\ \gamma_1, \quad , \gamma_p \end{array}\right\}$	Boundary coefficients
π	Ratio of circle circumference to diameter $\approx 3\ 141593$
$\nabla \times \mathbf{A}$	Curl of vector $\mathbf{A}$
∞	Infinity

PORT LABELLING CONVENTION

Port labels used in this text comply with the following convention (Johns' original notation in parentheses)

$V_{ypx}(V_{12})$

$V_{ypz}(V_7)$

$V_{xpy}(V_{11})$

$V_{xpz}(V_{10})$

$V_{zny}(V_4)$

$V_{znx}(V_2)$

$V_{zpx}(V_9)$

$V_{zpy}(V_8)$

$V_{xnz}(V_6)$

$V_{xny}(V_3)$

y

x

z

$V_{ynz}(V_5)$

$V_{ynx}(V_1)$
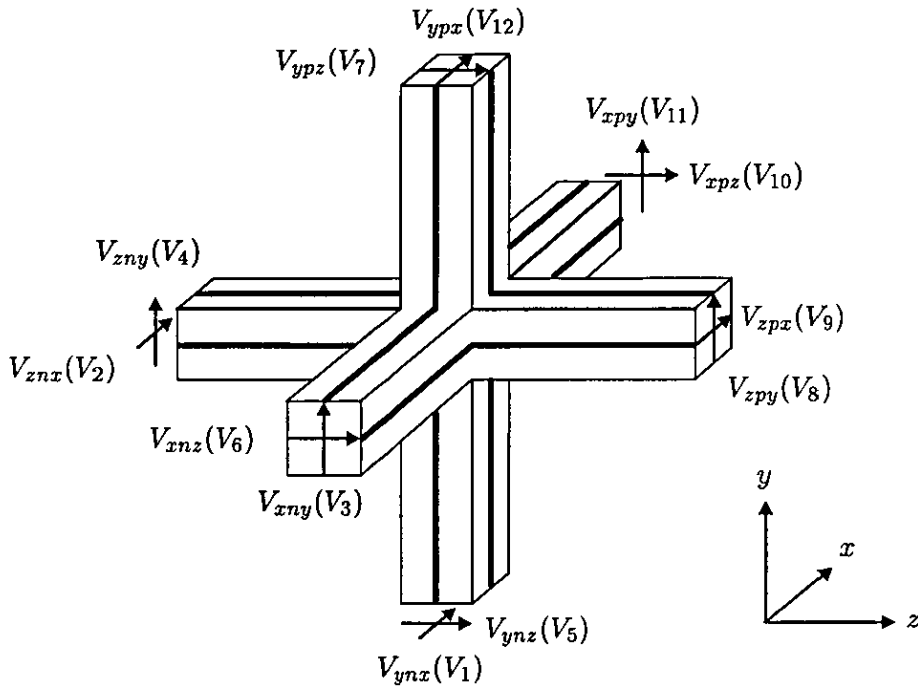
Other indices denote the time step and the pulse propagation direction, e g

$$_{n+1}^{\;\;i}V_{zpx}$$

"The incident voltage on the z-positive directed link-line, polarised in the x-direction at time step $n + 1$ "

A similar scheme is used for parameters associated with link and stub lines Symmetry is implied if 'n' or 'p' is omitted from the label subscript, e g $Z_{xpy} = Z_{xny} = Z_{xy}$.

Superscript or subscript	Denotes
e	Electric
i	Incident
m	Magnetic
o	Open circuit
r	Reflected
s	Short circuit

LIST OF FIGURES

LIST OF TABLES

CHAPTER 1:
INTRODUCTION

IN recent years the subject of electromagnetic (EM) immunity and emissions, usually referred to as electromagnetic compatibility (EMC), has become an increasingly important area of study in electrical engineering. All electronic and electrical devices generate radio frequency (RF) energy, either unintentionally by the acceleration or deceleration of electric charges during commutation, or by emission from RF power sources, such as in mobile communications equipment RF energy radiated from equipment (the *source* or *culprit*) can generate unwanted currents in neighboring equipment (the *victim*) by a variety of mechanisms. The effects of radio frequency interference (RFI) of this kind can be inconvenient such as degrading television reception, or more serious such as affecting the operation of medical equipment Concern about the effects of RFI on a range of equipment has been accentuated by the increasing density of use of the RF spectrum and increasing frequencies

Legislation and standards have developed in response to the growth in RFI sources, and now virtually all equipment must have:

- Intrinsic immunity to internal and external sources of RFI.

- Strictly limited emissions of RFI.

The automotive industry has a particularly strong interest in EMC, since modern vehicles often contain a number of electronic control systems such as engine management systems and anti-lock brakes The failure of such systems has serious safety implications and vehicle designs are legally required to undergo strict testing to ensure that they conform to set limits The importance of EMC to vehicle manufacturers also extends to product liability and quality issues.

1

1.1 The role of EM modelling in automotive design

Vehicles are amongst the most complex and expensive of all commonly owned consumer products Design optimisation is therefore a challenging and rewarding occupation for many businesses In order to meet market demands and gain competitive advantage, manufacturers have for many years sought the assistance of computers. The use of computers in automotive design is well established in disciplines such as geometric modelling[1], aerodynamics, and structural design

Computer modelling has gained in popularity in a wide range of disciplines because of the advantages it offers over experimental techniques. Modelling by no means replaces testing as a route to conformance with standards, but it does have a key diagnostic role. Designs can be evaluated at a much earlier stage than was previously possible, and this can reduce development time and costs significantly.

The quantity and detail of the data produced from models normally exceeds that possible with measurement alone. For example, EM simulation data gives field strength and current data in areas where it would be physically impossible to place measurement probes. Due to the increased amount of data available and the advent of advanced 3-D visualisation software, designers can now get a qualitative 'feel' for design as well as producing quantitative results for engineers This is particularly valuable in EM modelling, because experimental techniques only yield measurement data at individual points, unlike in a discipline such as aerodynamics where full-field visualisation of air flow has been realised by photographic means for many years

The electrical aspects of vehicle design have historically received relatively little attention because of their perceived minimal impact on the efficiency, safety and comfort of the vehicle In addition, the electronics content of vehicles was relatively low compared to their value

In older vehicles, the electrical system had a fairly simple design, and consisted almost exclusively of low-impedance wiring looms, relays, and switches This type of system is immune to virtually all commonly encountered sources of RF energy. However, the introduction of car radios in the 1950s and 1960s brought with it discrete components and amplifiers with high

---

[1] In fact, two of the pioneers of geometric modelling, de Casteljau and Bézier were both employed by vehicle manufacturers, (Citroen and Renault respectively) Geometrical modelling is the theoretical cornerstone of all computer-aided design (CAD) and other modelling methods rely heavily on it for representing and preprocessing geometrical data An excellent review of current methods can be found in Farin and Hamann [1 1]

input impedance Motorists rapidly became aware of radio noise caused by EM disturbances Significant internal and external RFI sources soon began to to be identified, and measures to correct the problem were devised Early EMC legislation was aimed at protecting domestic radio and TV reception from the broad-band noise emitted from vehicle spark ignition systems, and hence only covered broad-band emissions in the range 40–250 MHz

Later, the introduction of microprocessor-based control systems became more common, and this made the EMC performance of vehicles an important safety issue. Predicting the presence of EMC problems in modern vehicles can be demanding because of the wide range of materials in use and the geometrical complexity involved. For this reason EM modelling has grown to become an essential part of the design process [1 2], and the electrical aspects of vehicle design have become of equal importance to other more established areas

1.2 Test procedures

In principle, the test procedures adopted to study automotive EMC are extremely simple For whole-vehicle immunity tests illumination is provided at appropriate levels by a transmitting antenna and the effects on vehicle operation are observed For emission tests the RFI transmitted from the vehicle is measured with a broad-band antenna Details of the test procedures for whole vehicles, and for components have been described by Noble [1.3]

In practice there are difficulties in carrying out both types of test due to the nature of the measurements[2], and imperfections in the measuring environment. Emissions tests are usually carried out at an open-area test site (OATS), and immunity tests in a screened room or an anechoic or semi-anechoic chamber (see Figure 1 1). Semi-anechoic chambers are the most commonly used environments for whole-vehicle immunity tests. The metallic chamber walls are lined with RF-absorbing material (RAM) which absorbs the fields scattered by the vehicle and hence theoretically emulates free-space However some resonances are present due to the angular and frequency-dependent nature of these absorbers

At low frequencies the chamber walls are in the near field of the illuminating antenna and substantial coupling can occur [1.4] This complex situation makes it difficult to generate accurate,

---

[2] For example, it can be difficult to place field probes in immunity tests where standing waves are present Even very slight differences in position can yield large difference in the observed field strength
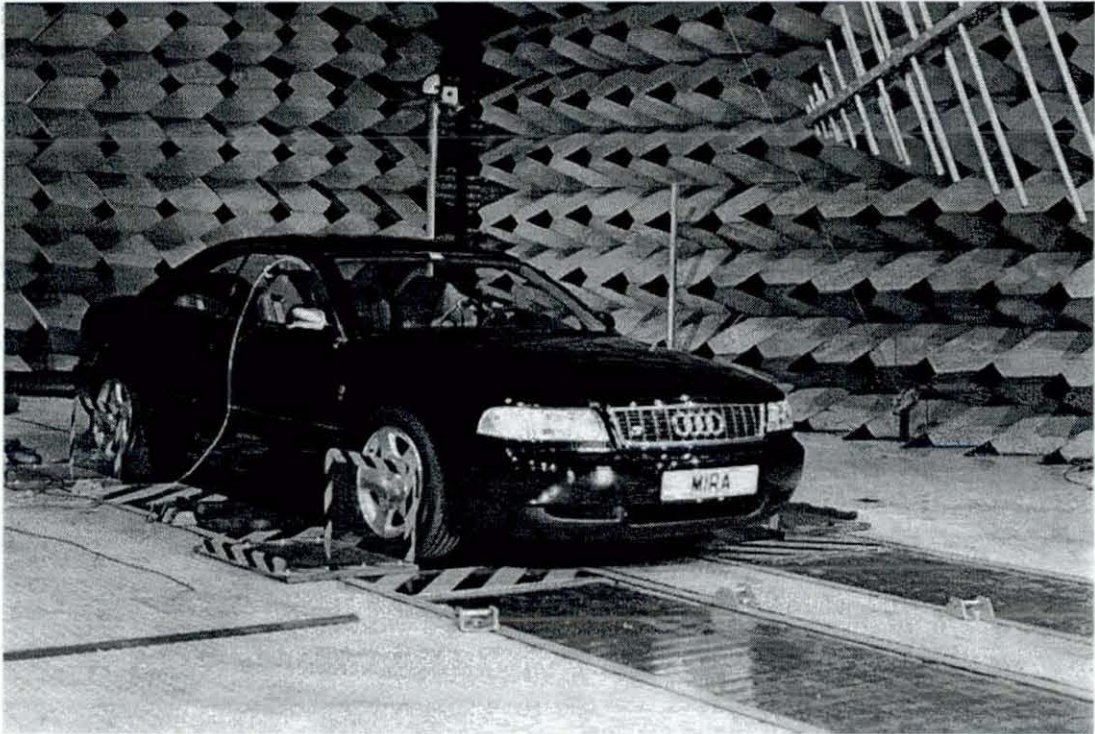
Figure 1.1: Vehicle immunity test carried out in the semi-anechoic chamber at MIRA, UK

uniform fields for tests, and indeed modelling has found a role in the design of cost-effective and efficient test environments [1.5]. Ideally a model should be capable of determining the vehicle's performance its test environment including the effects of the illuminating antenna and absorbers.

At high frequencies whole-chamber simulations are much more of a challenge in terms of the computer memory and model complexity required. Most semi-anechoic rooms are lined on the walls and roof with pyramidal absorbers which perform reasonably well at high frequencies[3], and thus it is a acceptable approximation to assume that the vehicle is surrounded by ideal free space. In the computer model this can be achieved by applying *absorbing* (or *radiation*) *boundary conditions*. These boundaries are be placed as close to the vehicle as possible in the model in order to conserve computer memory. This type of compromise is likely to be necessary more often in the future, since new innovations such as road-side communications at 5.8 GHz, and the first generation of forward-looking radars at 77 GHz are extending the band of interest (currently 20 MHz–1 GHz [1.6]) to the limits of current modelling capabilities.

---

[3] In some anechoic chambers ferrite tiles are used on the floor and as a backing for conventional RAM in order to improve low frequency performance.

1.3 Selection of a modelling method for automotive EMC

A wide range of numerical techniques have been developed for electromagnetic modelling Each method tends to have strengths in different types of problem, 1 e scattering, radiation or propagation This makes the choice of a modelling technique for EMC quite involved because fully self-contained EM simulations of the EMC test environment which include antennae etc can be partially classified in all three categories.

The propagation of EM waves in materials is concisely described by Maxwell's curl equations (1 1-1 4). Direct analytical solution is unrealistic except in cases where the geometry of the system of interest and the boundary conditions are extremely simple, although analytical techniques are widely used for validation purposes In most realistic physical situations a numerical solution method must be employed Numerical techniques often use a discretised version of either the differential (time domain) version of Maxwell's third and fourth equations

$$\nabla \times \mathbf{E} = -\mu \frac{\partial \mathbf{H}}{\partial t} \tag{1 1}$$

$$\nabla \times \mathbf{H} = \sigma_e \mathbf{E} + \epsilon \frac{\partial \mathbf{E}}{\partial t} \tag{1 2}$$

or the integral (frequency domain) forms:

$$\nabla \times \mathbf{E} = -j\omega\mu\mathbf{H} \tag{1 3}$$

$$\nabla \times \mathbf{H} = (\sigma_e + j\omega\epsilon)\mathbf{E} \tag{1 4}$$

These equations can be handled in a variety of different ways, each having distinct strengths and weaknesses. Some key features of a selection of methods are reviewed in Table 1.1, although more formal and comprehensive surveys have been conducted by Miller [1 7], and by Porter and Dawson [1 8].

The first choice to be made when selecting a technique is whether a time or frequency result is required Because of the nature of EMC problems, both time and frequency domain information are of interest. In order to cover a wide frequency band with a single simulation it is convenient to perform a time domain simulation with impulsive field excitation. The result can subsequently be transformed into the frequency domain using, for example, the discrete Fourier transform.

FINITE DIFFERENCE TIME DOMAIN (FDTD) [1.9], FINITE DIFFERENCE FREQUENCY DOMAIN (FDFD).	• Most commonly applied in the time domain form • Spatial discretisation into rectangular blocks • Time domain version produces **E** and **H** in alternate halves of the time step Frequency domain variant requires the solution of a set of simultaneous linear equations • Boundaries generally must lie on cell faces leading to a 'staircased' approximation of sloping boundaries, although special formulations are being devised to implement sloped and curved surfaces • High performance absorbing boundaries (boundaries at ∞) are not inherently easy to implement Successful schemes have been reported • Can deal with materials on a cell-by-cell basis and suitable for complex geometry
FREQUENCY DOMAIN FINITE ELEMENT METHOD (FDFEM) [1.10], TIME DOMAIN FINITE ELEMENT METHOD (TDFEM).	• Most commonly formulated in the frequency domain • Spatial discretisation into tetrahedral blocks bounded by elements • Operates by minimising an *energy functional*, which reduces the problem to a set of simultaneous linear equations • Absorbing boundaries can be difficult to formulate • Spurious solutions known as *vector parasites* must be handled • Complex material types and configurations are easily achieved • Accurate geometry representation possible as the elements may be individually scaled and distorted to fit the problem
METHOD OF MOMENTS (MoM) [1 11].	• Normally applied in the frequency domain, although time domain moment methods exist • Discretisation into wires, conducting patches or dielectric volumes • Integral form of Maxwell's equations are reduced to a set of simpler linear equations These are solved by a technique known as *the method of weighted residuals* • Different forms of the field integral equations determine which sort of problem the method solves, i e wires, patches or volumes This means that combining patches and dielectric volumes is nontrivial • Highly accurate absorbing boundaries can be implemented
GEOMETRICAL THEORY OF DIFFRACTION (GTD) [1 12].	• Based on optical methods • Only appropriate at very high frequencies where the free space wavelength of the incident wave is much smaller than the dimensions of the object • Differs from geometrical optics since the effects of diffraction are accounted for

Table 1.1: Features of alternative modelling methods to TLM

EMC simulations are distinct from simple radiation problems where, for example, the far-field radiation pattern of an antenna is to be evaluated Frequency domain methods such as the Method of Moments tend to be more efficient in terms of simulation times and memory usage for this type of problem

Time domain techniques are popular for a wide range of EMC problems, and are chosen as a starting point for this thesis A typical structure for a time domain modelling tool is shown in Figure 1 2 The most common time domain methods are the Finite Difference Time Do-
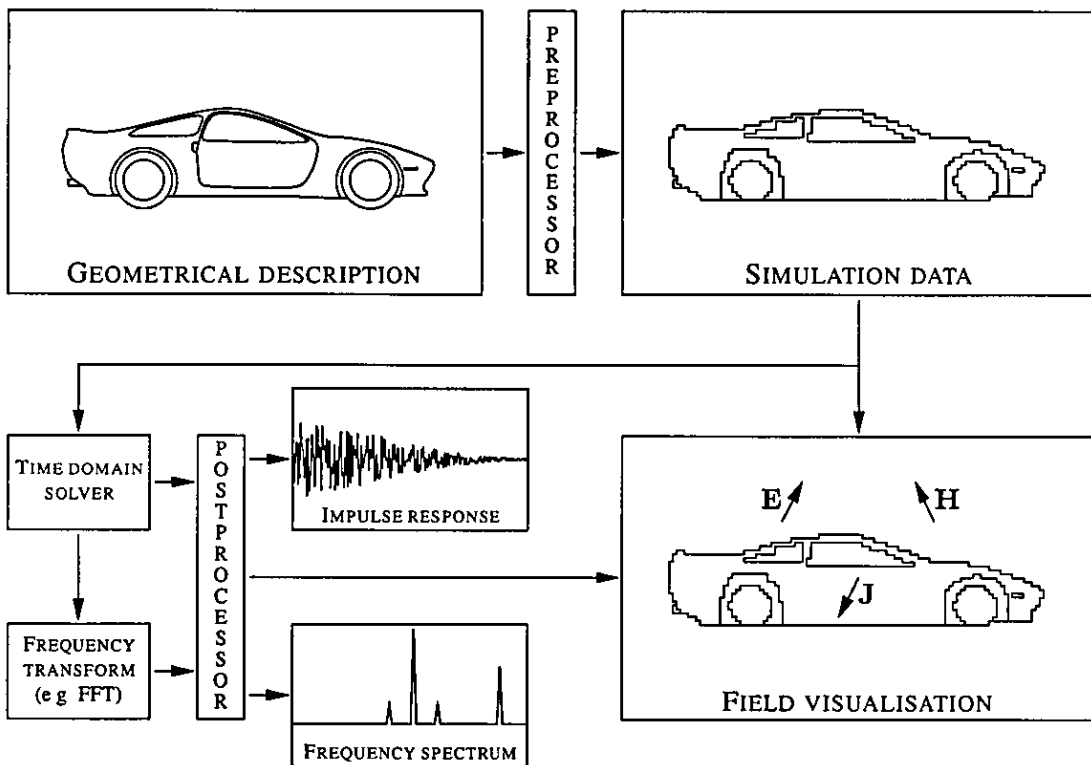
Figure 1 2· Simplified structure of a 3-D time domain EM modelling tool

main method (FDTD) and the subject of this thesis— the Transmission Line Modelling method (TLM) TLM and FDTD are very closely related and share many features, in fact TLM and FDTD have been shown to be equivalent in certain circumstances [1 13, 1 14, 1 15] The main difference between them lies in their formulation FDTD is formulated directly by mathematical methods, and TLM is formulated by conceptually replacing the problem with a set of equivalent electrical transmission lines. The fundamental unit of FDTD is the Yee cell [1 9], and in TLM is the point at which the transmission lines intersect— termed the *node* [1.16] Because TLM is based on the concept of electrical transmission lines it allows the engineer to draw on

existing knowledge of circuits and thus gives a good 'feel' for the modelling process TLM's power to abstract physical problems to electrical circuits has been used successfully in a wide variety of problems outside of electrical engineering, including acoustics [1 17], and thermal diffusion [1 18].

TLM also differs from traditional FDTD in the fact that both field components are available simultaneously, whereas in FDTD they are separated by one half of a time step The disadvantage of TLM appears to be in the additional memory that the 3-D symmetrical condensed node (SCN) [1.19] requires when compared to the Yee cell However, the stability of the TLM method tends to be better than FDTD for rectangular-faced cells where the side lengths differ, and this may mean that models with high permittivity materials can be represented more efficiently in TLM. Also, recent research suggests that TLM may perform significantly better than FDTD in modelling the fields around sharp conducting edges [1 20]. It is therefore debatable which method offers the best solution, although the use of FDTD seems more widespread in the radiation community, and TLM more common in the propagation and scattering communities. Whichever method offers the better alternative, there is no doubt that TLM has been used successfully in a wide range of problems. Since the advent of the SCN, it has been extensively applied in EMC both generally [1 21, 1 22, 1 23] and specifically in automotive EMC problems [1 24, 1.25, 1.26].

1.4 Objective of this thesis

Effective and efficient computation using any EM solution method depends fundamentally on

- Minimising the amount of computer memory in use.

- Minimising the number of calculations required to solve the problem

- Producing computer code with an optimised architecture

- Using high-performance computers

These requirement raise specific issues when applied to TLM. This thesis aims to target the parts of the TLM method where there is potential for achieving more efficient computation including

- The derivation and development of impulse reflection coefficient boundaries

- The evaluation of high performance absorbing boundary schemes for use in EMC simulations.

- Implementation issues including numerical accuracy, memory management and programming techniques.

The overall objective of this thesis is to develop methods for improving the effectiveness and efficiency of the TLM method. This is necessary to meet the challenges of increasing frequencies in the test environment and to maximise the potential of computing resources.

1 5   Thesis overview

Chapter 2 gives a brief introduction to the TLM method. The derivation and properties of different types of TLM node are described in the context of vehicle EM models. Finally, relevant recent developments in the TLM method are reviewed.

Chapter 3 identifies techniques which are based purely on the application of reflection coefficients between pairs of TLM nodes. A variety of common boundary types are derived and discussed, and a new method of applying asymmetric boundaries to achieve plane wave excitation in TLM is presented.

Chapter 4 analyses high-performance absorbing boundary schemes in the context of EM scattering problems. Performance tests are presented, and the merits of various schemes are discussed

Chapter 5 examines efficiency and accuracy of the TLM algorithm in terms of its implementation. Practical issues affecting the algorithm including the programming methodology, accuracy, and the efficient use of computational resources are addressed.

Chapter 6 concludes the findings, and proposes areas for further study

References

[1.1] G Farin and B. Hamann, "Current trends in geometric modeling and selected computational applications," *J Comp Phys.*, vol. 138, pp 1–15, 1997

[1.2] S. Lawton, "Numerical modelling for automotive EMC," in *Autotech Congress*, (Birmingham, UK), pp. 142–145, IMechE, 16–19 November 1993

[1.3] I E Noble, "Electromagnetic compatibility in the automotive environment," *IEE Proc Sci. Meas. Technol.*, vol. 141, no 4, pp 252–258, 1994

[1 4] C Christopoulos and I. Argyri, "Characterization of EMC environments using numerical simulations," in *Dig IEEE Int EMC Symposium*, (Denver, Colorado, USA), pp 334–338, 24–28 August 1998.

[1 5] J Clegg, M Alexander, L. Dawson, J. F. Dawson, J Jee, A C Marvin, B Loader, and S. J. Porter, "A method of reducing the number of ferrite tiles in an absorber lined chamber," in *Proc. EMC York'99*, (York, UK), pp. 59–64, IEE, 12–13 July 1999

[1 6] ISO 11451–1 1995 *Road vehicles— Electrical disturbances by narrowband radiated electromagetic energy— Vehicle test methods*, Part 1: General and definitions

[1 7] E. K. Miller, "A selective survey of computational electromagnetics," *IEEE Trans Antennas Propagat.*, vol. 36, no. 9, pp 1281–1305, 1988

[1 8] S. J Porter and J F Dawson, "Electromagnetic modelling for EMC using finite methods," *IEE Proc Sci. Meas. Technol.*, vol 141, no 4, pp 303–309, 1994

[1 9] K. S. Yee, "Numerical solution of initial value boundary value problems involving Maxwell's equations in isotropic media," *IEEE Trans Antennas Propagat*, vol 14, no 3, pp. 302–307, 1966

[1 10] J L Volakis, A. Chatterjee, and L. C Kempel, *Finite Element Method for Electromagnetics*. IEEE/OUP Series on Electromagnetic Wave Theory, New York, USA, Oxford, UK IEEE Press; Oxford University Press, 1998.

[1 11] R F Harrington, *Field computation by moment methods*. New York, USA. Macmillan, 1968

[1 12] V A Borovikov and B. Y Kinber, *Geometrical Theory of Diffraction*, vol 37 of *Electromagnetic Waves Series*. London, UK. Institution of Electrical Engineers, 1994

[1 13] P B Johns, "On the relationship between TLM and finite-difference methods for Maxwell's equations," *IEEE Trans Microw Theory Tech*, vol 35, no 1, pp 60–61, 1987.

[1 14] N R. S. Simons and E. Bridges, "Equivalence of propagation characteristics for the transmission-line matrix and finite-difference time-domain methods in two dimensions," *IEEE Trans. Microw Theory Tech*, vol 39, no 2, pp 354–357, 1991

[1.15] Z Chen, M. M. Ney, and W. J. R. Hoefer, "A new finite-difference time-domain formulation and its equivalence with the TLM symmetrical condensed node," *IEEE Trans Microw Theory Tech.*, vol 39, no. 12, pp. 2160–2169, 1991

[1 16] P. B Johns and R. L Beurle, "Numerical solution of 2-dimensional scattering problems using a transmission-line matrix," *Proc IEE*, vol 118, no 9, pp 1203–1208, 1971

[1 17] A. H. M. Saleh and P. Blanchfield, "Analysis of acoustic radiation patterns of array transducers using the TLM method," *Int. J Numerical Modelling· Electronic Networks Devices and Fields*, vol. 3, pp 39–56, 1990

[1.18] P B Johns, "A simple explicit and unconditionally stable numerical routine for the solution of the diffusion equation," *Int. J. Numerical Methods in Engineering*, vol 11, pp 1307–1328, 1977.

[1.19] P. B. Johns, "A symmetrical condensed node for the TLM method," *IEEE Trans Microw Theory Tech*, vol. 35, no 4, pp 370–377, 1987

[1.20] N. R. S. Simons, R. Siushansian, J LoVetri, and M. Cuhaci, "Comparison of the transmission-line matrix and finite-difference time-domain methods for a problem containing a sharp metallic edge," *IEEE Trans. Microw Theory Tech.*, vol 47, no 10, pp 2042–2045, 1999

[1 21] R. Allen, A Mallik, and P B. Johns, "Numerical results for the symmetrical condensed TLM node," *IEEE Trans. Microw Theory Tech*, vol. 35, no. 4, pp. 378–381, 1987

[1 22] J L Herring, P Naylor, and C. Christopoulos, "Transmission-line modelling in electromagnetic compatibility studies," *Int. J. Numerical Modelling Electronic Networks Devices and Fields*, vol. 4, pp 143–152, 1991.

[1 23] D. D. Ward and C. Christopoulos, "A three-dimensional model of the lightning channel," in *Int Conf on Lightning and Static Electricity*, (Bath, UK), pp 6B.3 1–6B 3 6, 26–28 September 1989.

[1.24] C. Christopoulos, P. B. Johns, A. Mallik, and P Naylor, "The use of numerical modelling techniques for EMC studies in vehicles," in *6th Int. Conf. Automotive Electronics*, (London, UK), pp. 159–163, IEE, October 1987

[1 25] J L Herring and C Christopoulos, "The vehicle body as an electromagnetic shield—numerical simulation for emission and susceptibility studies," in *7th Int Conf EMC*, (York, UK), pp 125–131, IEE, 28–29 August 1990

[1.26] D. D. Ward and S Lawton, "Numerical modelling for automotive EMC," in *IEEE Int Symp EMC*, (Atlanta, GA, USA), pp. 222–227, 14–18 August 1995

CHAPTER 2:

BACKGROUND AND FEATURES OF THE TRANSMISSION LINE MODELLING METHOD

THE TLM method has undergone considerable development since it was devised in the early 1970s In that time it has evolved into a comprehensive numerical technique with many powerful features. This chapter provides an introduction to the TLM method, including the development, derivation and errors of efficient and general 3-D nodes The state of current research is reviewed with an emphasis on the EM modelling of vehicles.

2.1 The history of TLM

Attempts to represent Maxwell's equations using equivalent electrical circuits date back as far as the 1940s [2.1], although the scope of these studies was restricted by the lack of fast, affordable digital computers. By the 1970s computers were readily available to perform the laborious and repetitive calculations involved, and a range of numerical techniques became popular The TLM method was first applied in pioneering work by Peter Johns to study wave guidance problems [1.16], but has since found applications in many areas of EM design and evaluation The first TLM nodes to be developed were the *2-D shunt node* and the *2-D series node* [2 2]. These types are limited to modelling phenomena which can be reduced to TM and TE modes respectively[1] The capabilities of these nodes are inadequate for modelling the complex EM characteristics of a 3-D vehicle body The 2-D nodes are important because their equivalent circuits are well understood and the concepts developed in their derivation are fundamental to the understanding and analysis of 3-D nodes

---

[1] That is, if the usual convention is adopted, where the node voltage is chosen to model the electric field and the node current is chosen to model the magnetic field

2 2 Two-dimensional nodes

In the 2-D TLM method, waves propagate on a *mesh* or *grid* of transmission lines which are joined at *nodes* [2 3]. If a voltage pulse of unit magnitude is injected into a node, as shown in Figure 2.1, and the transmission lines have characteristic (or *surge*) impedance Z_{TL}, then as it reaches the node centre it experiences a mismatch The pulse 'sees' the other three transmission lines in parallel, and thus a terminating impedance of $Z_{TL}/3$ By using transmission line theory it is possible to determine the magnitudes of the transmitted and reflected pulses as $\frac{1}{2}$ and $-\frac{1}{2}$ respectively. This process is known as *scattering*. The pulses then propagate along their respective transmission lines by a process known in TLM nomenclature as *connection* towards neighbouring nodes where they undergo further scattering.
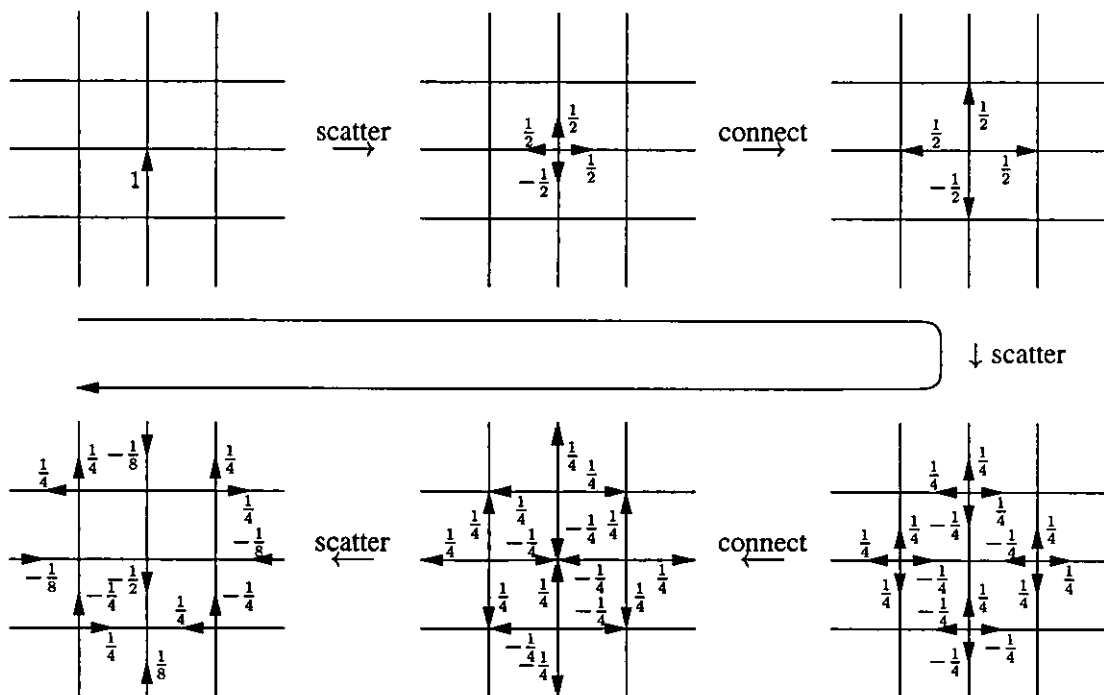
Figure 2 1· Nonzero voltage pulses on a shunt connected TLM mesh

The combined action of scattering and connecting pulses is consistent with Huygens' principle for light propagation [2.4]. In other words, each node acts as a secondary, isotropic, radiator for energy and by the net effect waves propagate on the mesh For this reason the TLM method is often viewed as a discretised version of Huygens' model for wave propagation, although more rigorous viewpoints have been adopted [2.5].

2 2 1   Shunt networks

If a single shunt connected node is isolated from the TLM mesh shown in Figure 2.1 the wave properties may be examined in more detail. Figure 2 2 shows an individual shunt node along with its lumped element equivalent circuit
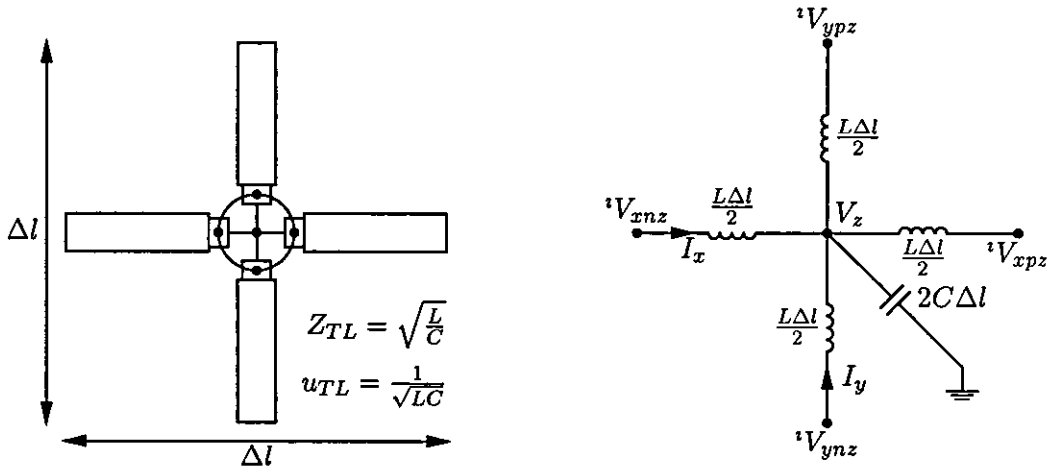
Figure 2.2 Shunt node made from coaxial transmission lines and the lumped element equivalent circuit

The network is conveniently analysed by assuming that the space step is small, i e $\Delta l \to 0$. By observing that $V = -L\frac{dI}{dt}$ for both propagation directions and that $\sum I = -C\frac{dV}{dt}$ at the node centre, the partial differential equations which govern the network may be expressed As shown in equation group (2.1), these are isomorphic to Maxwell's equations for TM field distributions (in this case containing nonzero field components of H_x, H_y and E_z only).

$$
\begin{aligned}
\frac{\partial E_z}{\partial y} &= -\mu \frac{\partial H_x}{\partial t} \\
-\frac{\partial E_z}{\partial x} &= -\mu \frac{\partial H_y}{\partial t} \\
\frac{\partial H_y}{\partial x} - \frac{\partial H_x}{\partial y} &= \epsilon \frac{\partial E_z}{\partial t}
\end{aligned}
\qquad \longleftrightarrow \qquad
\begin{aligned}
\frac{\partial V_z}{\partial x} &= -L \frac{\partial I_x}{\partial t} \\
\frac{\partial V_z}{\partial y} &= -L \frac{\partial I_y}{\partial t} \\
\frac{\partial I_x}{\partial x} + \frac{\partial I_y}{\partial y} &= -2C \frac{\partial V_z}{\partial t}
\end{aligned}
\qquad (2.1)
$$

Differentiating subsequent pairs of equations with respect to x, y and t respectively and substituting to remove the magnetic field components, an isomorphic pair of scalar wave equations is produced, i e.:

$$
\frac{\partial^2 E_z}{\partial x^2} + \frac{\partial^2 E_z}{\partial y^2} = \mu\epsilon \frac{\partial^2 E_z}{\partial t^2}
\quad \longleftrightarrow \quad
\frac{\partial^2 V_z}{\partial x^2} + \frac{\partial^2 V_z}{\partial y^2} = 2LC \frac{\partial^2 V_z}{\partial t^2}
\qquad (2 2)
$$

A mapping may therefore be established between components of the electric field (**E**) and electric potential (V), components of the magnetic field (**H**) and nodal current (I), permittivity (ϵ)

and capacitance (C), and permeability (μ) and inductance (L).

The propagation velocity in the medium and on the TLM mesh are obtained directly from wave equation pair (2 2)

$$u = \frac{1}{\sqrt{\epsilon\mu}} \quad \longleftrightarrow \quad u_{TLM} = \frac{1}{\sqrt{2LC}} = \frac{1}{\sqrt{2}} \frac{1}{\sqrt{LC}} \tag{2 3}$$

Therefore, if C models ϵ and L models μ, the propagation velocity on the TLM network for waves is $\frac{1}{\sqrt{2}}$ times the velocity in the medium. It can be further deduced that the intrinsic impedance of the network is $\frac{1}{\sqrt{2}}$ times the characteristic impedance of an individual link-line

A network with finite space step, Δl, shares these wave properties, providing Δl is sufficiently small The relationship between fields and circuit parameters are·

$$
\begin{aligned}
E_z &\longleftrightarrow &-\frac{V_z}{\Delta l} &= -\frac{1}{2\Delta l}\cdot({}^i V_{xnz} + {}^i V_{xpz} + {}^i V_{ynz} + {}^i V_{ypz}) \\
H_x &\longleftrightarrow &-\frac{I_y}{\Delta l} &= -\frac{1}{Z_{TL}\Delta l}({}^i V_{ypz} - {}^i V_{ynz}) \\
H_y &\longleftrightarrow &\frac{I_x}{\Delta l} &= \frac{1}{Z_{TL}\Delta l}({}^i V_{xpz} - {}^i V_{xnz})
\end{aligned}
\tag{2 4}
$$

The scatter process demonstrated in Figure 2 1 may be expressed algebraically by a scattering matrix, $\mathbf{S}$, i e.

$$ {}^r\mathbf{V} = \mathbf{S}\, {}^i\mathbf{V} \tag{2 5} $$

where

$$
{}^r\mathbf{V} = \begin{bmatrix} {}^r V_{xnz} \\ {}^r V_{xpz} \\ {}^r V_{ynz} \\ {}^r V_{ypz} \end{bmatrix}
$$

$$
\mathbf{S} = \frac{1}{2}\begin{bmatrix} -1 & 1 & 1 & 1 \\ 1 & -1 & 1 & 1 \\ 1 & 1 & -1 & 1 \\ 1 & 1 & 1 & -1 \end{bmatrix}
$$

$$
{}^i\mathbf{V} = \begin{bmatrix} {}^i V_{xnz} \\ {}^i V_{xpz} \\ {}^i V_{ynz} \\ {}^i V_{ypz} \end{bmatrix}
$$

and where superscripts i and r denote incident and reflected quantities respectively This process, combined with the connect process forms a time stepping algorithm operating with an interval Δt (hereafter known as the *time step*) defined by:

$$\Delta t = \frac{\Delta l}{u_{TLM}} = \Delta l \frac{\sqrt{2}}{u} \qquad (2\ 6)$$

2.2 2   Series networks

If the four transmission line segments in the shunt node are reconnected in series, another type of TLM network may be devised. The TLM series node is shown in Figure 2.3 along with its lumped element equivalent circuit. The partial differential equations which govern this network
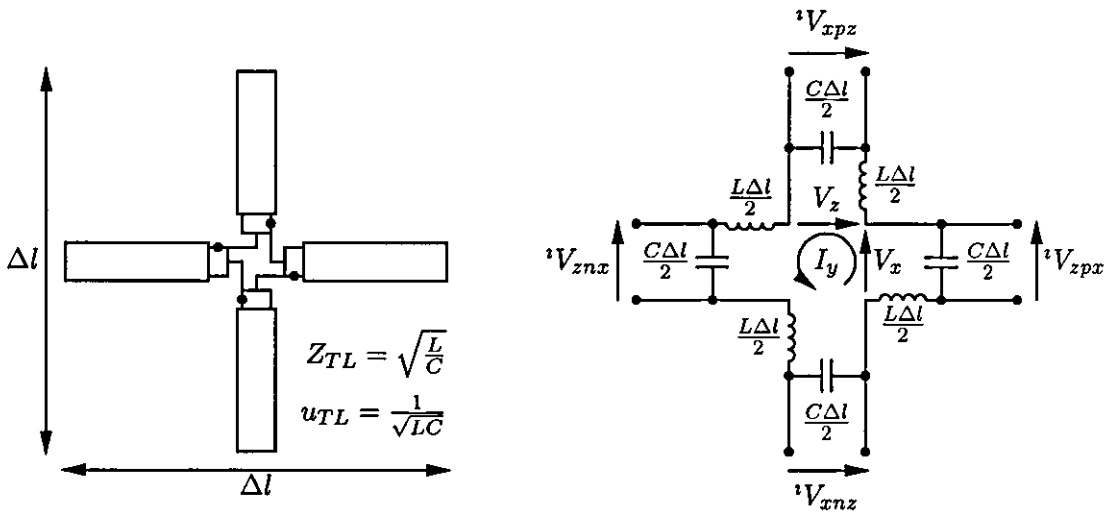
Figure 2 3 Series node made from coaxial transmission lines and the lumped element equivalent circuit

for $\Delta l \rightarrow 0$ are obtained in a similar manner to the shunt node Observing, in this instance, that $\sum V = -L\frac{dI}{dt}$ and that $I = -C\frac{dV}{dt}$ for each coordinate direction

$$
\begin{aligned}
\frac{\partial E_x}{\partial z} - \frac{\partial E_z}{\partial x} &= -\mu \frac{\partial H_y}{\partial t} & \frac{\partial V_x}{\partial z} + \frac{\partial V_z}{\partial x} &= -2L\frac{\partial I_y}{\partial t} \\
-\frac{\partial H_y}{\partial z} &= \epsilon \frac{\partial E_x}{\partial t} & \longleftrightarrow \qquad \frac{\partial I_y}{\partial z} &= -C\frac{\partial V_x}{\partial t} \\
\frac{\partial H_y}{\partial x} &= \epsilon \frac{\partial E_z}{\partial t} & \frac{\partial I_y}{\partial x} &= -C\frac{\partial V_z}{\partial t}
\end{aligned}
\qquad (2\ 7)
$$

As shown in equation group (2.7), the series node is equivalent to Maxwell's equations for a TE field distribution (with nonzero components in E_x, E_z and H_y only).

A scalar wave equation may be obtained by eliminating the electric field components

$$\frac{\partial^2 H_y}{\partial x^2} + \frac{\partial^2 H_y}{\partial z^2} = \mu\epsilon\frac{\partial^2 H_y}{\partial t^2} \quad \longleftrightarrow \quad \frac{\partial^2 I_y}{\partial x^2} + \frac{\partial^2 I_y}{\partial y^2} = 2LC\frac{\partial^2 I_y}{\partial t^2} \qquad (2\,8)$$

Examining equation (2.8) it can be seen that the wave velocity, and hence the time step are identical to that of the shunt node. The relationship between field components and circuit quantities are:

$$
\begin{aligned}
H_y &\longleftrightarrow & \frac{I_y}{\Delta l} &= \frac{1}{4Z_{TL}\Delta l}\cdot({}^{i}V_{znx} + {}^{i}V_{xpz} - {}^{i}V_{zpx} - {}^{i}V_{xnz}) \\
E_x &\longleftrightarrow & \frac{V_x}{\Delta l} &= \frac{1}{\Delta l}\cdot({}^{i}V_{znx} + {}^{i}V_{zpx}) \\
E_z &\longleftrightarrow & -\frac{V_z}{\Delta l} &= -\frac{1}{\Delta l}({}^{i}V_{xpz} + {}^{i}V_{xnz})
\end{aligned}
\qquad (2\,9)
$$

Because of the circuit topology, the scattering behaviour is different to that of the shunt node The scattering matrix for the series node is·

$$
\mathbf{S} = \frac{1}{2}\begin{bmatrix}
1 & 1 & 1 & -1 \\
1 & 1 & -1 & 1 \\
1 & -1 & 1 & 1 \\
-1 & 1 & 1 & 1
\end{bmatrix}
\qquad (2\,10)
$$

and the incident and reflected voltage vectors are:

$$
{}^{i}\mathbf{V} = \begin{bmatrix}
{}^{i}V_{xnz} \\
{}^{i}V_{xpz} \\
{}^{i}V_{znx} \\
{}^{i}V_{zpx}
\end{bmatrix}
$$

$$
{}^{r}\mathbf{V} = \begin{bmatrix}
{}^{r}V_{xnz} \\
{}^{r}V_{xpz} \\
{}^{r}V_{znx} \\
{}^{r}V_{zpx}
\end{bmatrix}
$$

2.2 3   Thévenin equivalent circuits

Once the propagation characteristics and field mappings for the TLM scheme have been established the focus can switch from Maxwell's equations to circuit theory.

A convenient method for analysing a variety of problems involving transmission lines is to generate a *Thévenin equivalent circuit.*
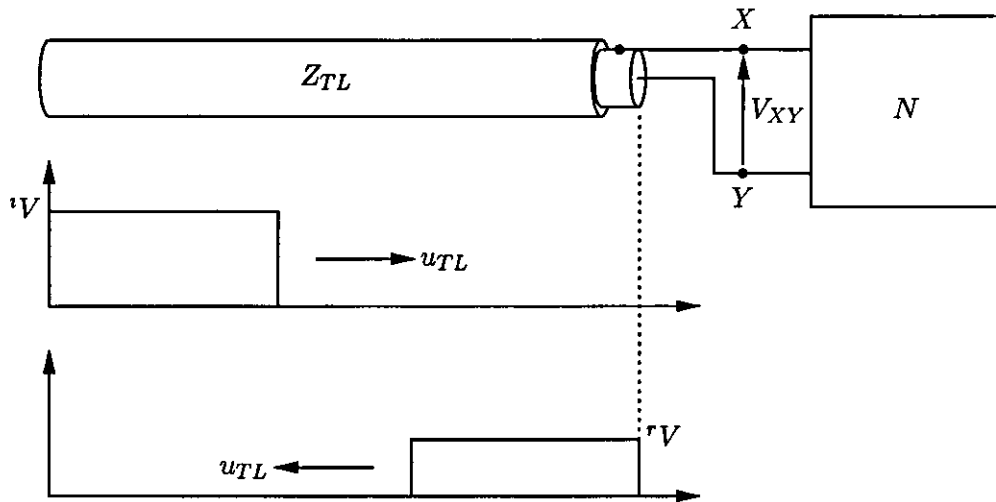
Figure 2 4 Transmission line carrying pulse of voltage ^iV, terminated with network N

The purpose is to simplify the circuit by replacing part of it with an equivalent voltage source (the *Thévenin voltage source*) and a series connected impedance (the *Thévenin impedance*) Figure 2.4 shows a transmission line connected to a general network N The objective of the following analysis is to replace the line with an equivalent Thévenin circuit and thus facilitate the solution of currents and voltages within network N

The first stage in obtaining the Thévenin equivalent circuit is to select a pair of reference terminals. These are denoted X and Y in the circuit shown in Figure 2.4. The next stage is to find the open circuit voltage V_{oc} at these terminals (see Figure 2.5(a)) When the line is unterminated the current flowing at XY is zero, and thus the reflected current magnitude must equal the incident current, i e :

$$\frac{^iV}{Z_{TL}} = \frac{^rV}{Z_{TL}} \qquad (2\ 11)$$

Furthermore, by applying Kirchoff's Voltage Law, it can be shown that

$$^rV = V_{oc} - {}^iV \qquad (2\ 12)$$

By substituting for ^rV in equation (2 12) (from equation (2 11)) the Thévenin voltage may be obtained, (see Figure 2.5(b)) i.e..

$$2\,^iV = V_{oc} \qquad (2\ 13)$$
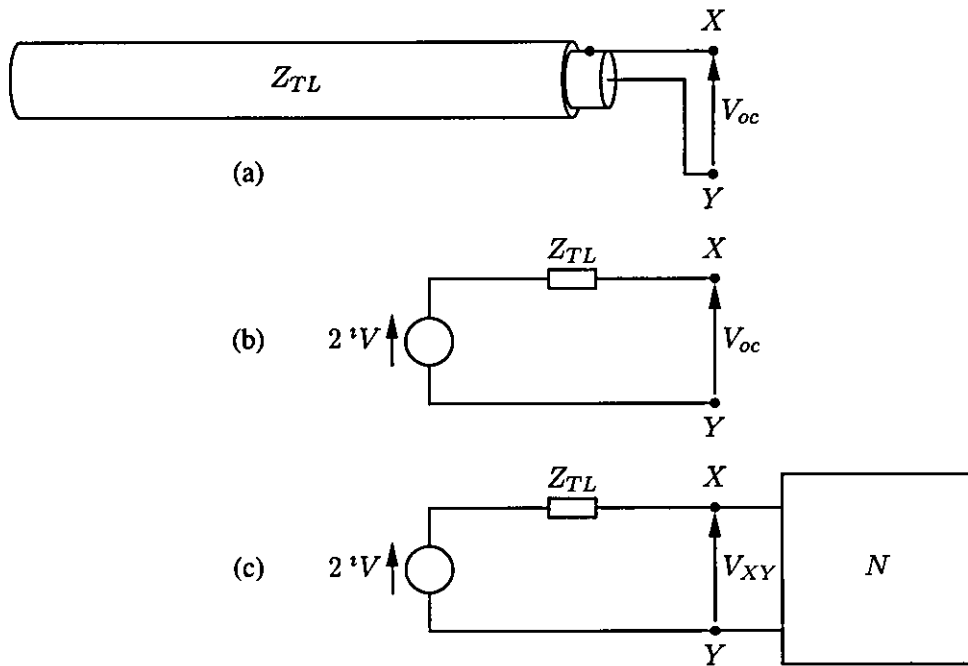
Figure 2 5 Stages in producing a Thévenin equivalent circuit

The Thévenin impedance is the value measured 'looking into' the reference terminals, which is simply the characteristic impedance of the transmission line

Therefore, the circuit in Figure 2 4 may be represented by the Thévenin equivalent shown in Figure 2.5(c) This is a useful result which aids the analysis of scattering both within the node and between nodes Internodal scattering will be covered in more detail in Chapter 3

This type of analysis may be applied to the series and shunt networks in the manner shown in Figure 2 6. In the diagram general values are assumed for the transmission line admittances (denoted Y_{xz} and Y_{yz}) in the shunt node and the impedances (denoted Z_{xz} and Z_{zz}) in the series node[2].

The reflected voltages are calculated by replacing each transmission line with its Thévenin equivalent and then applying equations of the form.

$$^rV = V_{XY} - {}^iV \qquad\qquad (2\ 14)$$

Although this analysis is relatively trivial in the case of simple shunt and series circuits, it becomes of greater importance when additional features such as stubs are added

---

[2] Note that by definition $Y_{xz} = \frac{1}{Z_{xz}}$ etc and the use of characteristic impedance or admittance is purely for mathematical convenience
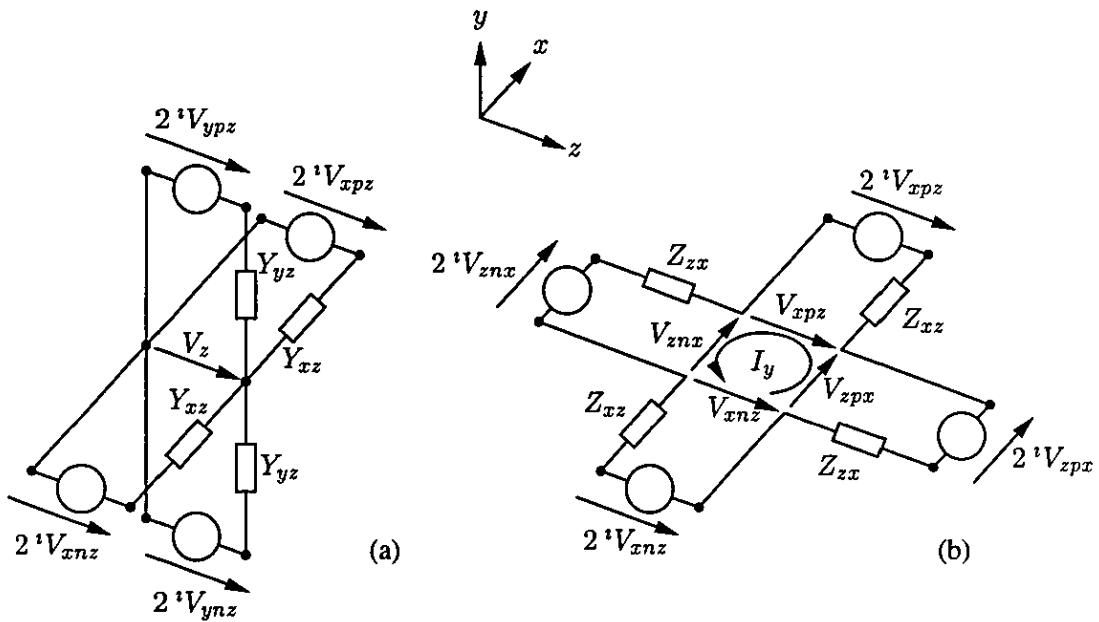
Figure 2 6 Thévenin equivalent circuits for (a) the shunt node and (b) the series node

2 2 4 Inhomogeneous and lossy materials

Real-world problems frequently contain dielectric and other materials where the speed of waves differs from that in the background material. The TLM formulations shown in the previous section cannot handle this property because in order to maintain synchronism it is necessary for the transit time of pulses to be uniform across the entire mesh, i e $\frac{1}{\sqrt{LC}}$ = a constant This means that in principle the wave velocity in the model must also remain constant (see equation (2 3)) To overcome this apparent difficulty, the concept of *stubs* has been introduced [2 6] Stubs are widely used in microwave circuits and are reactive elements formed from transmission line sections. This concept can be transferred directly to TLM.

Capacitive stubs are achieved by, conceptually, leaving one end of the transmission line section forming the stub as an open circuit (i e. numerically applying a +1 voltage reflection coefficient) This allows a localised increase in capacitance, and hence permittivity, to be modelled in shunt-connected networks The characteristic admittance of a capacitive stub associated with coordinate direction i of value C_{oi} may be expressed as a function of the time step

$$Y_{oi} = \frac{2C_{oi}}{\Delta t} \qquad (2\ 15)$$

Inductive stubs are achieved by, conceptually, short-circuiting one end of the transmission line

section forming the stub (i.e. numerically applying a −1 voltage reflection coefficient). This allows a localised increase in inductance, and hence permeability, to be modelled in series-connected networks. The characteristic impedance of an inductive stub associated with coordinate direction i of size L_{si} may be expressed by:

$$Z_{si} = \frac{2L_{si}}{\Delta t} \tag{2.16}$$

An example of a 2-D TLM model incorporating inhomogeneous material is shown in Figure 2.7.
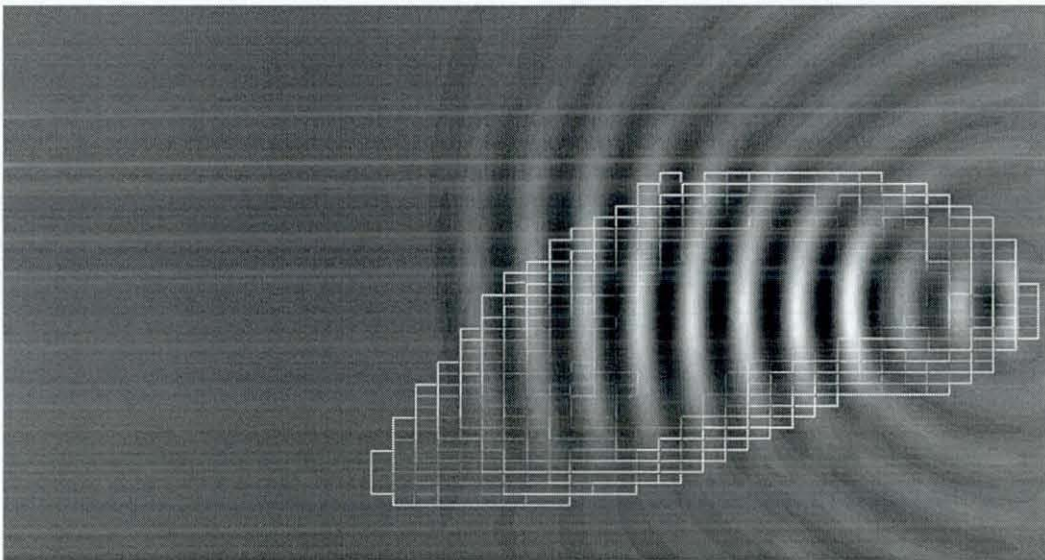
Figure 2.7: Beamforming action of the *melon* of the Harbour Porpoise— an example of inhomogeneous material modelling in an underwater acoustics problem

Stubs of this type are designed so that the time taken for a voltage pulse to propagate towards and then return from the mismatch is equal to the time step. In other words, the stub may be of any length providing any pulses reflected from it enter the node in synchronism with incident pulses from the link lines. By using stubs it is therefore possible to increase the local permittivity or permeability without affecting mesh synchronism or changing the link line impedance.

If the stub is infinite in length, it may be viewed as a lossy element, i.e. any pulse (and therefore energy) entering the stub is effectively dissipated. An infinite transmission line segment may therefore be represented by a resistor in the equivalent circuit of the node. Lossy stubs require no additional storage to implement since no reflections occur during connection.

Shunt conductance G_{ez} may be introduced into the shunt circuit to give electric losses (Figure 2 8) and series resistance R_{my} may be introduced into the series circuit to give magnetic losses (Figure 2.9).
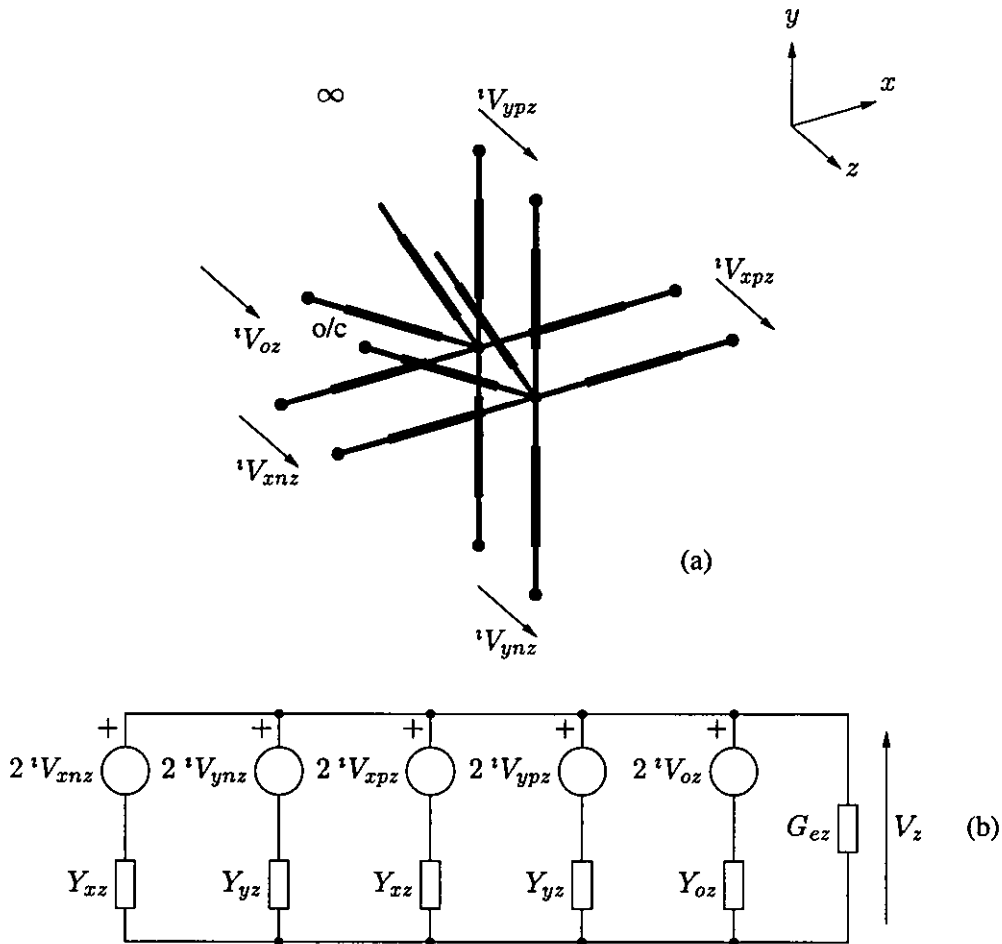
Figure 2 8: (a) Structure and (b) Thévenin equivalent circuit of a lossy shunt node
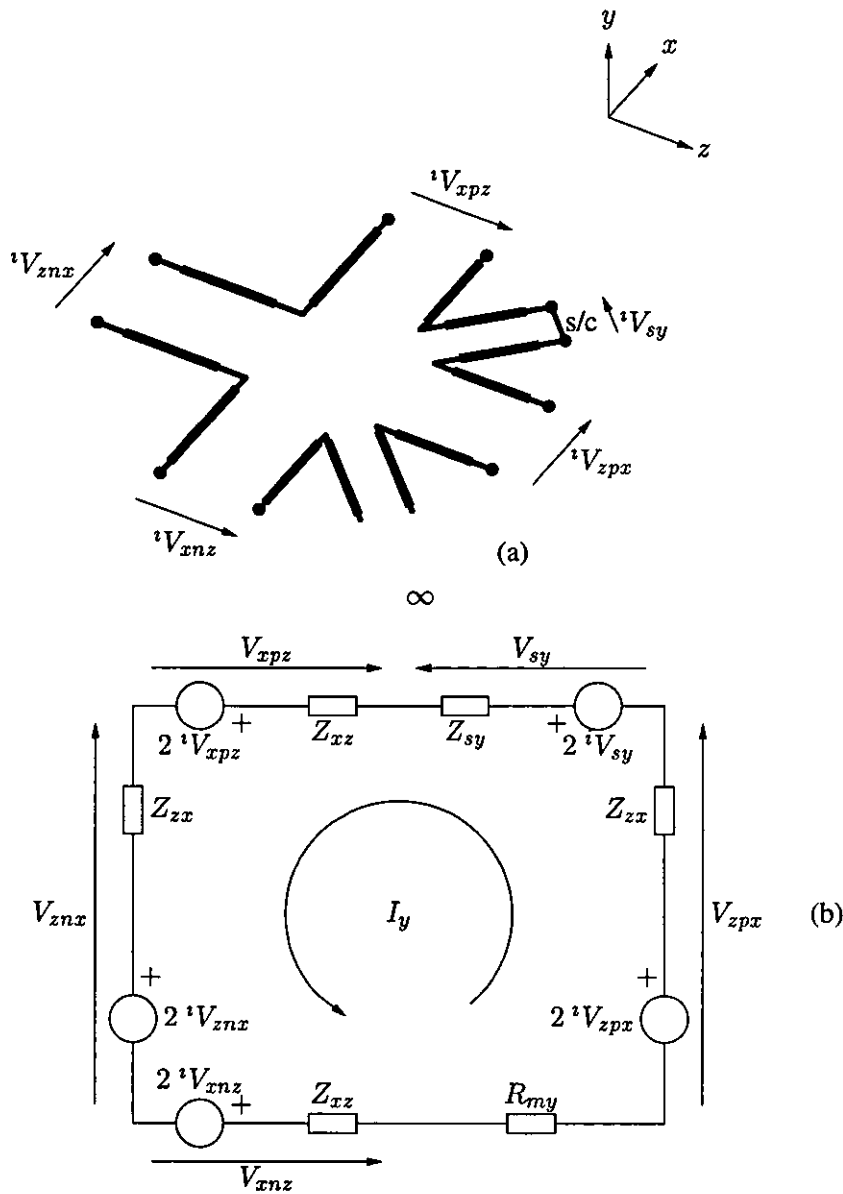
Figure 2 9 (a) Structure and (b) Thévenin equivalent circuit of a lossy series node

2.3   Three-dimensional node types

As explained at the start of this chapter, the capabilities of the shunt and series nodes are required in three dimensions for TEM field distributions. The first 3-D TLM algorithm, using the so-called *expanded node*, was described by Akhtarzad and Johns [2.7] The equivalent circuit consists of three shunt nodes and three series nodes electrically connected. The accuracy of the expanded node is limited as the field component measurements are made at different spatial

points within the node It is also regarded as inefficient in terms of computational resources since each 2-D node requires entirely separate treatment [2 8] The difficulties caused by spatial separation of the field components were later rectified by Saguet and Pic in the *Asymmetrical Condensed Node* (ACN) [2.9] The ACN uses less computer memory and provides all of the field components at a single point, however its asymmetry is inconvenient For example, the way in which problem boundaries are implemented depends on the orientation of the nodes to which they are applied.

A 3-D scalar node has been developed by Choi and Hoefer for solving problems which can be decomposed into TM or TE modes [2.10]. This is a natural development of the 2-D shunt node into three dimensions and as such is extremely efficient in terms of storage and computation Due to its lack of generality, however, it has few applications in EMC situations and has not been widely studied.

The most significant development in 3-D TLM is undoubtedly the *symmetrical condensed node* (SCN) introduced by Johns [1.19]. The success in producing a symmetrical node with all six field components available at a single point in space-time was initiated by a conceptual leap in TLM theory. Where earlier node types were developed by the *ad hoc* design of electrical networks, the SCN was formulated more directly from Maxwell's equations[3] As will be demonstrated, it is convenient to use a combination of circuit theory and Maxwell's equations in order to characterise the behaviour of the SCN and its derivatives.

Symmetrical condensed node types have been used exclusively for the work in this thesis as they are the most efficient and general nodes for use in EM models.

2 3 1   Symmetrical condensed nodes

The symmetrical condensed node may be derived in a variety of ways Originally, Johns generated the scattering matrix from first principles by inspecting Maxwell's curl equations, and applying the principles of energy and charge conservation to the node [1 19]. This method becomes cumbersome with more advanced SCN types. Other investigators have subsequently applied more general techniques, such as direct derivation by a process of centered differencing and averaging [2 12], or by jointly applying the principles of electric charge conservation,

---

[3] An equivalent circuit for the SCN has been derived by Mlakar [2 11], however it is very seldom useful in the modelling process due to its high complexity

magnetic flux conservation, electric field continuity and magnetic field continuity [2 13] In all of these derivations the convenience of applying circuit theory to derive the scattering matrix is somewhat redundant. This is unfortunate, since one of the more powerful features of TLM is its circuit analogy.

A more intuitive method has been recently reported by Portí *et al.* [2.14] which preserves the role of circuit theory more strongly in the modelling process This technique will be referred to as *the method of common and uncommon lines* The technique will be explained in the next section and it will be shown how this can be applied to symmetrical condensed nodes

2 3 2   The method of common and uncommon lines

If a pair of 2-D nodes are selected, such as the shunt and series nodes shown in Figures 2 2 and 2 3, a 3-D model can be imagined which satisfies Maxwell's equations for a pulse entering one of the ports common to both, i e xnz or xpz The shunt circuit is associated with E_z (by the voltage V_z) and the series circuit with H_y (by the current I_y)

The method of common and uncommon lines assumes that the shunt and series circuits are *somehow* connected, however no attempt is made to construct a full equivalent circuit Instead, the analysis assumes that a pulse is incident on one of the transmission lines common to both circuits (i e. $^iV_{xnz}$ or $^iV_{xpz}$ in Figure 2 6). Because there is no coupling between uncommon lines (on ports ypx, ynz, znx and zpx) the reflected voltages in those transmission lines may be calculated directly from the equivalent circuit of the appropriate 2-D node.

The reflected voltages in common lines are calculated by observing that scattering is an instantaneous process, and can be viewed as electro- and magnetostatic The coupling between common lines may therefore be mathematically imposed by ensuring that $\nabla \times \mathbf{H} = 0$ (charge is conserved) in the shunt node and $\nabla \times \mathbf{E} = 0$ (magnetic flux is conserved) in the series node during scattering. This condition leads to a pair of simultaneous linear equations which can then be solved to give the magnitude of pulses reflected into the common lines The technique is general and allows features developed in 2-D nodes to be rapidly incorporated into 3-D symmetrical condensed node formulations

2 3.3 The symmetrical condensed node without stubs

The method of common and uncommon lines may be illustrated by deriving the scattering matrix for the SCN without stubs. The equivalent circuits shown in Figure 2 6 are assumed with all link-lines of equal characteristic impedance and a unit magnitude pulse injected into a common line, i e $^iV_{xnz} = 1$. As has been explained, the reflected voltages into uncommon lines are produced from their respective shunt and series equivalent circuits, i e

$$^rV_{ypz} = \tfrac{1}{2}$$

$$^rV_{ynz} = \tfrac{1}{2}$$

$$^rV_{znx} = \tfrac{1}{2}$$

$$^rV_{zpx} = -\tfrac{1}{2}$$

Applying the principle of electric charge conservation to the shunt node

$$\tfrac{1}{2}(2C)(^iV_{xnz} + {}^iV_{xpz} + {}^iV_{ypz} + {}^iV_{ynz}) = \tfrac{1}{2}(2C)(^rV_{xnz} + {}^rV_{xpz} + {}^rV_{ypz} + {}^rV_{ynz})$$

Simplifying and substituting the known quantities:

$$\Rightarrow (1 + 0 + 0 + 0) = (^rV_{xnz} + {}^rV_{xpz} + \tfrac{1}{2} + \tfrac{1}{2})$$

$$\Rightarrow {}^rV_{xnz} + {}^rV_{xpz} = 0 \qquad (2.17)$$

Applying the principle of magnetic flux conservation to the shunt node

$$\tfrac{1}{2}(2L)(^iV_{xnz} + {}^iV_{zpx} - {}^iV_{xpz} - {}^iV_{znx}) = \tfrac{1}{2}(2L)(-^rV_{xnz} - {}^rV_{zpx} + {}^rV_{xpz} + {}^rV_{znx})$$

Simplifying and substituting

$$\Rightarrow (1 + 0 + 0 + 0) = (-^rV_{xnz} - (-\tfrac{1}{2}) + {}^rV_{xpz} + \tfrac{1}{2})$$

$$\Rightarrow {}^rV_{xnz} - {}^rV_{xpz} = 0 \qquad (2\ 18)$$

Therefore

$$^rV_{xnz} = 0$$

$$^rV_{xpz} = 0$$

By following similar analysis for other ports, the entire behaviour may be characterised by a surprisingly elegant scattering matrix

$$
^rV = S\,{}^iV \Rightarrow
\begin{bmatrix}
^rV_{ynx} \\
^rV_{znx} \\
^rV_{xny} \\
^rV_{zny} \\
^rV_{ynz} \\
^rV_{xnz} \\
^rV_{ypz} \\
^rV_{zpy} \\
^rV_{zpx} \\
^rV_{xpz} \\
^rV_{xpy} \\
^rV_{ypx}
\end{bmatrix}
= \frac{1}{2}
\begin{bmatrix}
0 & 1 & 1 & 0 & 0 & 0 & 0 & 0 & 1 & 0 & -1 & 0 \\
1 & 0 & 0 & 0 & 0 & 1 & 0 & 0 & 0 & -1 & 0 & 1 \\
1 & 0 & 0 & 1 & 0 & 0 & 0 & 1 & 0 & 0 & 0 & -1 \\
0 & 0 & 1 & 0 & 1 & 0 & -1 & 0 & 0 & 0 & 1 & 0 \\
0 & 0 & 0 & 1 & 0 & 1 & 0 & -1 & 0 & 1 & 0 & 0 \\
0 & 1 & 0 & 0 & 1 & 0 & 1 & 0 & -1 & 0 & 0 & 0 \\
0 & 0 & 0 & -1 & 0 & 1 & 0 & 1 & 0 & 1 & 0 & 0 \\
0 & 0 & 1 & 0 & -1 & 0 & 1 & 0 & 0 & 0 & 1 & 0 \\
1 & 0 & 0 & 0 & 0 & -1 & 0 & 0 & 0 & 1 & 0 & 1 \\
0 & -1 & 0 & 0 & 1 & 0 & 1 & 0 & 1 & 0 & 0 & 0 \\
-1 & 0 & 0 & 1 & 0 & 0 & 0 & 1 & 0 & 0 & 0 & 1 \\
0 & 1 & -1 & 0 & 0 & 0 & 0 & 0 & 1 & 0 & 1 & 0
\end{bmatrix}
\begin{bmatrix}
^iV_{ynx} \\
^iV_{znx} \\
^iV_{xny} \\
^iV_{zny} \\
^iV_{ynz} \\
^iV_{xnz} \\
^iV_{ypz} \\
^iV_{zpy} \\
^iV_{zpx} \\
^iV_{xpz} \\
^iV_{xpy} \\
^iV_{ypx}
\end{bmatrix}
\tag{2 19}
$$

By this method it is possible to generate all of the entries in a scattering matrix, S for the SCN by considering a total of three node pairs Unlike the expanded node, the shunt and series networks are purely used as analytical tools and do not require separate computation. As a result the node has all six field components condensed at a single point in space and with better efficiency than earlier 3-D nodes Because the circuit diagram of the SCN is complex it is normally shown schematically as a 3-D cruciform with the link lines shown in bold (see Figure 2 10)

The low-frequency propagation characteristics of the SCN may be obtained by considering a large mesh carrying a plane wave. It can be shown that the time step for the SCN is

$$
\Delta t = \frac{\Delta l}{2c}
\tag{2 20}
$$

The method of common and uncommon lines is extremely simple, but is suitable for all symmetrical condensed node types. It has been shown to be particularly useful for characterising scattering in nodes incorporating complex features such as thin wires [2 14]
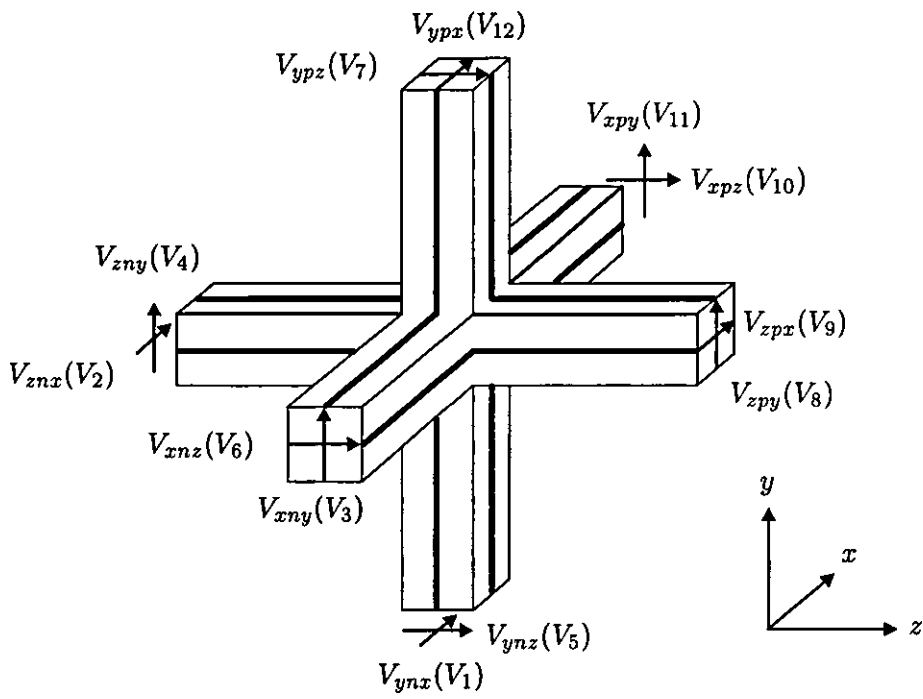
Figure 2.10: The Symmetrical Condensed Node (SCN) after Johns [1 19]

2 3 4 Symmetrical condensed nodes for inhomogeneous and anisotropic materials

So far, cubic cells and homogeneous material have been assumed for the symmetrical condensed node. In real models it is desirable to model cells which have rectangular faces in order to allow inhomogeneous materials to be efficiently incorporated. The ability to model anisotropic materials may also be required

By examining the electrical properties of the anisotropic, nonuniform, linear block of space shown in Figure 2 11, it is possible to write down the capacitance, inductance, electric con-
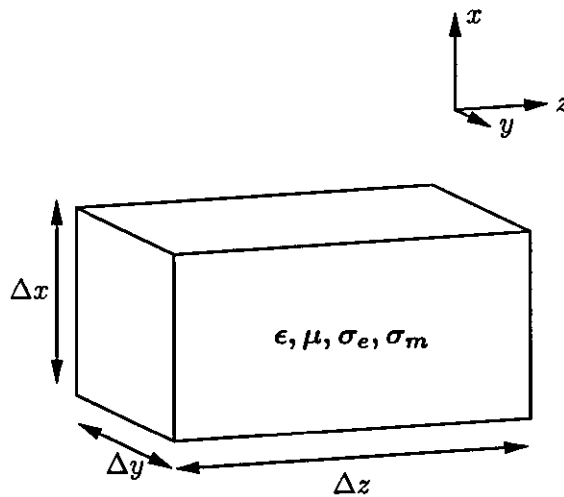
Figure 2 11 Arbitrary linear block of space

ductivity and magnetic conductivity for each coordinate direction. The constitutive parameters are:

$$L_i = \mu_i \frac{\Delta_j \Delta k}{\Delta i} \tag{2 21}$$

$$C_i = \epsilon_i \frac{\Delta_j \Delta k}{\Delta i} \tag{2 22}$$

$$G_{ei} = \sigma_{ei} \frac{\Delta_j \Delta k}{\Delta i} \tag{2.23}$$

$$R_{mi} = \sigma_{mi} \frac{\Delta_j \Delta k}{\Delta i} \tag{2.24}$$

where i, j, k are dummy indices such that $(i, j, k) \in \{(x, y, z), (y, z, x), (z, x, y)\}$ and L_i, C_i,

G_{ei}, and R_{mi} are the total inductance, capacitance, electric resistance and magnetic conductance of the block in coordinate direction i.

Parameters of the TLM node

There are only two fundamental constraints which must hold for a general SCN

1. The total capacitive and inductive contribution by link-lines and stubs must correspond to that of the block of space in each coordinate direction

2. The transit time of pulses on link-lines must be uniform for the node (and indeed, over the whole mesh).

The former constraint may be compactly expressed by a set of equations [2.15]

$$C_{ik}\Delta i + C_{jk}\Delta j + C_{ok} = C_k \tag{2 25}$$

$$L_{ij}\Delta i + L_{ji}\Delta j + L_{sk} = L_k \tag{2.26}$$

The latter constraint may be incorporated by expressing link-line impedances as a function of the time step

$$Z_{ij} = \frac{L_{ij}\Delta i}{\Delta t} \tag{2.27}$$

or as a link-line admittance, Y_{ij}:

$$Y_{ij} = \frac{C_{ij}\Delta i}{\Delta t} \tag{2 28}$$

By rearranging and substituting, the link-line capacitance and inductance terms may be eliminated from equations (2 25) and (2.26). Further substitution for C_k and L_k, and for the stub capacitance and inductance (obtained from equations (2.15) and (2 16)) yields·

$$Y_{ki} + Y_{ji} + \frac{Y_{oi}}{2} = \epsilon_i \frac{\Delta j \Delta k}{\Delta i \Delta t} \tag{2 29}$$

$$Z_{jk} + Z_{kj} + \frac{Z_{si}}{2} = \mu_i \frac{\Delta j \Delta k}{\Delta i \Delta t} \tag{2 30}$$

This pair of equations encompasses all of the fundamental constraints for the SCN and its derivatives.

Lossy nodes are accounted for by introducing infinite-length stubs in a similar manner to that described for 2-D nodes. The lossy stub impedances are those given in equation (2 23) for the equivalent shunt circuit and equation (2.24) for the equivalent series circuit [2 16, 2 17] A method which more closely models the permeability characteristics of ferrite materials by using parallel resistive elements on short-circuit stubs has also been described [2 18]

Advanced node types

Further conditions may be applied to equations (2 29) and (2 30) to obtain a variety of node types. Some of the more significant developments are summarised in Table 2.1.

For stubbed nodes, the time step and link line parameters are derived by insisting that the stub values are nonnegative[4] and substituting the appropriate constraints. For the symmetrical supercondensed node (SSCN), the parameters must be derived by solving a cubic inequality since there are no stubs

Once the parameters are obtained, the scattering behaviour may be determined from the Thévenin circuits described previously. Alternatively, the parameters may be substituted into the empirical form originally proposed by Naylor and Ait-Sadi [2.19]:

$$^{r}V_{inj} = V_j \pm I_k Z_{ij} -^i V_{ipj} \tag{2 31}$$

$$^{r}V_{ipj} = V_j \mp I_k Z_{ij} -^i V_{inj} \tag{2 32}$$

Calculations implemented in this form are known to be more computationally efficient (i e require fewer calculations) than scattering matrices, however deriving the parameters can be more difficult

---

[4] Negative stubs act as generators resulting in instability of the TLM algorithm

Node type	Conditions	Link lines	Lossless stubs	Time step constraints
SCN	$Z_{ij} = Z_0$ $Z_{si} = 0$ $Y_{oi} = 0$	$Z_{ij} = Z_0 = \dfrac{1}{Y_0} = \sqrt{\dfrac{\mu_0}{\epsilon_0}}$ (all identical)	none	$\Delta t = \dfrac{\Delta l}{2c}$
STUB-LOADED SCN	$Z_{ij} = Z_0$	$Z_{ij} = Z_0$ (all identical)	$Y_{oi} = 2Y_0\left(\dfrac{\epsilon_{ri}\Delta j \Delta k}{c\Delta t \Delta i} - 2\right)$ (three open circuit, electric) $Z_{si} = 2Z_0\left(\dfrac{\mu_{ri}\Delta j \Delta k}{c\Delta t \Delta i} - 2\right)$ (three short circuit, magnetic)	$\Delta t \le \dfrac{\epsilon_{ri}\Delta j \Delta k}{2c\Delta i}$ $\Delta t \le \dfrac{\mu_{ri}\Delta j \Delta k}{2c\Delta i}$
HYBRID SCN, TYPE I (HSCN (I)) [2 20, 2 21]	$Z_{ij} = Z_{ji}$ $Z_{si} = 0$	$Z_{ij} = Z_{ji} = Z_0\dfrac{\mu_{rk}\Delta i \Delta j}{2c\Delta t \Delta k}$ (three different)	$Y_{oi} = 2Y_0\left[\dfrac{\epsilon_{ri}\Delta j \Delta k}{c\Delta t \Delta i} - \dfrac{2c\Delta t}{\Delta i}\left(\dfrac{\Delta j}{\mu_{rj}\Delta k} + \dfrac{\Delta k}{\mu_{rk}\Delta j}\right)\right]$ (three open circuit, electric)	$\Delta t \le \dfrac{1}{2c}\sqrt{\dfrac{2\epsilon_{ri}}{[\mu_{rk}(\Delta j)^2]^{-1} + [\mu_{rj}(\Delta k)^2]^{-1}}}$
HYBRID SCN, TYPE II (HSCN (II)) [2 22, 2 21]	$Y_{ik} = Y_{jk}$ $Y_{oi} = 0$	$Y_{ik} = Y_{jk} = Y_0\dfrac{\epsilon_{rk}\Delta i \Delta j}{2c\Delta t \Delta k}$ (three different)	$Z_{si} = 2Z_0\left[\dfrac{\mu_{ri}\Delta j \Delta k}{c\Delta t \Delta i} - \dfrac{2c\Delta t}{\Delta i}\left(\dfrac{\Delta j}{\epsilon_{rj}\Delta k} + \dfrac{\Delta k}{\epsilon_{rk}\Delta j}\right)\right]$ (three short circuit, magnetic)	$\Delta t \le \dfrac{1}{2c}\sqrt{\dfrac{2\mu_{ri}}{[\epsilon_{rk}(\Delta j)^2]^{-1} + [\epsilon_{rj}(\Delta k)^2]^{-1}}}$
SYMMETRICAL SUPERCONDENSED NODE (SSCN) [2 23, 2 24]	$Y_{oi} = 0$ $Z_{si} = 0$	six different	none	see references [2 23] and [2 24]

Table 2 1 Properties of symmetrical condensed nodes

2.4 Discussion

The appropriate choice of SCN type depends strongly on the application If uniform cells, free space and perfect electrical conducting boundaries are a reasonable approximation, then the standard unstubbed SCN offers the most appropriate choice This node has the minimum storage requirement, computation and programming complexity.

Automotive components and whole vehicles are likely to require the ability to model materials in more detail, and this requires the use of one of the stubbed node types, or the SSCN In addition, the ability to use non-uniform aspect ratio cells is likely to be required for geometrical and efficiency reasons, and this also dictates the use of stubs or the SSCN.

Selecting which node to use depends on a range of factors including:

- The maximum time step available from the node.

- The minimum storage requirement which can be achieved

- The number of calculations in *scatter* and *connect*.

- The amount of complexity to implement.

The stub-loaded SCN is well established, widely verified, and is easy to implement in its standard form In the absence of internal boundaries, it requires no transmission/reflection process to be modelled between nodes (see Chapter 3 for more details) and this is convenient Unfortunately, the stub-loaded SCN requires 50% more storage than its unstubbed counterpart, and this is undesirable In addition, as is shown in Table 2.1, the time step is the minimum value of two expressions, one relating to permeability, and one to permeability

It has been shown that the SSCN offers a higher time step in certain circumstances, and has a lower storage requirement than other comparable SCNs. Another advantage of removing the stubs is that unstubbed nodes tend to have more uniform dispersion characteristics The SSCN has the disadvantage that it requires more computation than other nodes, and is more complex to implement In addition, it has not to date been tested as rigorously as other node types.

The hybrid node has some of the advantages of fully stubbed nodes and supercondensed nodes and appears to be a good compromise. If a uniformly graded mesh is required with dielectric

materials then it may be preferable to use type I HSCN since this will avoid having to apply reflection coefficients between nodes. In addition, the type I needs marginally less computation as no sign change is required when computing the incident voltages for stubs during connection

2 4.1 Excitation and measurement

Excitation and measurement of fields in the symmetrical condensed node is achieved by injecting or measuring voltage pulses at the node's ports. It is conventional to perform these operations on incident voltages, although it is equally possible to use reflected voltages.

Measurement is simply a matter of determining the voltage at the centre of the equivalent shunt circuit, V_t, which is sometimes referred to as the *equivalent total voltage* The electric field is determined from:

$$E_t = -\frac{V_t}{\Delta t} \tag{2 33}$$

The current in the series circuit, I_t, termed the *equivalent total current* is used to determine the magnetic field:

$$H_t = \frac{I_t}{\Delta t} \tag{2 34}$$

Excitation is the reverse process, with the important difference that the injected voltages are applied symmetrically about the node centre. This prevents uncompensated charges being introduced   If, for example, a field of $\mathbf{E} = E_0\hat{z}$ is to be excited in an unstubbed SCN in free space

$$E_o = -\frac{1}{2\Delta l}({}^iV_{xnz} + {}^iV_{xpz} + {}^iV_{ynz} + {}^iV_{ypz}) \tag{2.35}$$

By applying symmetry, the injected pulse magnitudes required are

$${}^iV_{xnz} = {}^iV_{xpz} = {}^iV_{ynz} = {}^iV_{ypz} = -\frac{1}{2}E_0\Delta l \tag{2 36}$$

Conducting nodes are sometimes used in models to represent structures They are implemented by applying a short-circuit condition to the node centre, and thus the scatter operation is merely

$$
\begin{aligned}
{}^rV_{ipj} &= -{}^iV_{ipj} \\
{}^rV_{inj} &= -{}^iV_{inj}
\end{aligned} \tag{2 37}
$$

Currents may be injected into this type of node by exciting space nodes in a continuous path, p, surrounding the conductor to satisfy Ampere's law

$$I_{conductor} = \int_p \mathbf{H} \cdot d\mathbf{l} \qquad (2\ 38)$$

where $d\mathbf{l}$ is the vector which describes the path around the contour p

Whichever method is used, it is important to ensure that the spectral components of the excitation function do not exceed the upper frequency limit of the mesh This is achieved by choosing a function which has very low magnitude high-frequency components, such as a Gaussian pulse, or by prefiltering arbitrary excitation with a low pass filter to remove any unwanted spectral components

2.5   Source of errors in condensed node formulations

The sources of error in the TLM method are generally well understood In automotive applications the complexity of geometry means that the individual contribution of a particular source of error is difficult to estimate For this reason the minimisation of all types of error is an important issue.

2 5 1   Velocity error

Due to the discretised nature of the TLM model, the propagation characteristics are anisotropic, i.e. the model is dispersive. The effects of dispersion are minimised at low frequencies where the space step, Δl, is much smaller than the wavelength, λ, in the model. The provision of a suitable number of nodes is therefore fundamental to the overall model accuracy The first formal analysis of the propagation characteristics of the unstubbed SCN was conducted by Nielsen and Hoefer [2.25]. The key findings of the study were:

- On-axis dispersion is zero

- Maximum dispersion occurs in the [1 1 1] direction

- The dispersion characteristics of the SCN are superior to both the expanded TLM node and the Yee cell (FDTD)
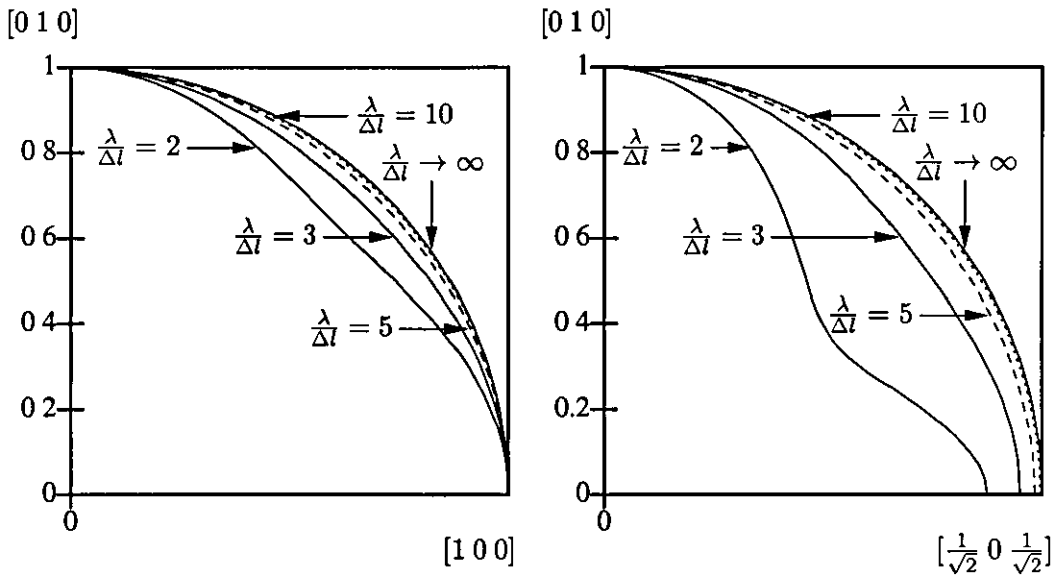
Figure 2 12 Normalised wave vector magnitude for different grid resolutions from the analytical form of Nielsen and Hoefer [2 25]

Similar analysis has been completed for the stub-loaded SCN [2 26], and for a range of advanced node types [2 27] In practice, for all node types the space step must be chosen so that $\lambda/\Delta l \geq 10$ to minimise the effects of dispersion This limit is typical of most low frequency modelling methods, and is often referred to as the *cutoff frequency*. In automotive models there is likely to be a mix of materials in use which may have differing wave properties, and thus the minimum number of nodes required in each region of the model varies This is an important consideration because the inclusion of even a small volume of very high permittivity material may mean that a large number of nodes is required

2 5 2   Spurious modes

As with most numerical methods, TLM suffers from some non-physical solutions These are termed *spurious modes* and were first characterised analytically for the SCN by Nielsen [2 28] Spurious modes occur at high spatial frequencies ($\lambda \approx 2\Delta l$) which are well beyond the cutoff frequency of the TLM mesh, and can be viewed as the resonant modes of the numerical method itself. In some cases they propagate without attenuation and can have significant relative magnitude, especially in models of highly lossy systems.

Due to their high frequency nature, they propagate with severe dispersion. This is in itself a problem since the energy distribution in the model can be severely disrupted, but it can also

accentuate the stability problems found in certain specialised techniques such as time-space extrapolated absorbing boundaries (see Chapter 4)   In addition, the energy coupled into spurious modes can lead to unpredictable losses and thus errors in the modelled Q-factor. Other problems such as frequency shift of observed resonances are also attributable to the presence of spurious modes

Spurious solutions are generated by temporal or physical discontinuities in the modelled system They are either caused by high-frequency components in the excitation, or by sharp corners of objects or excitation volumes within the model   Avoiding high-frequency components in the time domain is easily achieved through signal processing of the excitation signal (low-pass filtering), or by selecting a function which is band limited   However, avoiding spatial discontinuities can be more difficult, since sharp edges often occur in models.

In the vast majority of situations encountered in automotive EM models, providing reasonable care is exercised, spurious solutions can be reduced to a negligible level. Even if spurious modes are accidentally excited, they occur well beyond the cutoff frequency of the mesh and can often be ignored or filtered out of the results.

2.5 3   Coarseness error

Another important consequence of the discrete nature of the TLM method is termed *coarseness error*. Coarseness error occurs where the grid resolution is inadequate to resolve rapid spatial variations in the field distribution. This typically occurs near to sharp corners of objects or between adjacent conductors. The error can be reduced by a number of means, such as locally increasing the grid resolution, or by employing specialised *corner nodes* [2.29]   Some of the features of vehicle geometry are prone to modelling error related to coarseness, although it is not clear how significant this type of error is when compared to that originating from other sources.

2 5 4   Geometrical approximation error

A rectangular coordinate system is normally used to discretise objects for modelling, although curvilinear meshes may be used [2.30, 2.31]. Whichever coordinate system is in use, a loss of resolution during the discretisation process is inevitable since surfaces and volume regions

must be mapped onto the midpoints of the link lines and nodes respectively. The model is often termed a *staircased* (2-D TLM) or *sugar-cubed* (3-D TLM) approximation of the physical system This type of geometrical approximation can introduce significant error, particularly where the surfaces to be modelled are curved or inclined at an angle to the coordinate axes

A number of investigators such as German [2 32] and Melton *et al* [2 33] have proposed algorithms to allow reflective boundaries to be more accurately placed in SCN meshes and thus achieve better conformity to real-world geometry.

Curved and sloped boundaries are a prominent feature of modern vehicles for aerodynamic and aesthetic reasons The ability to improve the geometrical accuracy without increasing the number of nodes in the model is therefore highly desirable.

2 5 5   Implementation related errors

As with all numerical methods, the actual algorithm implementation has a fundamental role to play in accuracy Digital computers operate with a finite numerical accuracy and certain numerical operations introduce error by their nature. Errors from this source are covered in detail in Chapter 5.

2.6   A pictorial review of capabilities for automotive models

The last section has highlighted some of the inherent limitations with the TLM method. As has been commented, many of these have knock-on effect on the efficiency. Fortunately, the situation can be improved by applying specialised modelling techniques to cope with problematic features in the physical system. A brief review of some of the methods which have been developed is shown in Figure 2 13 This thesis aims to address the efficiency implications in more general terms; in particular the number of nodes and amount of computation required

Absorber models The characterisics of RF absorbing materials require specialised treatment Several schemes for modelling the behaviour of absorbers have been proposed [2 34, 2 35, 2 36]

Thin wire models[†] The dimensions of wires (e g. in antennas) are often small compared with the TLM space step, leading to significant errors Thin wire nodes have been developed to allow wires to be accurately and efficiently modelled [2 42, 2 43]

Narrow slot formulations[†] Small gaps between panels cause highly significant disturbances in the field distribution (see Section 2 5 3) The resulting computational overhead may be minimised by incorporating a sub-cellular slot model [2 37]

Thin films Some vehicle shells are made from non-metallic materials, such as Carbon Fibre Composite (CFC), which allow significant field penetration Methods have been developed to model the diffusion of fields through this type of material [2 38, 2 39, 2 40, 2 41]

Multiconductor models Vehicles normally contain looms of tightly packed, thin wires A technique has been proposed which allows multiple conductors to be efficiently placed in TLM models [2 44]

Curved and sloping surfaces See Section 2 5 4

†According to Babinet's principle, the problems of thin wires and of narrow slots are closely related [2 45]

Figure 2 13 Features of the TLM method of particular relevance to EMC studies of vehicles

2.7   Conclusion

The origins, principles and errors of the TLM method have been described It has been shown that 3-D condensed node types are closely related to 2-D shunt and series types. The method of common and uncommon lines has been applied to the SCN for illustrative purposes

It has been argued that the Hybrid SCN offers the most appropriate selection for current automotive EM modelling, based on simplicity of computation and time step considerations

The TLM method has the ability to model complex material types, thin conductors, thin films and narrow slots. The ability to represent these physical features makes it well suited to automotive EM models.

References

[2.1]   G Kron, "Equivalent circuit of the field equations of Maxwell—I," *Proc Inst Radio Engrs* , vol. 32, pp. 289–299, May 1944

[2 2]   S. Akhtarzad and P. B. Johns, "Generalised elements for t l m. method of numerical analysis," *Proc. IEE*, vol. 122, no. 12, pp 1349–1352, 1975.

[2 3]   C. Christopoulos, *The Transmission-Line Modeling Method TLM*. IEEE/OUP Series on Electromagnetic Wave Theory, New York, USA; Oxford, UK IEEE Press, Oxford University Press, 1995.

[2.4]   C. Huygens, *Traité de la Lumière*. Leiden, 1690.

[2 5]   M Krumpholz and P Russer, "Two-dimensional FDTD and TLM," *Int J Numerical Modelling· Electronic Networks, Devices and Fields*, vol 7, pp 141–153, 1994

[2 6]   P B Johns, "The solution of inhomogeneous waveguide problems using a transmission-line matrix," *IEEE Trans. Microw. Theory Tech.*, vol. 22, no. 3, pp. 209–215, 1974

[2 7]   S Akhtarzad and P. B. Johns, "Solution of 6-component electromagnetic fields in three space dimensions and time by the t l m method," *Electron. Lett* , vol. 10, no 25/26, pp. 535–537, 1974.

[2.8]   P. Saguet, "The 3D transmission-line matrix method Theory and comparison of the processes," *Int J Numerical Modelling Electronic Networks Devices and Fields*, vol 2, pp. 191–201, 1989.

[2 9]   P Saguet and E. Pic, "Utilisation d'un nouveau type de noeud dans la méthod TLM en 3 dimensions," *Electron. Lett* , vol. 18, no. 11, pp. 478–480, 1982

[2 10] D. H. Choi and W. J. R. Hoefer, "The simulation of three-dimensional wave propagation by a scalar TLM model," in *MTT Symposium Digest*, (San Francisco, CA, USA), pp 70–71, IEEE, 1984.

[2.11] J. Mlaker, "Circuit model for a symmetrical condensed TLM node," *Int. J Numerical Modelling: Electronic Networks Devices and Fields*, vol 6, pp 183–193, 1993.

[2 12] H. Jin and R. Vahldieck, "Direct derivations of TLM symmetrical condensed node and hybrid symmetrical condensed node from Maxwell's equations using centered differencing and averaging," *IEEE Trans. Microwave Theory Tech* , vol 42, no 12, pp 2554–2561, 1994.

[2 13] V. Trenkić, C. Christopoulos, and T. M. Benson, "Simple and elegant formulation of scattering in TLM nodes," *Electron. Lett* , vol 29, no. 18, pp 1651–1652, 1993

[2.14] J. A. Portí, J A Morente, and M. C Carrión, "Simple derivation of scattering matrix for TLM nodes," *Electron Lett.*, vol. 34, no. 18, pp 1763–1764, 1998

[2.15] V. Trenkić, *The development and characterization of advanced nodes for the TLM method.* PhD thesis, University of Nottingham, November 1995. pt. 1, pp 18–19

[2 16] P. Naylor and R. A. Desai, "New three dimensional symmetrical condensed lossy node for solution of electromagnetic wave problems by TLM," *Electron Lett* , vol 26, no 7, pp 492–494, 1990.

[2.17] F J. German, G. K. Gothard, and L. S Riggs, "Modelling of materials with electric and magnetic losses with the symmetrical condensed TLM method," *Electron Lett* , vol 26, no. 16, pp 1307–1308, 1990.

[2.18] J F. Dawson, "Improved magnetic loss for TLM," *Electron. Lett.*, vol. 29, no 5, pp 467–468, 1993.

[2 19] P Naylor and R Ait-Sadi, "Simple method for determining 3-D TLM nodal scattering in nonscalar problems," *Electron Lett* , vol. 28, no 25, pp 2353–2354, 1992

[2 20] R A. Scaramuzza and A. J. Lowery, "Hybrid symmetrical condensed node for the TLM method," *Electron Lett.*, vol. 26, no. 23, pp 1947–1949, 1990

[2 21] V Trenkić, C Christopoulos, and T. M. Benson, "On the time step in hybrid symmetrical condensed TLM nodes," *IEEE Trans. Microw. Theory Tech* , vol. 43, no 9, pp 2172–2174, 1995

[2 22] P. Berini and K Wu, "A pair of hybrid symmetrical condensed TLM nodes," *IEEE Microw. and Guided Wave Lett.*, vol. 4, no. 7, pp. 244–246, 1994

[2 23] V. Trenkić, C Christopoulos, and T. M Benson, "New symmetrical super-condensed node for the TLM method," *Electron Lett*, vol. 30, no. 4, pp. 329–330, 1994

[2.24] V. Trenkić, C. Christopoulos, and T. M Benson, "Theory of the symmetrical super-condensed node for the TLM method," *IEEE Trans. Microw. Theory Tech*, vol 43, no 6, pp. 1342–1348, 1995

[2 25] J. Nielsen and W J R. Hoefer, "A complete dispersion analysis of the condensed node TLM mesh," *IEEE Trans. Magnetics*, vol. 27, no. 5, pp. 3982–3985, 1991

[2 26] J A Morente, G. Giménez, J. A Portí, and M. Khalladi, "Dispersion analysis for a TLM mesh of symmetrical condensed nodes with stubs," *IEEE Trans. Microw Theory Tech*, vol 43, no 2, pp. 452–456, 1995

[2.27] V. Trenkić, *The development and characterization of advanced nodes for the TLM method* PhD thesis, University of Nottingham, November 1995 pt 3, pp 102–177

[2 28] J Nielsen, "Spurious modes of the TLM-condensed node formulation," *IEEE Microw and Guided Wave Lett*, vol 1, no 8, pp 201–203, 1991.

[2 29] J L Herring and W J R Hoefer, "Improved correction for 3-D TLM coarseness error," *Electron. Lett.*, vol. 30, no. 14, pp. 1149–1150, 1994.

[2.30] H. Meliani, D. de Cogan, and P. B. Johns, "The use of orthogonal curvilinear meshes in TLM models," *Int. J. Numerical Modelling: Electronic Networks Devices and Fields*, vol 1, pp 221–238, 1988.

[2.31] D. D. Ward, *A three-dimensional model of the lightning return stroke*. PhD thesis, University of Nottingham, May 1991. ch 8

[2.32] F. J German, "Infinitesimally adjustable boundaries in symmetrical condensed node TLM simulations," in *Proc. 9th Annual Review of Progess in Applied Comput Electromagn*, (Monterey, CA, USA), pp 482–490, ACES, 22–26 March 1993.

[2 33] M. D. Melton, S. C. Pomeroy, and D. D. Ward, "Improved object definition within a TLM model for automotive applications," in *EMC York '99*, (York, UK), pp 12–15, IEE, 12–13 July 1999.

[2 34] J. F Dawson, "Representing ferrite absorbing tiles as frequency dependent boundaries in TLM," *Electron Lett* , vol. 29, no. 9, pp. 791–792, 1993.

[2 35] J. F. Dawson, J Ahmadı, and A. C. Marvin, "Modelling the damping of screened room resonances by ferrite tiles using frequency dependent boundaries in TLM," in *Proc 2nd Int Conf Comput. Electromagn* , (Nottingham, UK), pp 271–274, IEE, 12–14 April 1994.

[2.36] J. Paul, C. Christopoulos, and D. W. P. Thomas, "Modelling of RF absorbing materials for anechoic chambers," in *Digest of the Second International Workshop on TLM modeling*, (Munich, Germany), pp. 165–176, IEEE, 27–29 October 1997

[2 37] A. Centeno and R A Scaramuzza, "The use of TLM in the EMC design and analysis of aircraft hatches," in *Digest of the Second International Workshop on TLM modeling*, (Munich, Germany), pp. 155–164, IEEE, 27–29 October 1997.

[2 38] A. Mallık and C. P Loller, "The modelling of EM leakage into advanced composite enclosures using the TLM technique," *Int. J. Numerical Modelling Electronic Networks Devices and Fields*, vol 2, pp 241–248, 1989

[2 39] D. P. Johns, J Wlodarczyk, and A Mallık, "New TLM models for thin structures," in *Proc. Int Conf Comput Electromagn.*, (London, UK), pp. 335–338, IEE, 25–27 November 1991.

[2.40] V. Trenkıć, C. Christopoulos, and T. M Benson, "Numerical simulation of polymers and other materials for electronic shielding applications," in *POLYMAT '94*, (London, UK), pp 384–387, September 1994.

[2 41] J A. Cole, J F. Dawson, and S. J Porter, "Efficient modelling of thin conducting sheets within the TLM method," in *Proc. 3rd Int Conf. Comput Electromagn* , (Bath, UK), pp 45–50, IEE, April 1996.

[2 42] J. A. Morente, J. A. Portí, G Giménez, and A. Gallego, "Loaded-wire node for TLM method," *Electron. Lett.*, vol. 29, no. 2, pp 182–184, 1993.

[2.43] A. P. Duffy, J. L. Herring, T. M. Benson, and C. Christopoulos, "Improved wire modelling in TLM," *IEEE Trans Microw Theory Tech.*, vol. 42, no. 10, pp 1978–1983, 1994

[2 44] A. J Wlodarczyk, V Trenkić, R. A Scaramuzza, and C. Chrıstopoulos, "A fully ın-
tegrated multıconductor model for TLM," *IEEE Trans Mıcrow Theory Tech* , vol 46,
no. 12, pp 2431–2437, 1998

[2 45] C. A. Balanıs, *Antenna Theory— Analysıs and Desıgn*, ch. 12, pp 616–620 New York
John Wıley, 2nd ed , 1997

CHAPTER 3:

INTERNODAL REFLECTION COEFFICIENT BOUNDARIES

M ANY physical properties of a system being modelled may be effectively and efficiently incorporated by applying reflection coefficients to the pulses transferred between nodes during the connect process This chapter describes the application and derivation of various boundaries of this type and discusses their relative merits An improved method of producing plane-wave excitation using asymmetric boundaries is developed

3.1 Introduction

Connection is, by definition, a one-dimensional concept and therefore operations performed on a single pair of connected link-lines can only be expected to model one-dimensional phenomena [3.1]. Since the transit time of pulses is uniform over the entire mesh, and computation is carried out at distinct time steps, boundary placement is, theoretically, restricted to the node centre (accounted for during scattering at $n\Delta t$) or to the link lines joining adjacent nodes (accounted for during connection at $(n + \frac{1}{2})\Delta t$) Often it is simplest to handle boundary placement between nodes because it avoids having to produce a new scattering matrix. For the purposes of this chapter, internodal boundaries will be assumed, however it has recently been shown that placing conducting boundaries within the node can yield good results [3 2]

Internodal boundaries are relatively straightforward to design in the TLM method by applying circuit theory, although it has been shown that certain frequency dependent boundaries are more conveniently obtained using filter theory [2 34, 2 41]

47

Boundaries can be broadly categorised into:

Internal boundaries to model thin objects within the model, such as metals or thin layers of non-
ferrous materials The nodes joining either side of the layer may be electrically isolated
if there is no significant penetration of fields

External boundaries to terminate the computational domain. The nature of the test environment
will dictate the appropriate modelling boundary Open region scattering problems such
as those found in anechoic EMC test situations require boundaries which absorb fields,
whereas in conductive environments symmetry boundaries are more appropriate

3 2   Idealised boundary types

Several commonly used boundary conditions may be conveniently studied by evaluating the
reflection and transmission processes which occur between nodes The first stage is to analyse
the circuit shown in Figures 3 1 and 3.2.
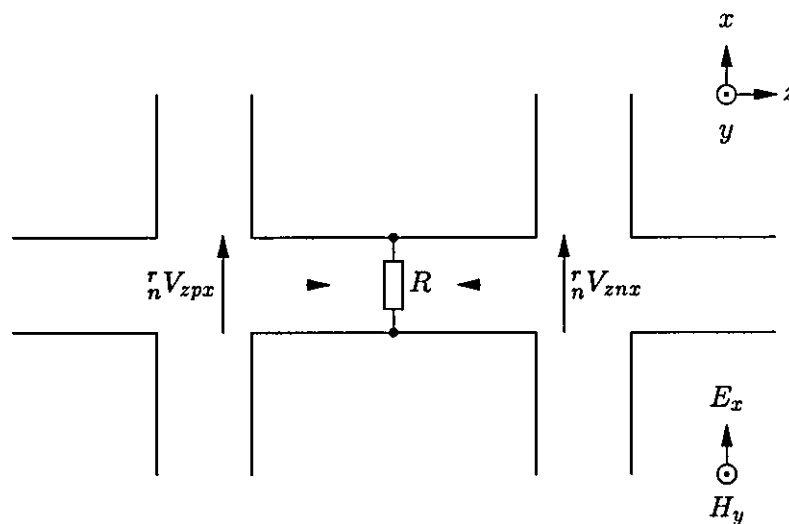
Figure 3.1: Reflected pulses in a pair of SCNs after scattering

The Thévenin equivalent circuit at time $(n + \frac{1}{2})\Delta t$, shown in Figure 3 3, is obtained in a similar
manner to that adopted for the node itself (see Section 2.2 3, p 18ff)

The reflection and transmission coefficients are found by applying Kirchoff's Voltage Law and
Kirchoff's Current Law:
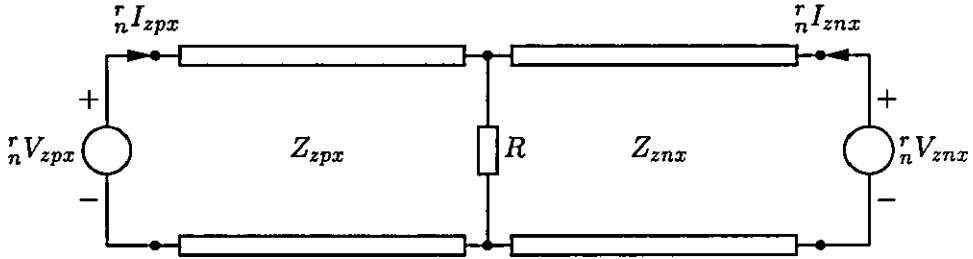
Figure 3 2 Pair of transmission lines extracted from Figure 3 1 with a parallel resistor, R
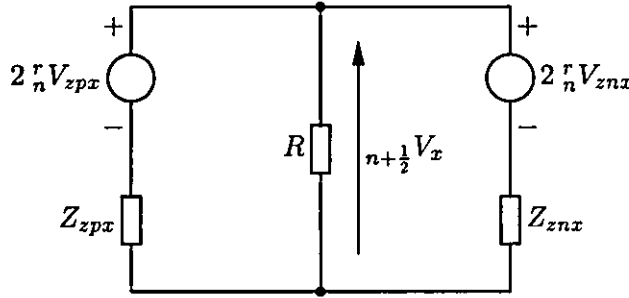
Figure 3 3: Thévenin equivalent of the circuit shown in Figure 3 2

$$\frac{{}_{n+\frac{1}{2}}V_x}{R} = \frac{2\,{}_{n}^{r}V_{zpx} - {}_{n+\frac{1}{2}}V_x}{Z_{zpx}} + \frac{2\,{}_{n}^{r}V_{znx} - {}_{n+\frac{1}{2}}V_x}{Z_{znx}}$$

$$\Rightarrow {}_{n+\frac{1}{2}}V_x = \frac{2\left({}_{n}^{r}V_{zpx}Z_{znx} + {}_{n}^{r}V_{znx}Z_{zpx}\right)}{\frac{Z_{zpx}Z_{znx}}{R} + Z_{zpx} + Z_{znx}} \tag{3 1}$$

The incident voltages at the next time step may be evaluated from.

$$\begin{aligned} {}_{n+1}^{i}V_{zpx} &= {}_{n+\frac{1}{2}}V_x - {}_{n}^{r}V_{zpx} \\ {}_{n+1}^{i}V_{znx} &= {}_{n+\frac{1}{2}}V_x - {}_{n}^{r}V_{znx} \end{aligned} \tag{3 2}$$

By substituting into these equations from equation (3.1), a four element link-line scattering matrix[1] may be derived containing link-line reflection coefficients, Γ_{zpx} and Γ_{znx} and transmission coefficients T_{zpx} and T_{znx}.

$$\begin{bmatrix} {}_{n+1}^{i}V_{zpx} \\ {}_{n+1}^{i}V_{znx} \end{bmatrix} = \begin{bmatrix} \frac{2Z_{znx}}{\alpha} - 1 & \frac{2Z_{zpx}}{\alpha} \\ \frac{2Z_{znx}}{\alpha} & \frac{2Z_{zpx}}{\alpha} - 1 \end{bmatrix} \begin{bmatrix} {}_{n}^{r}V_{zpx} \\ {}_{n}^{r}V_{znx} \end{bmatrix} = \begin{bmatrix} \Gamma_{zpx} & T_{znx} \\ T_{zpx} & \Gamma_{znx} \end{bmatrix} \begin{bmatrix} {}_{n}^{r}V_{zpx} \\ {}_{n}^{r}V_{znx} \end{bmatrix} \tag{3 3}$$

where $\alpha = \frac{Z_{zpx}Z_{znx}}{R} + Z_{zpx} + Z_{znx}$. This expression will be used in the following sections to assist the derivation of a several frequently-encountered boundaries

---

[1] Not to be confused with the *nodal* scattering matrix

3 2.1   Field measurement on link-lines

The field components may be extracted at time $(n + \frac{1}{2})\Delta t$, from the voltage and currents on link lines at the boundary.

Considering equation (3 1) with $R \to \infty$:

$$_{n+\frac{1}{2}}V_x = \frac{2\left(^r_nV_{zpx}Z_{znx} + ^r_nV_{znx}Z_{zpx}\right)}{Z_{zpx} + Z_{znx}}$$

Since the mapping in the TLM formulation is $E_x \mapsto -V_x/\Delta x$, the electric field may be obtained directly from:

$$_{n+\frac{1}{2}}E_x = -\frac{2\left(^r_nV_{zpx}Z_{znx} + ^r_nV_{znx}Z_{zpx}\right)}{\Delta x(Z_{zpx} + Z_{znx})} \tag{3 4}$$

In general, for a k-directed link line pair polarised in the i-direction

$$_{n+\frac{1}{2}}E_i = -\frac{2\left(^r_nV_{kpi}Z_{kni} + ^r_nV_{kni}Z_{kpi}\right)}{\Delta i(Z_{kpi} + Z_{kni})} = -\frac{2\left(^r_nV_{kpi}Y_{kpi} + ^r_nV_{kni}Y_{kni}\right)}{\Delta i(Y_{kni} + Y_{kpi})} \tag{3 5}$$

These expressions are also valid if the stub parameters are directly substituted for their normalised equivalents

In the SCN formulation the loop current is contributed by the stubs and the appropriate circulating ports, i e. I_i is supplied by ports jnk, jpk, knj and kpj and stubs As was explained in the previous chapter, the loop current is related to the field by, $H_y \mapsto I_y/\Delta y$. By considering the direction of current flow in the circuit under consideration, the magnetic field on the boundary is

$$_{n+\frac{1}{2}}H_y = \frac{2\left(^r_nV_{znx} - ^r_nV_{zpx}\right)}{\Delta y(Z_{zpx} + Z_{znx})} \tag{3 6}$$

In general, the magnetic field at the boundary may be obtained directly from

$$_{n+\frac{1}{2}}H_i = \frac{2\left(^r_nV_{jnk} - ^r_nV_{jpk}\right)}{\Delta i(Z_{jpk} + Z_{jnk})} \tag{3 7}$$

Note that in this case, the normalised stub values may not be directly substituted These measures of the field components on the boundary are useful for evaluating the fields on equivalent surfaces, as will be demonstrated later.

3 2 2   Electric wall

In order to obtain a plane of electric symmetry (known as an *electric wall*) on an external problem boundary, the situation shown in Figure 3 4 may be considered   By maintaining the
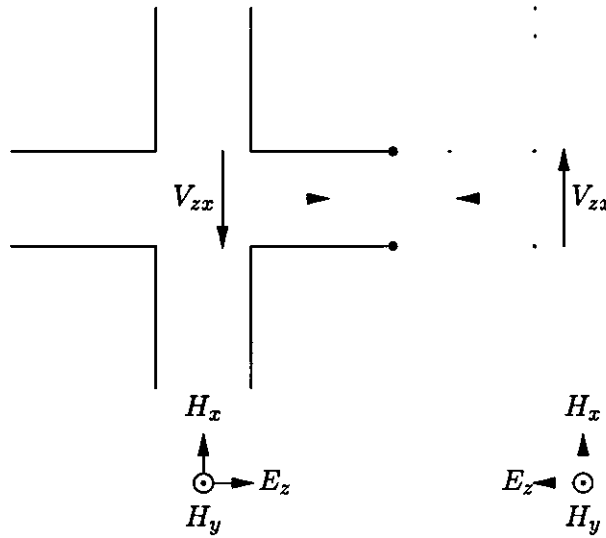
Figure 3 4   Nonzero field components at an electric wall

magnetic field in the x and y directions, electric field symmetry tangential to z is enforced V_{zx} is an arbitrary quantity, chosen to give positive field components. If the two identical nodes shown in the diagram carry the same magnetic field in the y direction, then $_n^r V_{zpx} = -V_{zx}$ and $_n^r V_{znx} = V_{zx}$ After connection, the pulses present on link-lines are

$$_{n+1}^{i} V_{zpx} = V_{zx}$$

$$_{n+1}^{i} V_{znx} = -V_{zx}$$

This implies that the right hand-node could be omitted (and hence the computational domain could be terminated) if a reflection coefficient of $\Gamma_{zpx} = -1$ were applied to the voltage impulse emerging from the left-hand node A similar argument holds for the x-directed magnetic component, yielding $\Gamma_{zpy} = -1$.

By substituting into equation (3.3) and setting $Z_{znx} \to \infty$, it can be shown that the equivalent resistive load is $R = 0$ In other words, an electric wall represents a short-circuited load

Electric walls may also be incorporated into internal boundaries to represent perfect electrically conducting (PEC) objects

3 2 3 Magnetic wall

A plane of magnetic symmetry (known as a *magnetic wall*) may be obtained by following a broadly similar analysis to that of the electric wall. The tangential field components at the boundary in this case are E_x and E_y. If the identical nodes in Figure 3 5 carry the same electric field, then $_n^r V_{zpx} = -V_{zx}$ and $_n^r V_{znx} = -V_{zx}$
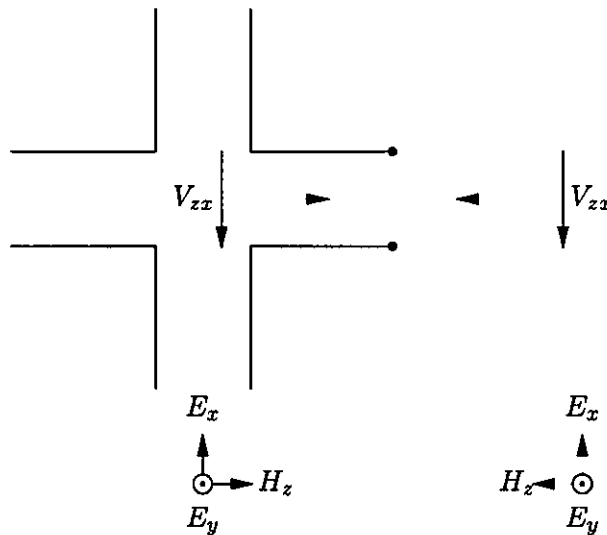
Figure 3 5 Nonzero field components at a wall of magnetic symmetry

After connection, the pulses on link-lines are·

$$_{n+1}^i V_{zpx} = -V_{zx}$$

$$_{n+1}^i V_{znx} = -V_{zx}$$

This implies that the right-hand node could be removed, and the domain truncated, if a reflection coefficient of $\Gamma_{zpx} = +1$ were applied. A similar argument holds for E_y, giving $\Gamma_{zpy} = +1$

Substituting into equation (3 3) and setting $Z_{znx} \to \infty$, the equivalent resistive load is $R = \infty$ In other words, a magnetic wall represents an open-circuited load.

3.2 4 Wrap-around symmetry

Another type of symmetry condition can be enforced by *wrapping* pulses (i e. exchanging pulses between opposite boundaries) during connection [3 3]. The operation can be expressed alge-

braically by

$$_{n+1}^{i}V_{zpx} = {_n^r}V_{znx}$$

$$_{n+1}^{i}V_{znx} = {_n^r}V_{zpx}$$

Similar equations apply to the y-polarised ports.

Because the voltage impulses must be identical to maintain symmetry, this type of boundary is only appropriate for a one-node thick slice of mesh It can be seen by examining Figure 3 6 and carrying out a similar analysis to the electric and magnetic walls, that both types of symmetry are enforced automatically.
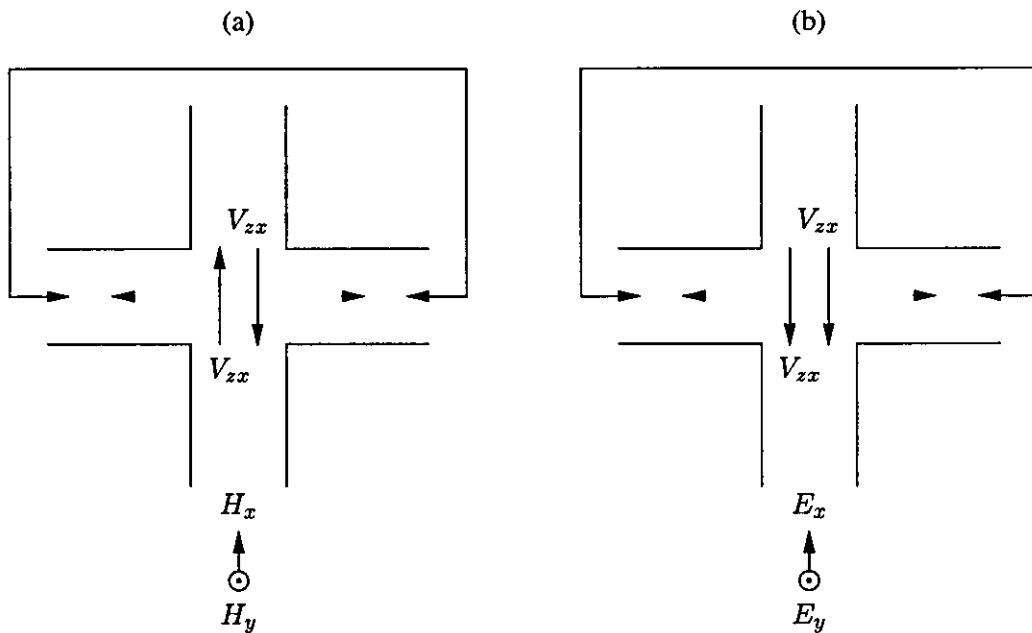
Figure 3 6. Wrapped-around boundaries operating as (a) an electric wall and (b) a magnetic wall

Wrapped around boundaries of this type are often used for convenience, to avoid the programmer having to decide which sort of symmetry wall to use

3 2 5   Absorbing wall

If field absorption is required at the boundary, a number of methods are possible   One approach, known widely as the *matched termination*, assumes an infinitely long transmission line is connected to each of the outermost nodes of the mesh. Each line is chosen to have electrical parameters which are equivalent to the physical parameters of the infinite space surrounding the

problem The TLM parameters of a z-directed line in x-polarisation are (see Section 2.3 4 for details)

$$C_x = \epsilon_0 \epsilon_{rx} \frac{\Delta y \Delta z}{\Delta x}$$

and,

$$L_y = \mu_0 \mu_{ry} \frac{\Delta x \Delta z}{\Delta y}$$

The characteristic impedance of the link-line is therefore:

$$Z_{znx} = \sqrt{\frac{L_y}{C_x}} = \sqrt{\frac{\mu_0 \mu_{ry} \Delta x \Delta z}{\Delta y} \cdot \frac{\Delta x}{\epsilon_0 \epsilon_{rx} \Delta z \Delta y}} = Z_0 \sqrt{\frac{\mu_{ry}}{\epsilon_{rx}}} \frac{\Delta x}{\Delta y} \qquad (3\ 8)$$

By substituting this value and allowing $R \to \infty$ in equation (3 3), the voltage reflection coefficient, Γ_{zpx}, may be evaluated:

$$\Gamma_{zpx} = \frac{Z_0 \sqrt{\frac{\mu_{ry}}{\epsilon_{rx}}} \frac{\Delta x}{\Delta y} - Z_{zpx}}{Z_0 \sqrt{\frac{\mu_{ry}}{\epsilon_{rx}}} \frac{\Delta x}{\Delta y} + Z_{zpx}} \qquad (3\ 9)$$

The reflection coefficient with R present, and with $Z_{znx} \to \infty$ may also be written

$$\Gamma_{zpx} = \frac{2}{\frac{Z_{zpx}}{R} + 1} - 1$$

Equating the two expressions for reflection coefficient the terminating resistance may be derived

$$R_{MT} = Z_0 \sqrt{\frac{\mu_{ry}}{\epsilon_{rx}}} \frac{\Delta x}{\Delta y}$$

In general the equivalent resistance required for a TLM node on the mesh boundary with dimensions, Δi, Δj, Δk on the i-oriented link-line and j-polarisation is

$$R_{MT} = Z_0 \sqrt{\frac{\mu_{rk}}{\epsilon_{rj}}} \frac{\Delta j}{\Delta k} \qquad (3\ 10)$$

The corresponding TLM reflection coefficient is·

$$\Gamma_{ij} = \frac{R_{MT} - Z_{ij}}{R_{MT} + Z_{ij}} \qquad (3\ 11)$$

Evaluation

A simple simulation was performed with a $101 \times 101 \times 1$ node mesh The z-boundaries were connected using a wrapped-around boundary, and the node at $(50, 50, 0)$ was excited with a field of $\mathbf{E} = \exp(-\frac{n^2}{2 \times 10^2})\hat{z}$

$$50\Delta t \qquad\qquad 100\Delta t$$

$$150\Delta t \qquad\qquad 200\Delta t$$

-30 -27 -24 -21 -18 -15 -12 -9 -6 -3 0 $|\mathbf{E}|$ (dB)
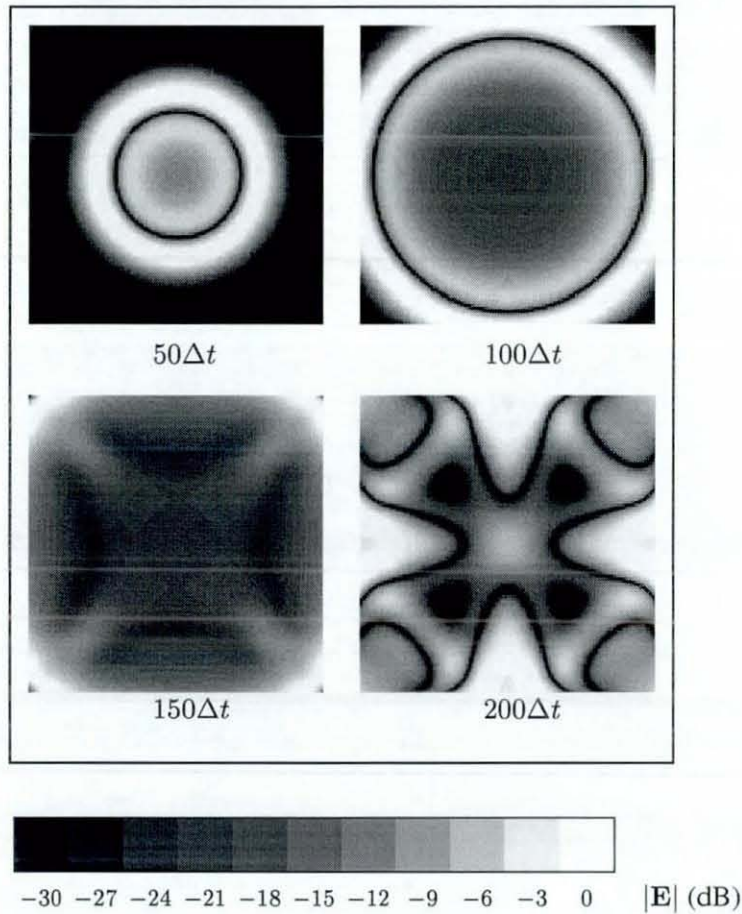
Figure 3.7: Normalised electric field distribution for matched termination boundaries

The evolution of the wavefront was examined at each time step and the plots normalised. The results shown in Figure 3.7 demonstrate that the wavefront is significantly distorted in its transition from the problem boundary. At near normal incidence the reflections are minimal, however as the wave incident angle moves away from the normal significant reflections occur. The reason for this behaviour is that the boundary is only matched where all the incident field components are tangential.

In practice, this means that there are considerable restrictions on how close the boundary may be placed to objects. If, for example, the radiation pattern of an antenna is the subject of study, sufficient distance must be provided between the conductors in the antenna and the boundary. This distance may be appreciable, and thus large numbers of cells may be required around objects simply to allow for limitations in the mesh termination method.

Despite their clear disadvantages, matched boundaries are employed widely in commercial

TLM simulators. This is because they are easy to apply, and are fundamentally stable in operation. More sophisticated absorbing boundaries are the subject of Chapter 4.

3.3 Non-ideal conducting boundaries

In many situations, it is inappropriate to assume that conducting objects are made of PEC material. Real conductors exhibit frequency dependent, lossy properties. They also allow penetration of fields. Accurately modelling these effects can be computationally expensive, and so usually approximations must be made to avoid long run times. However, modelling losses in boundaries can be advantageous because the fields will decay more quickly, reducing the number of time steps required.

3 3.1 Conducting boundaries

Lossy internal and external conducting walls can be thought of as combining the properties of electric and absorbing walls. If the absorbing wall is chosen as a starting point, the conductive properties may be inserted by substituting a lossy term into the equation for the line impedance

The conductance required in a z-directed line in x-polarisation is:

$$G_x = \sigma_{ex} \frac{\Delta y \Delta z}{\Delta x}$$

The impedance of the infinite link-line which models the conducting medium is therefore

$$Z_{znx} = \sqrt{\frac{j\omega L_y}{j\omega C_x + G_x}} = \frac{\Delta x}{\Delta y} \sqrt{\frac{j\omega \mu_0 \mu_{ry}}{j\omega \epsilon_0 \epsilon_{rx} + \sigma_{ex}}}$$

Frequency domain expressions such as this cannot be directly handled by time domain numerical methods This problem has been overcome by Cacoveanu *et al* by applying a recursive algorithm to model the frequency dependent nature [3 4].

If narrow-band results are acceptable it is possible to approximate the medium impedance For example, if the 'good conductor' approximation is applied (i e. $\omega\epsilon \ll \sigma$) then·

$$Z_{znx} \simeq \frac{\Delta x}{\Delta y} \sqrt{\frac{j\omega \mu_0 \mu_{ry}}{\sigma_{ex}}}$$

After substitution into equation (3 11) with $R \rightarrow \infty$ and algebraic manipulation (including the use of the identity $\sqrt{j} = \frac{(1+j)}{\sqrt{2}}$) an approximate TLM reflection coefficient may be obtained

$$\Gamma_{zx} \simeq -1 + \frac{\Delta x}{Z_{zx}\Delta y}\sqrt{\frac{2\omega\mu_0\mu_{ry}}{\sigma_{ex}}} \qquad (3\ 12)$$

This expression is consistent with that derived by Hoefer for 2-D TLM [3 1]

Alternatively the skin depth, δ, may be quoted, in which case the TLM reflection coefficient to be applied is

$$\Gamma_{zx} \simeq -1 + \frac{\Delta x}{Z_{zx}\Delta y}\omega\mu_0\mu_{ry}\delta \qquad (3\ 13)$$

Thin internal conducting boundaries with field penetration can modelled using the circuit shown at the start of this chapter, however much more accurate methods have been devised [2.39, 2 41] These methods are particularly important in EMC simulations where the coupling of fields into enclosures is of interest

3 3 2 Applying physical reflection coefficients

In some circumstances the physical reflection coefficient is a known quantity. It is in general necessary to convert this into a TLM voltage reflection coefficient

From basic circuit theory, it can be shown that the resistive load required to terminate a transmission line is related to the real reflection coefficient, ρ, and the matching resistance R_{MT} by.

$$R_\rho = R_{MT}\left(\frac{1+\rho}{1-\rho}\right) \qquad (3\ 14)$$

If this equation is rearranged and substituted into equation (3 11), the corresponding TLM reflection coefficient may be evaluated:

$$\Gamma_{ij} = \frac{R_p(1-\rho) - Z_{ij}(1+\rho)}{R_p(1-\rho) + Z_{ij}(1+\rho)} \qquad (3\ 15)$$

3 3 3 Discussion

Conducting boundaries are an important feature in models of EMC problems   In the most basic form they may be efficiently included into problems by applying the concept of surface

impedance or skin depth. However, to model the penetration effects of fields much more so-phisticated models are required, which may impact on the computational overhead   In most production road vehicles, the materials used for bodywork (often ferrous metals such as steel) are good conductors and the penetration effects are minimal   In this case, applying conduc-tor models in their most basic form should in most cases be acceptable Increasingly, however, lighter composite materials such as CFC (carbon fibre composite) are being used These materi-als are poorer conductors, and field penetration is appreciable. This has important consequences for both the computer model, and the EM properties of the vehicle.

3 4   A compact partial Huygens' surface for TLM simulations

In a number of circumstances, it is desirable to illuminate scattering objects with ideal plane waves. Examples of where this might be necessary are

- Where incident waves in the physical system have reached far field conditions before striking the scatterer

- Where the simulation results are to be compared with analytical solutions, which often assume ideal plane-wave illumination.

Unfortunately, illuminating the TLM mesh across the entire cross-section in free space scatter-ing problems does not normally produce perfect plane waves The reason lies in the boundary implementation, which typically in a scattering problem will be an absorbing boundary such as the matched condition discussed earlier. The source is physically truncated at the mesh bound-ary, and thus appears finite in extent In addition, although to a lesser extent, sources in the near vicinity of the mesh boundary can cause other errors which are related to the ABC performance

3 4 1   Theory

In order to provide an absorbing boundary to the scattered field, and to maintain an infinite source, a special type of boundary known as a *Huygens' surface* may be used.

Huygens' surfaces were first employed in the FDTD method by Merewether and Fisher in order to simplify the analysis of dielectric and poorly conducting scatterers [3 5] The formulation

is based on the equivalence principle, which may be demonstrated by considering the two situations shown in Figures 3 8(a) and 3.8(b). In case (a) the external sources radiate from the
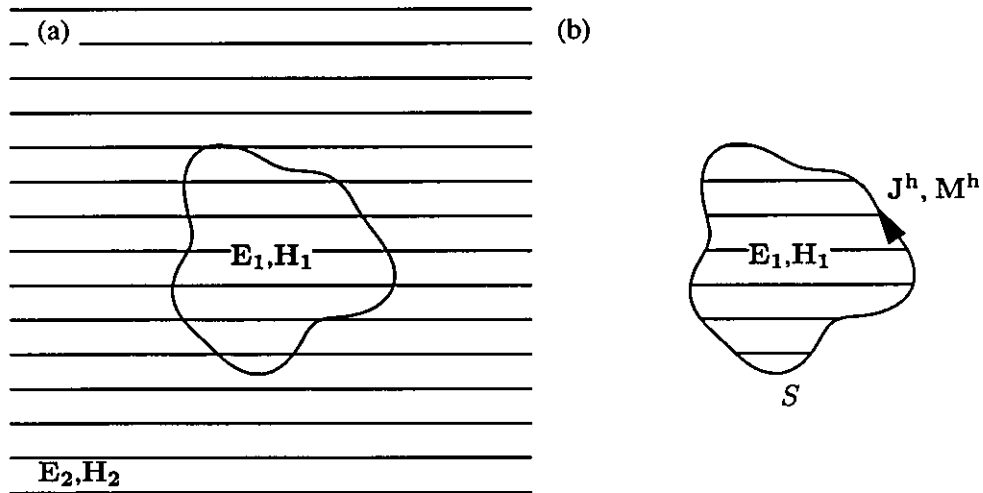
Figure 3 8 Generation of equivalent current sources

external region (2) to the internal region (1) passing through an artificial surface S The surface currents flowing on S may be quantified

$$(E_1 - E_2) \times \hat{n} = M^s = 0$$
$$\hat{n} \times (H_1 - H_2) = J^s = 0$$

If $E_2 = 0$, $H_2 = 0$ and equivalent Huygens' source magnetic and electric currents are introduced at the interface as shown in Figure 3 8(b), then the fields inside the bounded region will replicate those in the original problem providing

$$M^h = E^h \times \hat{n} \qquad (3\ 16)$$

$$J^h = \hat{n} \times H^h \qquad (3\ 17)$$

The new problem is bounded if the correct Huygens' currents can be obtained, and is therefore more easily analysed by numerical methods

The excitation of plane waves is amenable to this technique since the external fields are easily determined. Chen *et al.* [3 6] and German [3.7] have successfully used analytical expressions to generate the Huygens' currents. Another approach employing TLM reflection coefficients has been described by Porter and Dawson [3 8, 3.9]. The technique described here is akin to the Porter and Dawson method, but has some distinct advantages

3.4.2 Implementation

The TLM mesh is split into two regions· the problem space, which is surrounded by an absorbing boundary, and an auxiliary region which has a symmetry boundary Symmetry in the latter region is achieved by 'wrapping round' pulses in the manner described in Section 3.2 4

This process ensures that undistorted plane waves can propagate in the auxiliary region regardless of polarisation Ideal plane wave propagation is obtained by exciting the TLM mesh across the entire cross-section and feeding pulses from the auxiliary region into the problem space The edges of a propagating wavefront are consequently reinforced, and thus the excitation appears infinite in extent The voltage reflection coefficients which need to be applied at the boundaries are shown in Figure 3.9

The reflection and transmission processes required by the technique are handled in the connect phase of the TLM algorithm i e.:

$$_{n+1}^{i}V_{ipj}^{p} = \Gamma_{ij} \, _{n}^{r}V_{ipj}^{p} + (1 - \Gamma_{ij}) \, _{n}^{r}V_{inj}^{a}$$

$$_{n+1}^{i}V_{inj}^{p} = \Gamma_{ij} \, _{n}^{r}V_{inj}^{p} + (1 - \Gamma_{ij}) \, _{n}^{r}V_{ipj}^{a}$$

$$(3.18)$$

$$_{n+1}^{i}V_{ipk}^{p} = \Gamma_{ik} \, _{n}^{r}V_{ipk}^{p} + (1 + \Gamma_{ik}) \, _{n}^{r}V_{ink}^{a}$$

$$_{n+1}^{i}V_{ink}^{p} = \Gamma_{ik} \, _{n}^{r}V_{ink}^{p} + (1 + \Gamma_{ik}) \, _{n}^{r}V_{ipk}^{a}$$

for ports on the extremities of the problem space, and:

$$_{n+1}^{i}V_{ipj}^{a} = _{n}^{r}V_{inj}^{a}$$

$$_{n+1}^{i}V_{inj}^{a} = _{n}^{r}V_{ipj}^{a}$$

$$(3\ 19)$$

$$_{n+1}^{i}V_{ipk}^{a} = _{n}^{r}V_{ink}^{a}$$

$$_{n+1}^{i}V_{ink}^{a} = _{n}^{r}V_{ipk}^{a}$$

for ports on the periphery of the auxiliary region. Superscript a denotes port voltages in the auxiliary region, superscript p denotes port voltages at the edge of the problem space, and Γ_{ij}, Γ_{ik} are reflection coefficients for the matched condition, given in equation (3.11).

Figure 3 9 Reflection/transmission processes applied to form a partial Huygens' surface

3 4 3 Analytical verification

If the problem is set up as shown in Figure 3 10, then the equivalent Huygens' currents on surface S for a plane wave with instantaneous magnitude of $\mathbf{E} = E_x \hat{x} + E_y \hat{y}$, and $\mathbf{H} = H_x \hat{x} + H_y \hat{y}$ can be obtained from equations (3 16) and (3.17)

On the artificial surface only three faces (labelled A, B, C) require consideration, the others follow through symmetry.

Figure 3 10· Plane wave incident on artificial surface S

Face A

$$\mathbf{M^h} = \mathbf{E} \times \hat{n}_A = E_y \hat{z} - E_x \hat{y}$$
$$\mathbf{J^h} = \hat{n}_A \times \mathbf{H} = -H_y \hat{z} + H_x \hat{y} \qquad (3\ 20)$$

Face B

$$\mathbf{M^h} = \mathbf{E} \times \hat{n}_B = E_y \hat{z}$$
$$\mathbf{J^h} = \hat{n}_B \times \mathbf{H} = -H_y \hat{z} \qquad (3\ 21)$$

Face C

$$\mathbf{M^h} = \mathbf{E} \times \hat{n}_C = -E_x \hat{z}$$
$$\mathbf{J^h} = \hat{n}_C \times \mathbf{H} = H_x \hat{z} \qquad (3\ 22)$$

It should be noted that these currents are for the special case where the plane wave is propagating in a direction normal to face A. A full implementation of a Huygens' surface would impose no such restriction [3.7]

3 4 4   Equivalent currents in the TLM model

In order to verify that the correct currents are produced by the reflection/transmission processes, the fields at the boundary are required. For the case where the boundary intersects a pair of transmission lines of equal characteristic impedance Z_{ij}, equations (3 5) and (3.7) may be simplified to give·

$$E_j = -\frac{V_{ipj} + V_{inj}}{\Delta j} \qquad (3\ 23)$$

$$H_k = \frac{V_{inj} - V_{ipj}}{Z_{ij}\Delta k} \qquad (3\ 24)$$

These equations will be used in the following analysis

Face A

No special reflection coefficients need be applied, and so the scattered voltages, V_x and V_y, (shown in Figure 3.11)
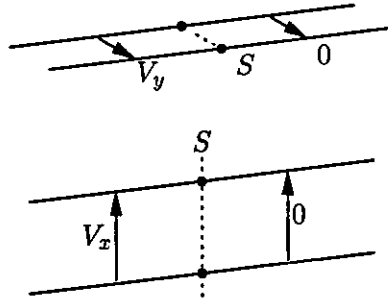
Figure 3 11· Voltages at face A after scattering

are simply exchanged during connection. The field vectors obtained from equations (3 23) and (3 24) are.

$$\begin{aligned}
\mathbf{E} &= -\frac{V_x}{\Delta x}\hat{x} - \frac{V_y}{\Delta y}\hat{y} \\
\mathbf{H} &= \frac{V_y}{Z_{zy}\Delta y}\hat{x} + \frac{V_x}{Z_{zx}\Delta y}\hat{y}
\end{aligned}$$

producing magnetic and electric current densities of:

$$\mathbf{M^h} = -\frac{V_y}{\Delta y}\hat{x} + \frac{V_x}{\Delta x}\hat{y}$$

$$\mathbf{J^h} = -\frac{V_x}{Z_{zx}\Delta x}\hat{x} + \frac{V_y}{Z_{zy}\Delta x}\hat{y} \qquad (3\,25)$$

Face B

A similar process is followed for B, however, this time the reflection/transmission coefficients are applied in the manner described. Note that for this face V_{xz} models H_y and to produce positive-directed current after connection, the outer port voltage is chosen as negative (Figure 3.12).
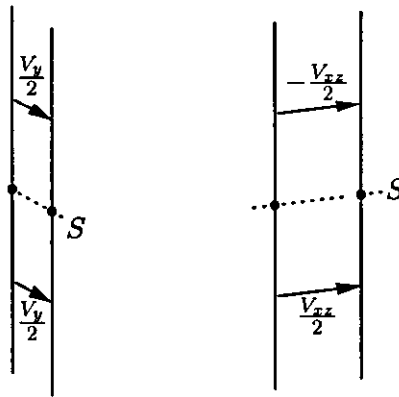
Figure 3 12 Voltages at face B after scattering

Therefore

$$
\begin{aligned}
\mathbf{E} &= -\frac{1}{\Delta y}\left[\left(\Gamma\frac{V_y}{2} + (1-\Gamma)\frac{V_y}{2}\right) + \frac{V_y}{2}\right]\hat{y} \\
&= -\frac{V_y}{\Delta y}\hat{y} \\
\mathbf{H} &= \frac{1}{Z_{xz}\Delta y}\left[\frac{V_{xz}}{2} - \left(\Gamma\frac{V_{xz}}{2} - (1+\Gamma)\frac{V_{xz}}{2}\right)\right]\hat{y} \\
&= \frac{V_{xz}}{Z_{xz}\Delta y}\hat{y}
\end{aligned}
$$

giving equivalent current densities of:

$$
\begin{aligned}
\mathbf{M^h} &= -\frac{V_y}{\Delta y}\hat{z} \\
\mathbf{J^h} &= -\frac{V_{xz}}{Z_{xz}\Delta y}\hat{z} \qquad (3.26)
\end{aligned}
$$
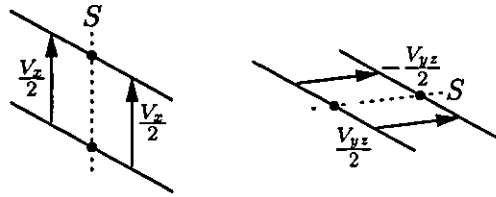
Face C

Figure 3 13. Voltages at face C after scattering

By applying similar analysis to that described for B the fields are.

$$\mathbf{E} = -\frac{V_x}{\Delta x}\hat{x}$$

$$\mathbf{H} = -\frac{V_{yz}}{Z_{yz}\Delta x}\hat{x}$$

giving currents

$$\mathbf{M}^h = \frac{V_x}{\Delta x}\hat{z}$$

$$\mathbf{J}^h = \frac{V_{yz}}{Z_{yz}\Delta x}\hat{z} \qquad (3\ 27)$$

These equivalent currents are consistent with those previously derived (equations (3 20)–(3 22)) and therefore applying the reflection/transmission coefficients in equations (3.18) and (3 19) produces a Huygens' surface. In addition, it is fairly straightforward to show that in the absence of auxiliary region field components, scattered fields meet a reflection coefficient of Γ_{ij}, Γ_{ik} and hence a matched condition exists.

3.5 Plane-wave test results

In order to validate the partial Huygens' surface, a number of simulations were carried out. Tests were chosen to investigate the basic operation, and also to validate the method in more complex cases involving features such as grading.

3.5 1 Free space

Linearly polarised waves were generated by exciting fields in a plane parallel to and near to the z-minimum boundary of a TLM mesh

A relatively small mesh containing $10 \times 10 \times 30$ nodes was employed, and matched termination boundaries were introduced Excitation was provided by a unit magnitude Gaussian pulse injected into both E_x and E_y component directions, giving a field of strength $\sqrt{2}$ Vm^{-1} polarised at $45°$ The time domain field was measured at a point $(4, 2, 28)$ and the output was plotted (Figure 3.14)

This result was compared with the output of a similar simulation, but this time introducing the auxiliary regions to the x- and y-boundaries and applying the reflection/transmission coefficients described in equations (3.18) and (3.19) (see Figure 3.15).

Results

The graphs show that the E_x and E_y fields components are attenuated significantly in the matched case, and also a z-component is present These anomalies are eliminated entirely by applying the Huygens' surface This test was repeated for meshes with different grading and similar results were found.

E

(Vm^{-1})
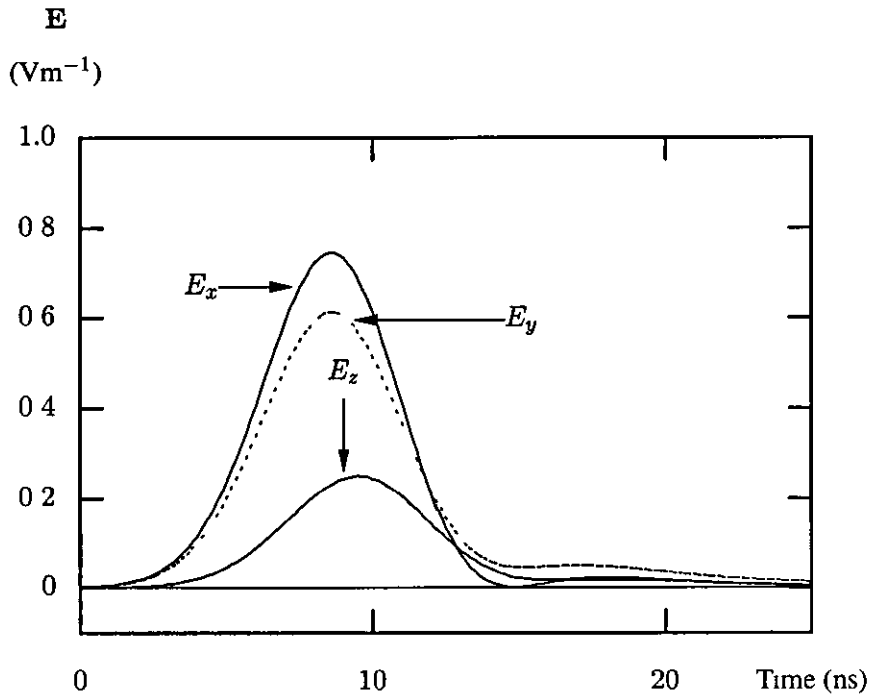
Figure 3 14 Electric field near to a matched termination wall

E

(Vm^{-1})
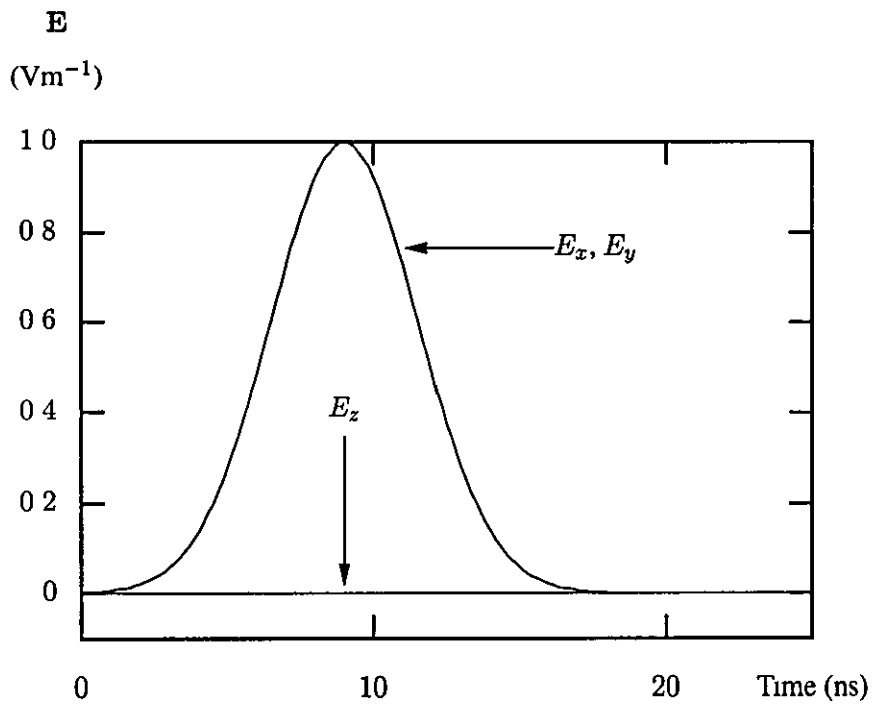
Figure 3 15· Electric field near to a partial Huygens' surface

As a further test an elliptically polarised plane wave of $\mathbf{E} = 2 \sin(2\pi 10^8 t)\hat{x} + \cos(2\pi 10^8 t)\hat{y}$ was generated in the same mesh As demonstrated in Figure 3 16, the wave propagates in the desired manner.
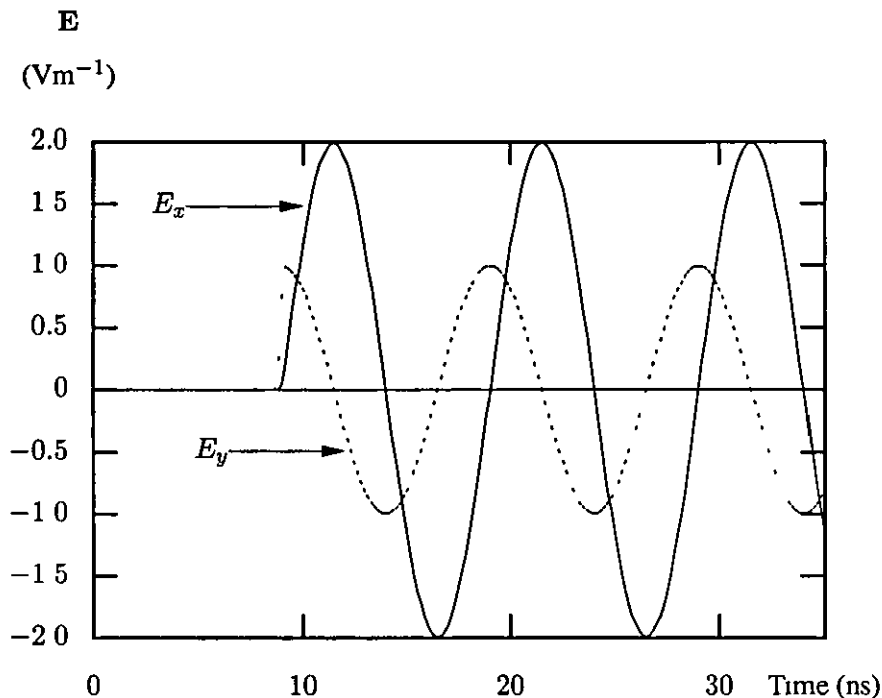
Figure 3 16 Electric field with elliptically polarised excitation at $z = 0$

3 5 2   Sinusoidal grating

Sinusoidal gratings are sometimes found embedded in vehicle windscreens in the form of very fine metallised wires These wires are intended to act as heaters for demisting, but they also exhibit interesting properties at RF, including a strong polarising effect

Two test objects were modelled in an attempt to examine the properties of this type of device The first was a simple model using conducting nodes (see Figure 3 17(a)). The second was more advanced and used thin conductors on a glass substrate (see Figure 3 17(b))

Each object was enclosed in a $100 \times 100 \times 100$ node TLM mesh Object (a) was modelled on a cubic mesh, and object (b) was modelled on a graded mesh in order to efficiently and accurately incorporate the dielectric material ($\epsilon_{r,glass} = 6$).

(a)

■ = conducting node

(b)

306 × 245 × 2 mm
$\epsilon_r = 6\,0$

thin PEC
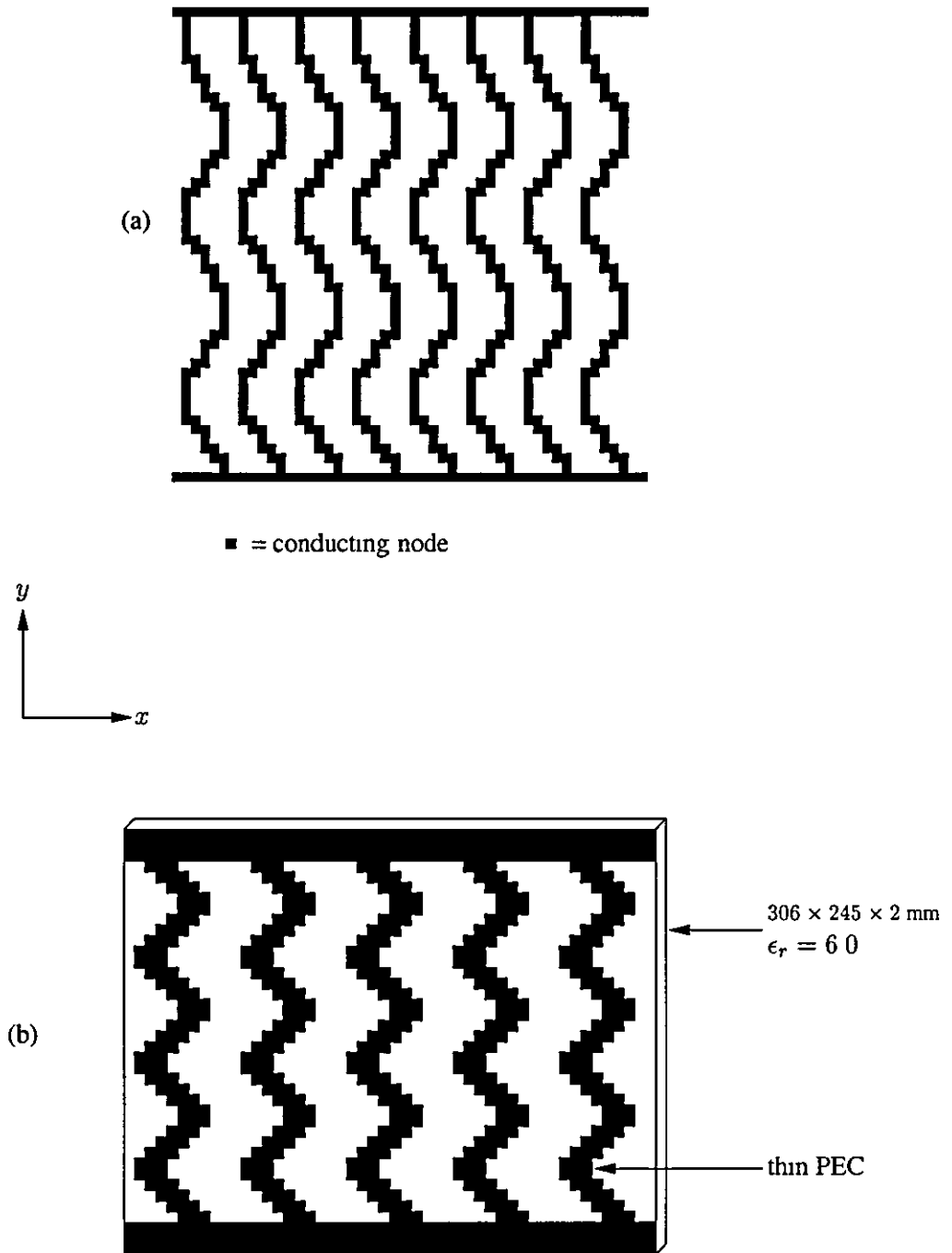
Figure 3 17 Sinusoidal grating test objects with $\Delta x = \Delta y \approx 6$ mm and $\Delta z \approx 2$ mm

Measurement points were placed at suitable positions in front of each object in order to observe the incident and reflected waves. Once again, results were generated for matched termination boundaries to act as a comparison. Model (b) required many more time steps to complete than (a) since the maximum time step for the model was reduced significantly by the inclusion of dielectric material. Excitation was provided at 45° in an identical manner to the free space tests

Results

The results for object (a) demonstrate the polarising effect. For the x-polarisation (Figure 3 18) very little of the incident wave is reflected, whereas approximately 80% of the y-polarised field is reflected (Figure 3 19). This result is masked by anomalies in the matched termination simulations.

The results for object (b) (Figure 3.20) demonstrate that partial Huygens' surfaces can be used with equal success in graded meshes.

E_x

(Vm^{-1})
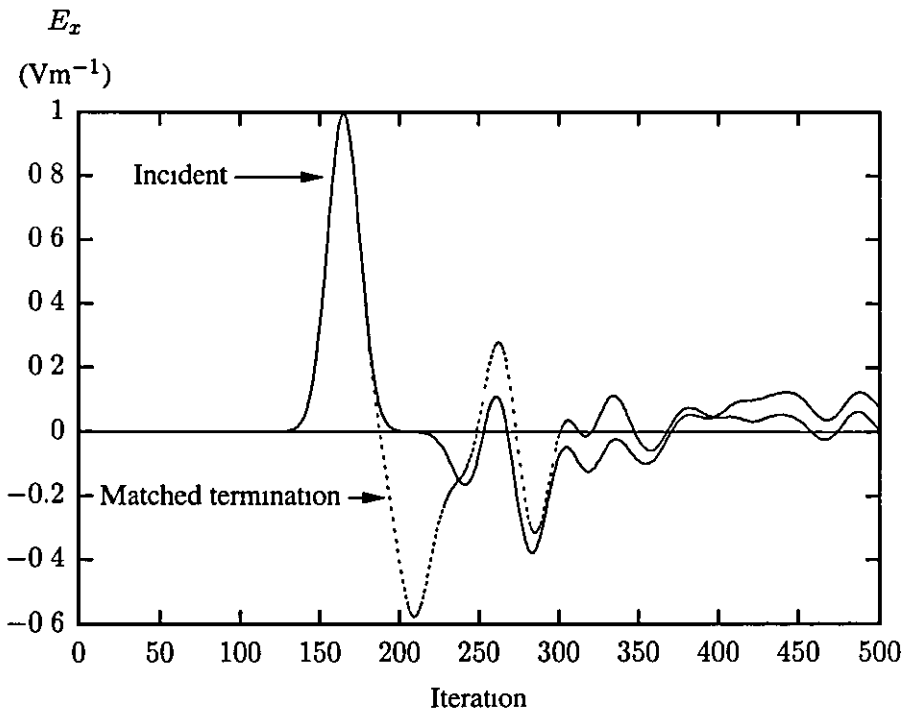
Figure 3 18 x-component of the electric field in front of object (a)

E_y

(Vm^{-1})
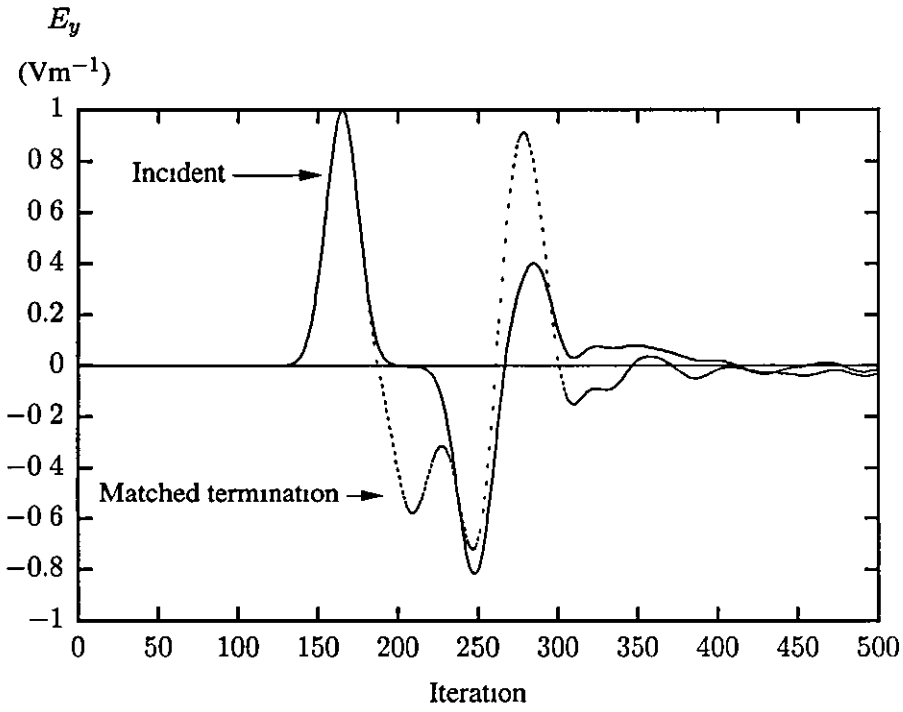
Figure 3 19. y-component of the electric field in front of object (a)

E_x

(Vm^{-1})
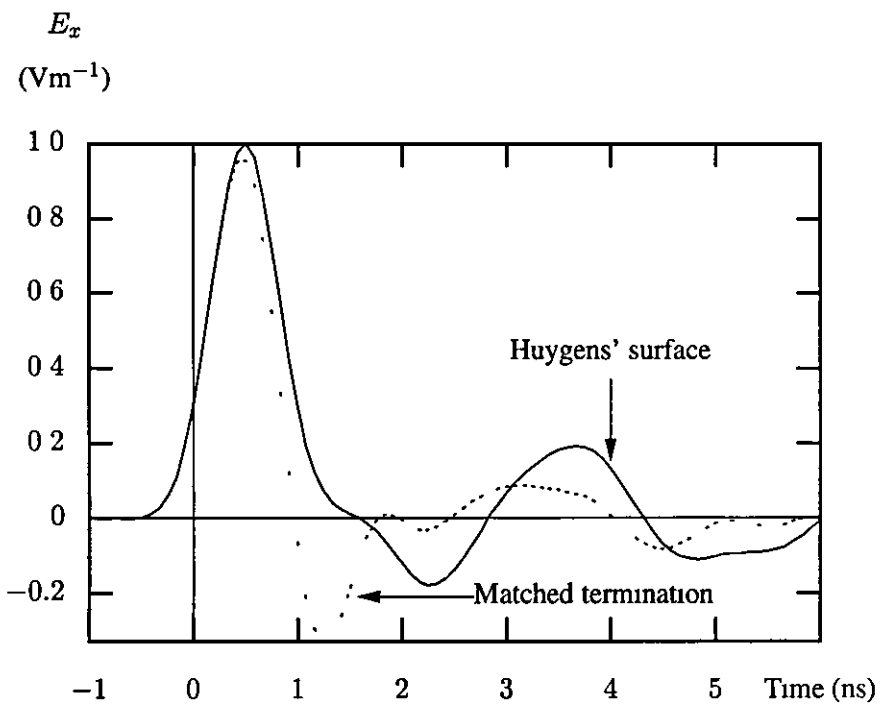
Figure 3 20 x-component of the electric field in front of object (b)

3 5 3   Vehicle body

A CAD model of a car body was prepared in a commercial CAD software package, and a *grid* or *tartan mesh* was applied to the surface. The resulting data (see Figure 3.21) was used in the TLM model and all surfaces were modelled as PEC Plane wave excitation was once again
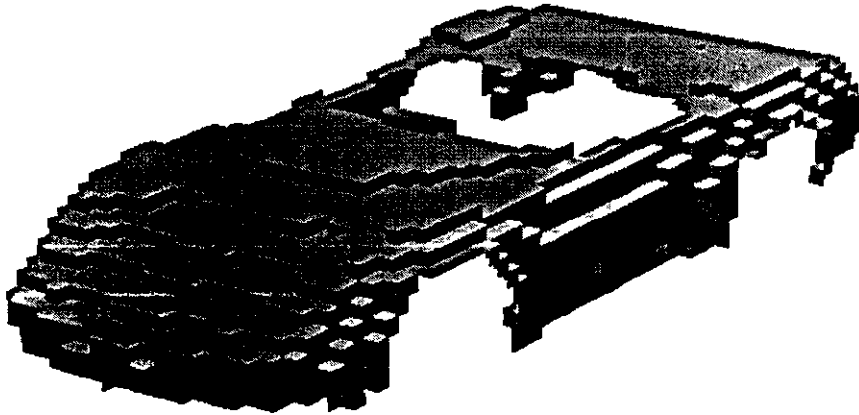
Figure 3 21 Vehicle body test object

applied at 45°, and the result from using matched termination boundaries and partial Huygens' surfaces were compared The electric field intensity was plotted as a grey scale pixel map, and was captured as a series of time snapshots

Results

Figure 3 22 shows that the field intensities for the partial Huygens' surface are considerably improved over the matched termination case. This demonstrates that the technique can be used to improve results for full-field visual data as well as that obtained from individual measuring points
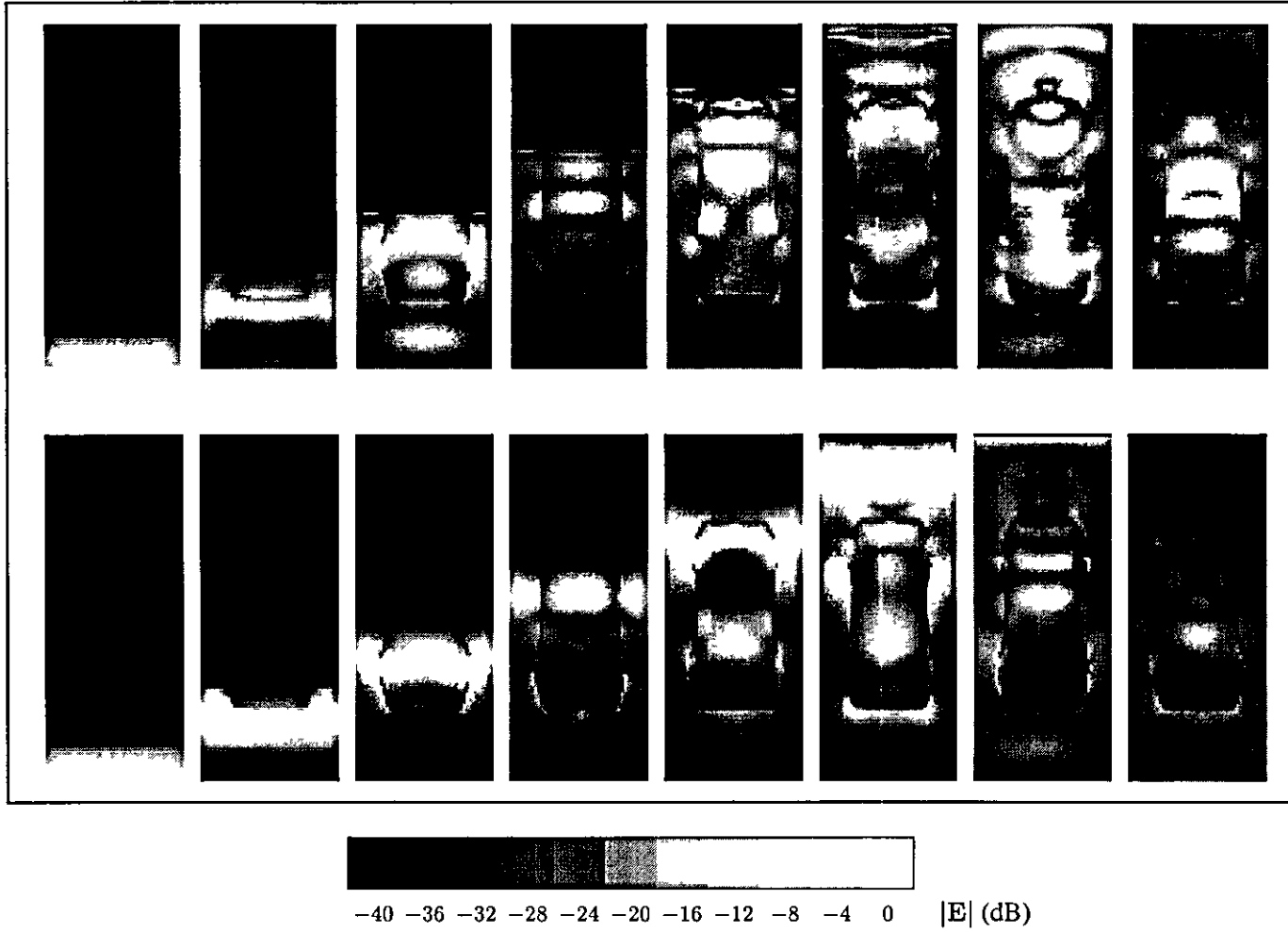
Figure 3 22 Whole-vehicle plane-wave illumination for (top) matched termination boundaries and (bottom) partial Huygens' surface
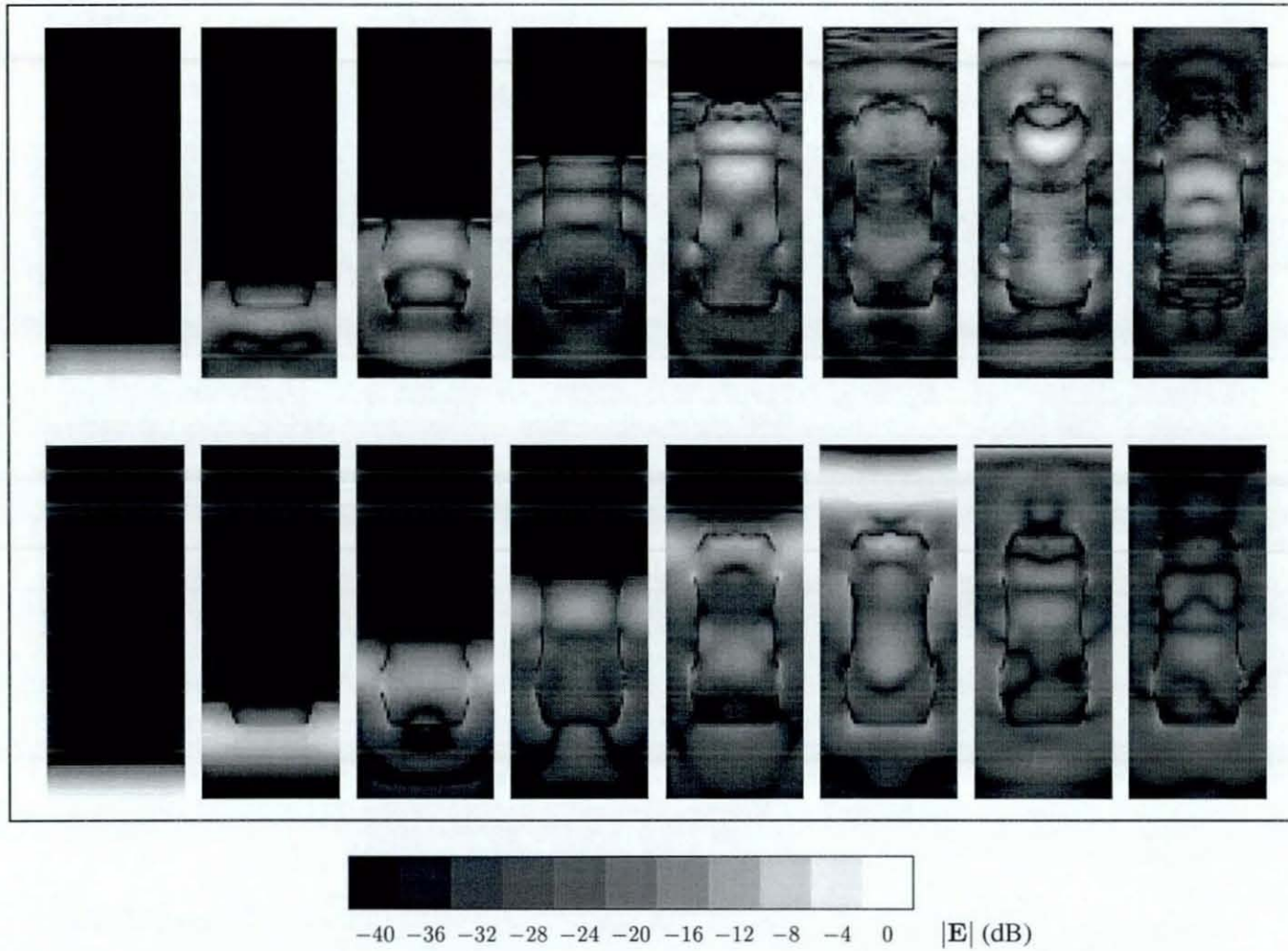
Figure 3.22: Whole-vehicle plane-wave illumination for (top) matched termination boundaries and (bottom) partial Huygens' surface

3 5 4   Discussion

The method described is easy to implement in a TLM program It has been tested in a variety of situations with success, and appears to perform equivalently to the method described by Porter and Dawson [3 8, 3 9]. The advantages over this technique are:

- The boundary is polarisation independent, i e. reflection coefficients need not be altered for different polarisations.

- Only one auxiliary region is required per pair of boundaries (however it is relatively straightforward to modify the earlier method to use only one region instead of two)

The method is limited by its use of link line reflection coefficients, and its use is restricted to situations where illumination is provided parallel to the mesh axes. In some circumstances, this may prove problematic, especially for the computation of radar cross-section where a wide variety of illumination angles are required A full Huygens' surface has been demonstrated by German [3.7] for this purpose, however, this technique does not automatically account for the effects of dispersion. It is therefore preferable where the excitation is parallel to the mesh axes to use a method which does automatically account for dispersion such as the one described here

Extensive tests have shown that the method is stable regardless of the mesh grading in use, and even when the effects of dispersion are appreciable.

3.6   Conclusion

Symmetry conditions are available in TLM which can be used to reduce the computational overhead dramatically Lossy electric walls may be used to represent the surface impedance of highly conducting materials. Electric and magnetic walls are the most commonly used symmetry conditions So-called 'wrap-around' boundary conditions are only appropriate for reducing the total number of dimensions in a problem As an example, it might be used for terminating the z-boundaries of a $10 \times 10 \times 1$ node TLM mesh of SCNs

Absorbing boundaries based purely on 1-D implementations perform relatively poorly, and can only be relied upon to provide an accurate representation of free space where the wave incident angle on the boundary is a fixed and known quantity

The matched termination boundary has been successfully combined with the 'wrap-around' symmetry condition to provide a new method of plane-wave excitation in the TLM mesh Effectively, the symmetry condition is applied to the propagating wavefront, whilst a matched condition is presented to scattered waves.

Generally, boundaries derived from one-dimensional assumptions are easily formulated and applied They are also efficient and stable in their operation. The main disadvantage is that where a true 3-D phenomenon requires modelling, such as an absorbing boundary, the effectiveness is severely limited.

References

[3 1] W J. R Hoefer, "The transmission-line matrix method— theory and applications," *IEEE Trans Microw. Theory Tech* , vol. 33, no. 10, pp. 882–893, 1985.

[3 2] A Centeno, "Modified conducting boundaries in symmetrical condensed node (SCN) transmission line matrix (TLM) modelling," *Electron. Lett* , vol 35, no 10, pp 802–803, 1999

[3 3] Kimberley Communications Consultants, *Micro-Stripes V3 0 2 Manual.* 1997.

[3.4] R. Cacoveanu, P. Saguet, S. Ciochina, and D Homentcovschi, "Recursive method for modelling metallic boundaries using TLM method," *Electron Lett* , vol 31, no 15, pp 1266–1267, 1995

[3 5] D E. Merewether, R. Fisher, and F W. Smith, "On implementing a numeric Huygen's source scheme in a finite difference program to illuminate scattering bodies," *IEEE Trans Nuclear Science*, vol. 27, no. 6, pp. 1829–1833, 1980.

[3 6] Z Chen, M. M. Ney, and W. J. R. Hoefer, "Absorbing and connecting boundary conditions for the TLM method," *IEEE Trans Microw Theory Tech.*, vol 41, no 11, pp 2016–2024, 1993

[3.7] F. J. German, "General electromagnetic scattering analysis by TLM method," *Electron Lett.*, vol. 30, no. 9, pp. 689–690, 1994.

[3 8] S J. Porter and J. F. Dawson, "Improved plane-wave illumination for TLM method," *Electron Lett.*, vol. 29, no 18, pp 1663–1664, 1993.

[3.9] J. F. Dawson and S J Porter, "Plane-wave illumination for the TLM method using a partial Huygen's surface," in *Proc 9th Int. Conf. EMC*, (Manchester, UK), pp 246–250, 5–7 September 1994.

CHAPTER 4:
HIGH-PERFORMANCE ABSORBING BOUNDARIES

A S the upper frequency of interest increases, performing whole chamber simulations becomes impractical In order to restrict the amount of computer memory used it becomes essential to truncate the domain of the problem with an artificial absorbing boundary condition (ABC). The better the performance of the ABC, the closer the boundary may be placed to the vehicle in the model and the fewer the number of cells which are required Thus, ABCs have an essential role to play in the efficiency of high frequency models of electrically large objects

This chapter focuses on the performance and practicality of high-performance ABC schemes in EM models of vehicles.

4.1   Properties of absorbing boundary conditions

The purpose of applying absorbing (or *radiating*) boundary conditions is to truncate the computational domain without introducing non-physical reflections or, put in other terms, to emulate the effects of an infinite TLM mesh. As was shown in Subsection 3 2 5 (p 53ff), applying a simple matched condition meets this specification only for waves striking the boundary at a single, fixed angle.

Desirable properties for a high-performance absorbing boundary are·

- Low magnitude wave reflection coefficient

- The ability to absorb incident waves from a variety of angles

- Frequency-independent wave reflection coefficient.

- Efficient use of memory and simple computation.

- High stability

$$ (x, y, z_{max} - 2) \quad (x, y, z_{max} - 1) \quad (x, y, z_{max}) $$

ABC
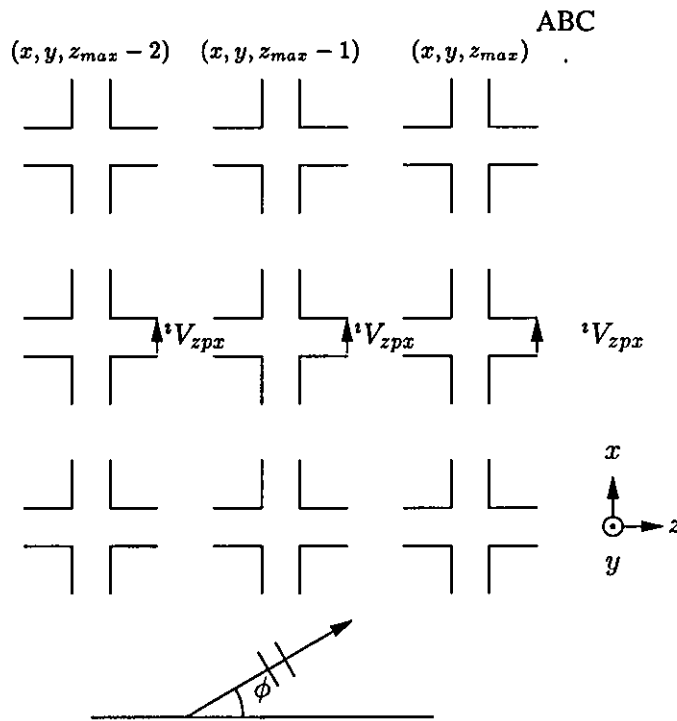
Figure 4 1 Wave incident angle on a boundary placed at z_{max}

The type of open region scattering problems encountered in EM models of vehicles are characterised by their broad-band nature, the unpredictability of the wave incident angle on the boundary (see Figure 4.1), and the complex nature of the scattered fields A number of the high-performance schemes reported in recent years have been demonstrated in wave guidance problems where the bandwidth is relatively low, and fields are reasonably predictable. The implications for models of semi- and fully-anechoic EMC situations are not always clear from these studies

4 1.1 Test method

ABCs have been extensively tested using a variety of experimental and analytical techniques [4 1, 4.2, 4.3]. The majority of these studies have focused on the quantification of localised reflection errors. Whilst these studies are valuable for assessing performance, it is difficult to use the results to understand how to make best use of the ABC in real problems. The approach adopted for the test cases in this chapter recognises that the choice of absorbing boundary type and usage needs to be made carefully, especially when computational resources are limited

The problem to be addressed is this: A certain number of free space nodes are always required

around the object being modelled in order to allow for inaccuracy in the absorbing boundary
If the ABC behaves poorly, then more cells are required, and thus the number of cells wasted
modelling free space increases. Therefore, a larger space step must be selected leading to
poorer geometrical accuracy and lower model bandwidth. It is important to choose a value for
the space step (and hence the amount of free space allowed around objects) which yields the
highest bandwidth model where ABC accuracy can be maintained.

The test cases employed in this chapter attempt to assess this trade-off by artificially imposing
a limit on the number of nodes A common object which has been discretised using different
space steps and with corresponding amounts of surrounding free-space nodes is used These
models are then compared against a reference solution obtained by placing the most finely
discretised model in a much bigger mesh.

4 1 2 Model definition

The geometry employed was the complex vehicle-like object[1] shown in Figure 4 2
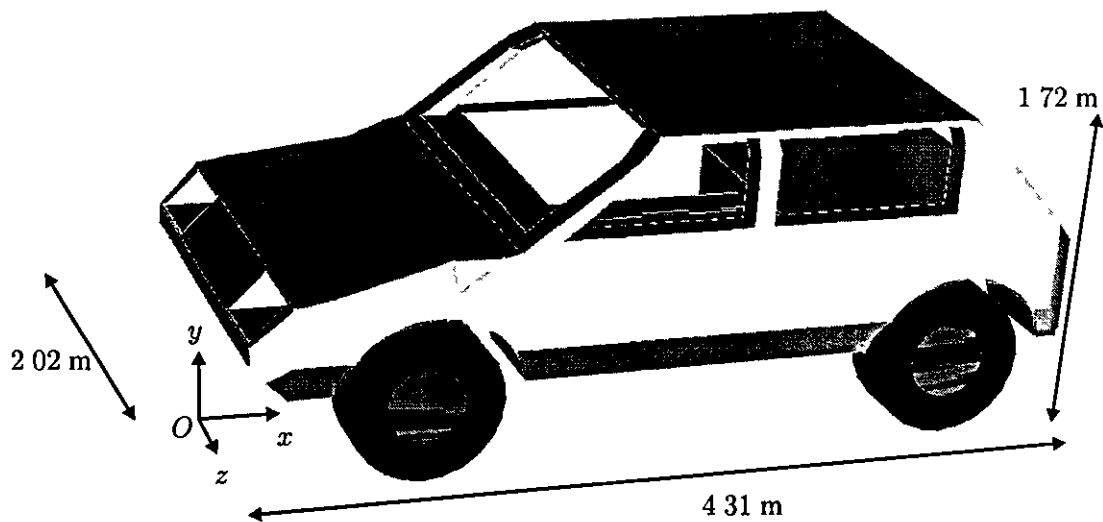
Figure 4 2 Complex vehicle-like geometry modelled in ABC tests

All surfaces in the geometrical model were assumed to represent PEC, except the tyres which
were not included in the final TLM model. The excitation source was a finite thickness tube of

---

[1] This geometrical model is a modified version of that used by Ruddle *et al* [4 4], and is used with permission

electric free space field polarised in E_x placed in the foot well of the car from the front to rear Various measuring points in and around the vehicle were monitored to assess the performance

The geometrical model was discretised onto meshes of $115 \times 46 \times 54$ nodes with varying space steps. A summary of the discretisation level and time step for each model is shown in Table 4 1

Cutoff frequency f_c (MHz)	Space step Δl (m)	Time step Δt (s)	Number of iterations n
200	0 1498962	$2.5000000 \times 10^{-10}$	1334
300	0 0999308	$1.6666667 \times 10^{-10}$	2001
400	0 0749481	$1.2500000 \times 10^{-10}$	2668
500	0 0599585	$1.0000000 \times 10^{-10}$	3335
600	0 0499654	$8 3333333 \times 10^{-11}$	4002
700	0.0428275	$7 1428571 \times 10^{-11}$	4669

Table 4 1 Model statistics for a vehicle-like geometry placed in the centre of a $115 \times 46 \times 54$ cell mesh

In each case the object was placed in the centre of the mesh and the surrounding volume was populated with free space nodes The results of the discretisation process are shown in Figure 4.3.

The reference model was prepared using the smallest space step (corresponding to a model cutoff frequency of 700 MHz), but this time the object was placed in the centre of a much bigger mesh containing $230 \times 92 \times 108$ nodes.

All 7 models were run for a suitable number of iterations to allow the transients to decay to a low level The time-domain impulse response obtained at each measurement point was subsequently transformed into the frequency domain by means of a discrete Fourier transform for analysis

The 6 small models were computed using the software developed for this thesis and the reference model was run on *Microstripes*[2]. This had the added advantage that it allowed the software to be verified against a commercial package which has been validated against experimental data

In the remainder of this chapter a variety of reported schemes will be described, implemented

---

[2] Microstripes is a commercial TLM software package supplied by Kimberley Communications Consultants The version used is known to employ matched termination absorbing boundaries

and tested. In some cases the ABC scheme will be dismissed by consideration of the methodology, and in other more promising cases the vehicle test model will be used to evaluate performance

4 2   Local ABCs

The matched termination boundary condition (MTBC) is implemented on a node-by-node basis, and for this reason is referred to as a *local* absorbing boundary condition   The advantage of local schemes is that they are very easy to implement, and require the modification of a single voltage impulse. Care must be taken however, as some more sophisticated schemes make use of field theory to determine the reflected voltage impulse at the boundary This indirect approach can lead to difficulties with stability because of differences between the analytical (continuous) domain and the discrete domain.

4 2.1   MTBC

The results for the matched termination are shown in Figures 4 4 to 4 6. The results show that the boundary placement has a very strong influence on accuracy in the frequency domain

For the coarser meshes reasonable accuracy can be obtained (Figure 4 4). Minor frequency shifts which do occur can be accounted for by the geometrical errors caused by the discretisation process.

In contrast, the finely meshed models give poor accuracy over the whole band, even at low frequency (Figure 4.5). The errors and frequency shifts in the resonances cannot be explained merely by the geometrical approximation of the mesh. Figure 4 6 shows the results for cutoff frequencies of 400 MHz and 500 MHz. There is a marked reduction in accuracy between these two responses and therefore it is suggested that, given the artificial resource limitations imposed, 400 MHz is the maximum frequency which can be produced from this model.

This result has important consequences, since it is tempting to place objects closer to the boundary to extend the frequency limit of the model. This action is liable to destroy the integrity of the model across the frequency spectrum and should be avoided at all costs

$f_c = 200$ MHz $\qquad\qquad f_c = 300$ MHz $\qquad\qquad f_c = 400$ MHz

E output points

$f_c = 500$ MHz $\qquad\qquad f_c = 600$ MHz $\qquad\qquad f_c = 700$ MHz
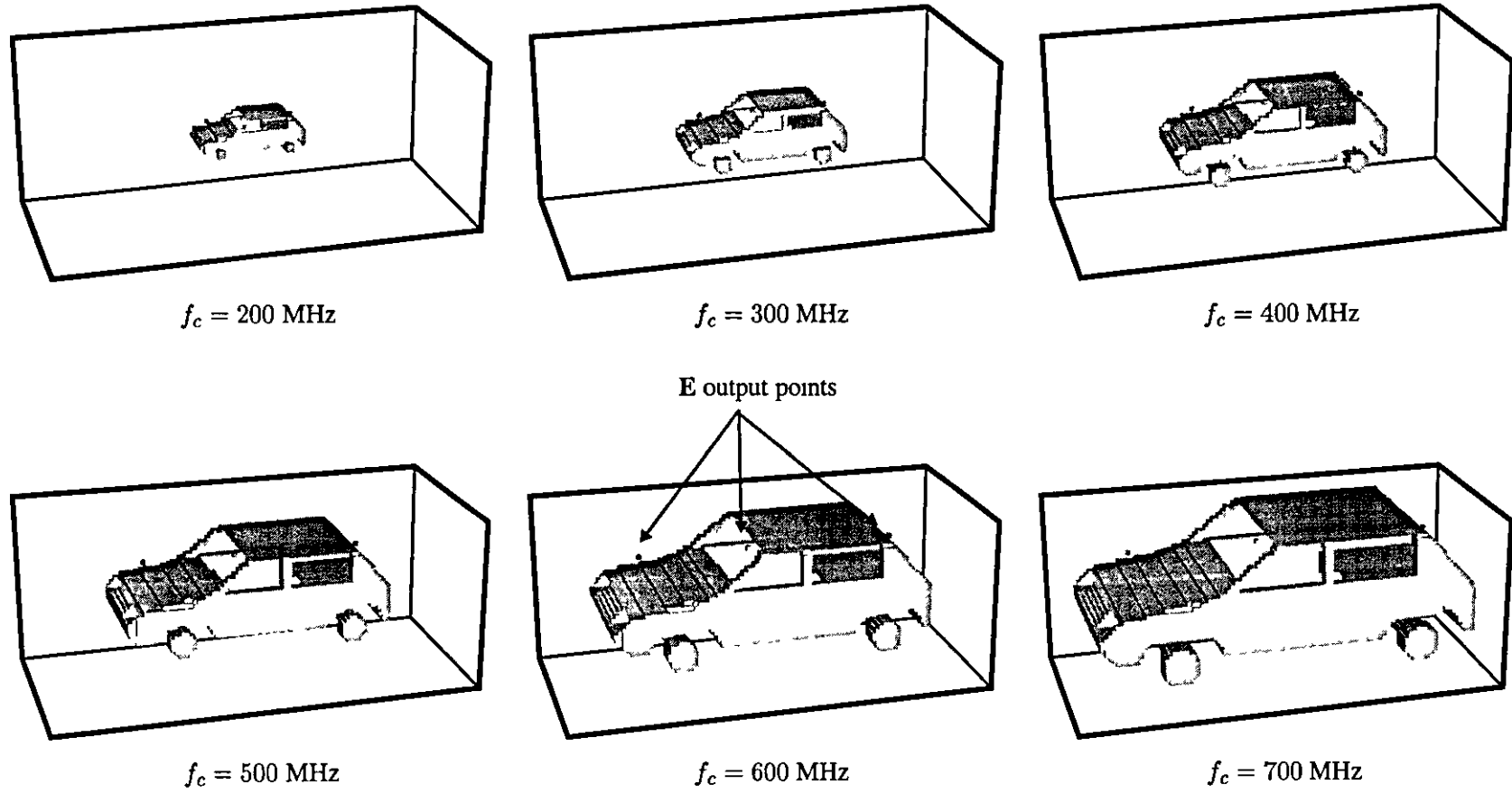
Figure 4 3 Vehicle geometry discretised on coarse and fine meshes
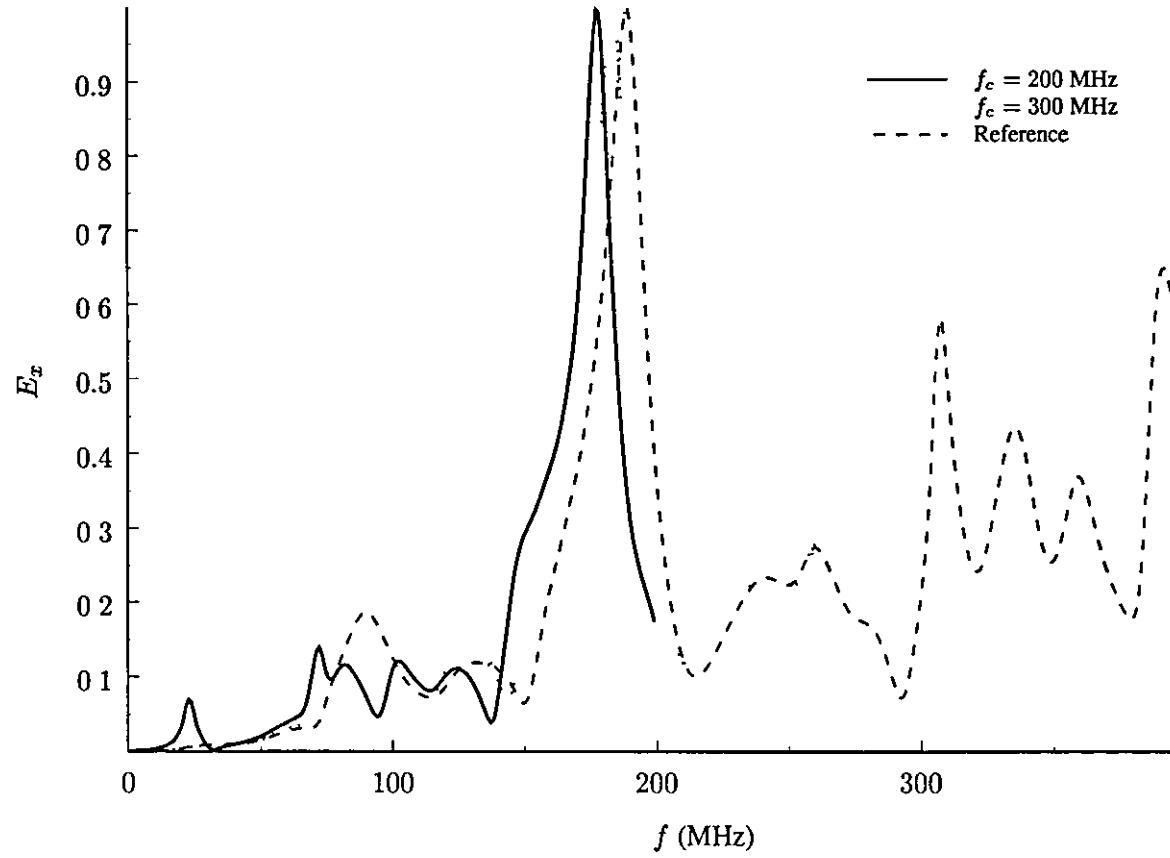
Figure 4 4 Normalised coarse mesh results at (0 25, 1 6, 0) for MTBC
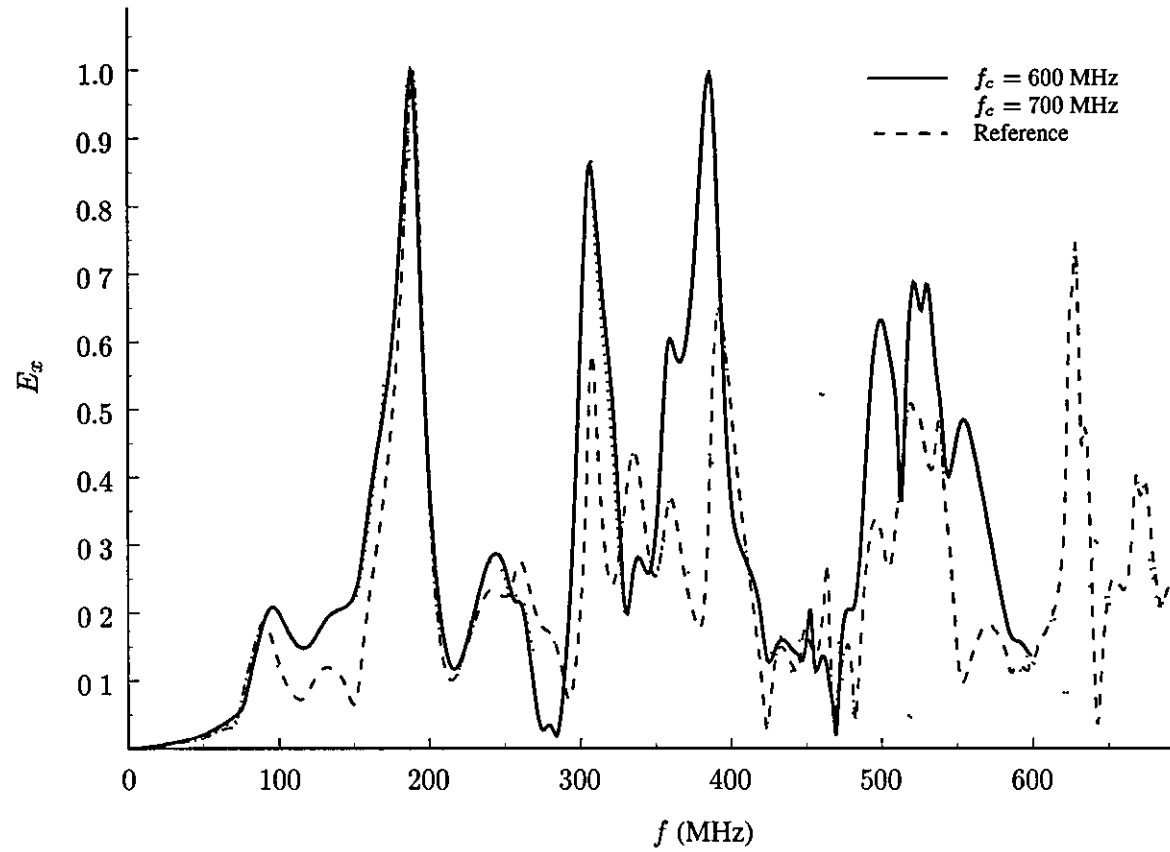
Figure 4 5 Normalised fine mesh results at (0 25, 1 6, 0) for MTBC
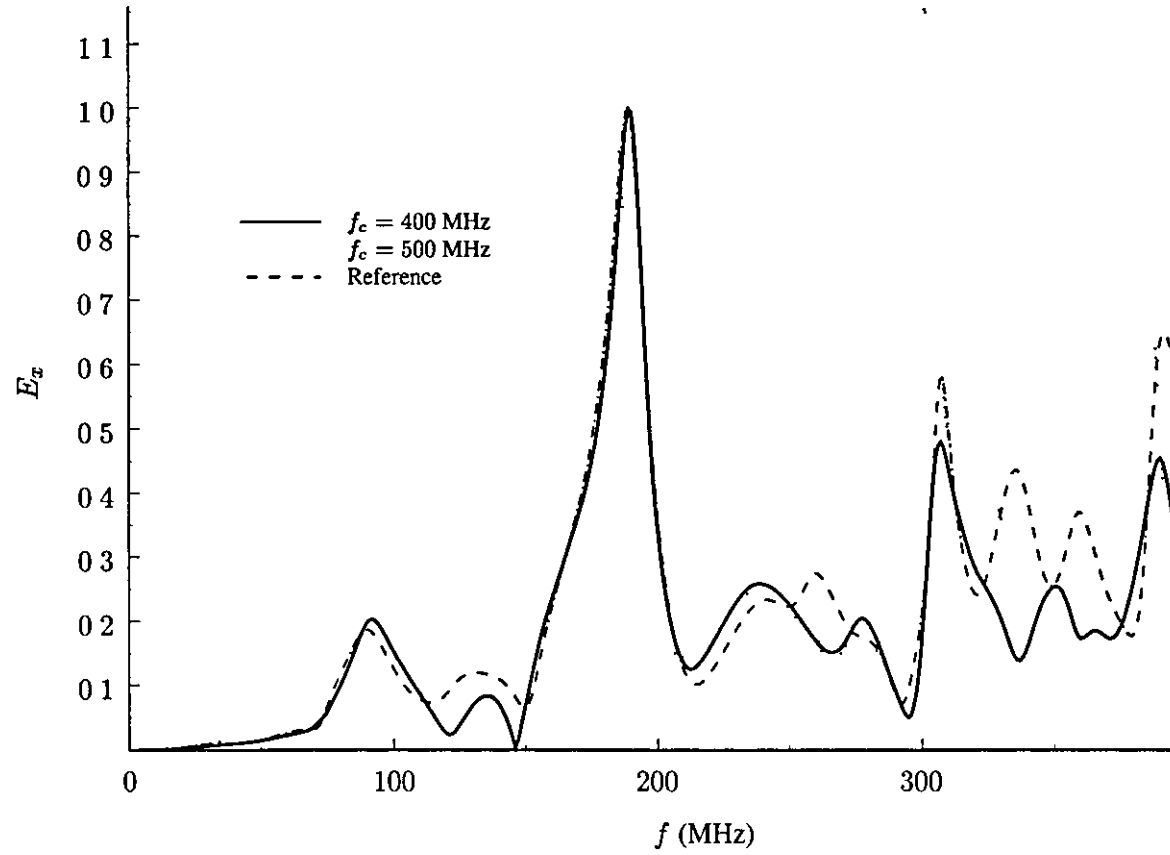
Figure 4 6 Comparison of $f_c = 400$ MHz and $f_c = 500$ MHz results with the reference solution

4 2 2   Variable impedance boundary condition

Simons and Bridges have proposed a method for improving the MTBC, known as the variable impedance boundary condition (VIBC) [4 5]. The VIBC improves the MTBC by using the instantaneous field distribution to predict the wave incident angle. Once the arrival angle has been estimated the impedance of the boundary is selected to match the boundary-directed component of the wave. Thus a wave striking the boundary at any angle can in theory be absorbed The TLM reflection coefficient to be selected for a boundary at z_{max} is:

$$\Gamma_{zpx} = \frac{\frac{Z_0}{\cos\phi_e}\sqrt{\frac{\mu_{ry}}{\epsilon_{rx}}}\frac{\Delta x}{\Delta y} - Z_{zpx}}{\frac{Z_0}{\cos\phi_e}\sqrt{\frac{\mu_{ry}}{\epsilon_{rx}}}\frac{\Delta x}{\Delta y} + Z_{zpx}} \tag{4 1}$$

where ϕ_e is the estimate of the wave incident angle A similar expression may be obtained for y-polarised waves

A brief test of the VIBC has revealed several features which make it unsuitable for use in vehicle EM models. In virtually all realistic problems, the wave striking the boundary is the result of superposition In many cases this causes rapid changes in the wave incident angle ϕ which makes the parameter ϕ_e extremely difficult to calculate from the field distribution. For this reason, the method is practically limited to situations where a single, smooth wave strikes the boundary.

The VIBC is an attractive technique, and can in principle give better performance than the MTBC in problems with a very simple field distribution at little computational cost However, it fails to deliver the performance and reliability required to analyse large, complex structures such as vehicles.

4 2 3   One-way equations

Another class of local ABC is formulated by solving a type of partial differential equation which allows waves to propagate only in specific directions These equations are termed *one-way equations*. One-way equation ABCs originate in the FDTD community [4 6], and have been subsequently applied to TLM. Early attempts in FDTD focused on the theory developed by Engquist and Majda [4.7], although virtually all implementations in TLM have been based on the later and more general approach proposed by Higdon [4.8, 4 9]

Higdon's boundary condition states that for the wave equation:

$$\frac{\partial^2 E}{\partial x^2} + \frac{\partial^2 E}{\partial y^2} + \frac{\partial^2 E}{\partial z^2} = \frac{1}{c^2}\frac{\partial^2 E}{\partial t^2} \tag{4 2}$$

the analytical boundary condition for waves travelling in the positive z-direction is

$$BE = \prod_{m=1}^{p} B_m E = \prod_{m=1}^{p} \left(\frac{\partial}{\partial z} + \frac{\cos\theta_m}{c}\frac{\partial}{\partial t} + \delta_m\right)E = 0 \tag{4 3}$$

B is the boundary operator which ensures perfect absorption for linear combinations of waves propagating at angles $\theta_1, \theta_2, \cdots, \theta_p$, p is the order of the boundary operator, and $\delta_1, \delta_2, \quad, \delta_p$ are small positive constants which are chosen to damp low frequency components and D C. (hereafter known as *damping factors*).

Theoretical reflection coefficient

The magnitude of the reflection coefficient obtained from the analytical boundary condition given in equation (4.3) has been shown by Higdon to be [4 8]

$$|\rho_T| = \prod_{m=1}^{p} \left|\frac{\cos\theta_m - \cos\phi}{\cos\theta_m + \cos\phi}\right| \tag{4 4}$$

As an example, for first order conditions ($p = 1$), it is possible to select a value for θ_1 to absorb waves approaching the boundary from a preselected angle (see Figure 4.7). In guided wave problems, such as in the simulation of a matched load for a waveguide, it is often possible to select an appropriate incident angle from *a priori* knowledge of the fields. In scattering problems, the choice is more difficult since waves may strike the boundary from a variety of angles, depending on the geometry of the scatterer and on the type and positioning of the excitation

It is possible to improve the range of angles at which absorption takes place by constructing higher order operators. Figure 4 8 shows the analytical reflection coefficient of second order ($p = 2$) and third order ($p = 3$) operators where the selected absorption angles are spread evenly over the interval $0° \leq \theta_m \leq 90°$. In theory it is possible to continue to increase the order, however in practice this increases the memory requirement and reduces stability.

|ρ_T|

(dB)
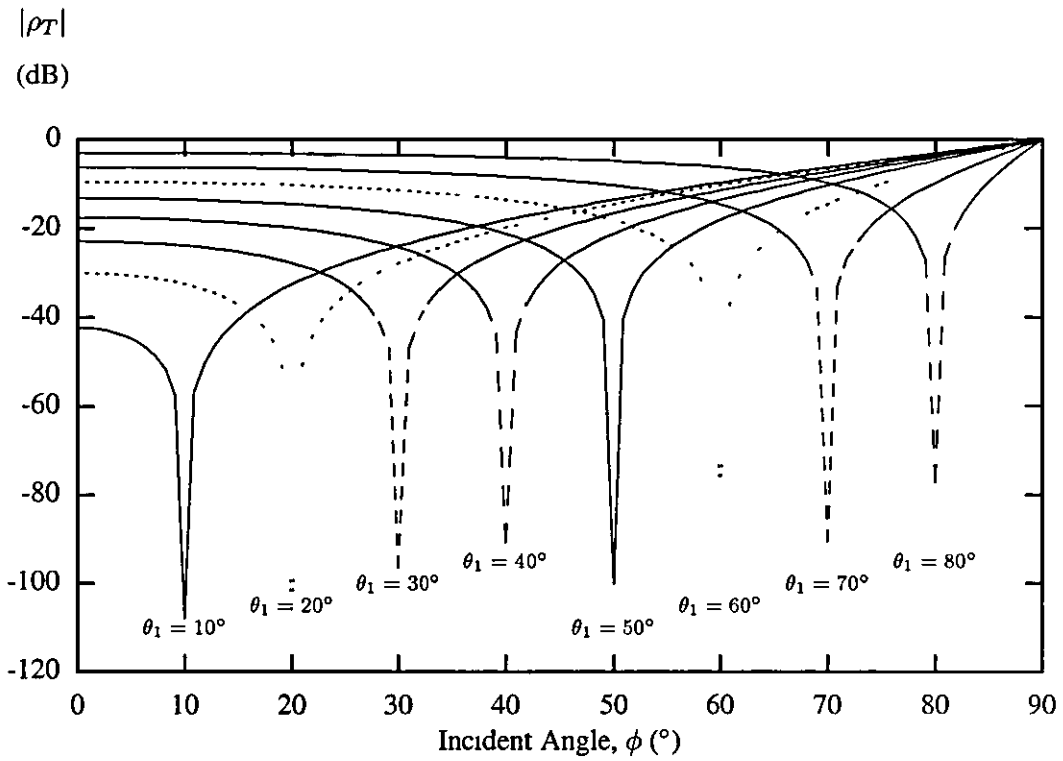
Figure 4 7 Theoretical reflection coefficient of Higdon's method for various first order operators

|ρ_T|

(dB)
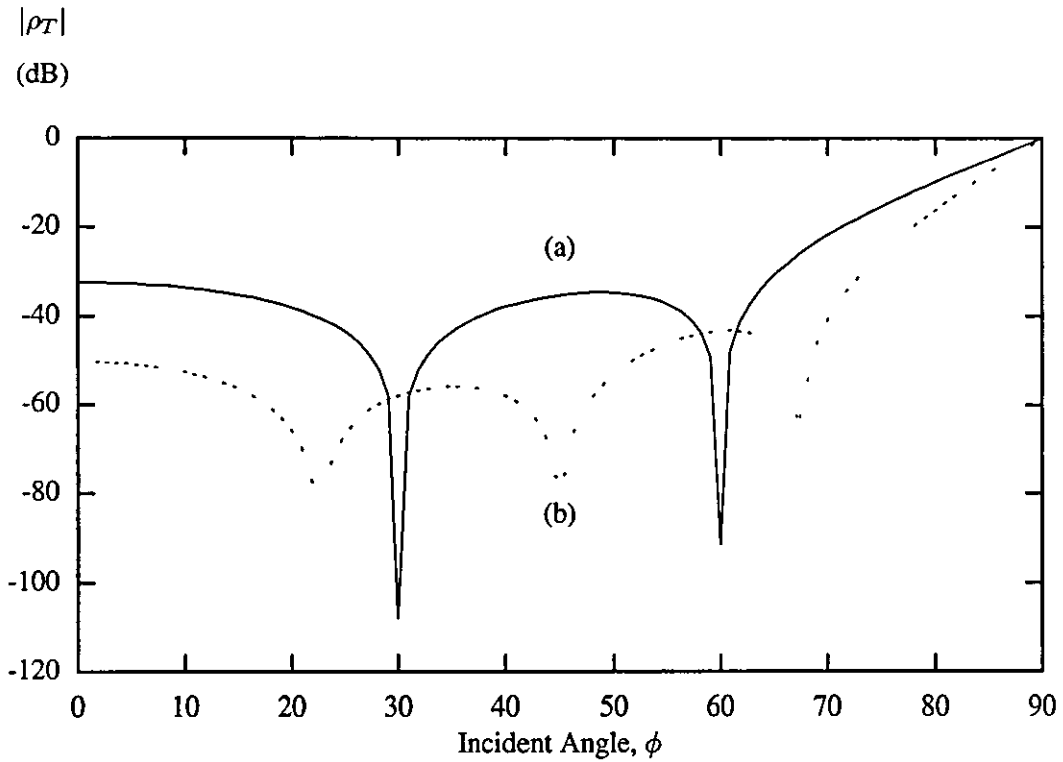
Figure 4 8. Theoretical reflection coefficient for (a) second order, $\theta_1 = 30°$ and $\theta_2 = 60°$ (b) third order, $\theta_1 = 22\ 5°$, $\theta_2 = 45°$ and $\theta_3 = 67\ 5°$

Application to TLM

Several authors have reported implementations of Higdon's method to 3-D SCN TLM [4 10, 3 6]. The most successful method reported appears to be that of Eswarappa and Hoefer [4 11] The discrete boundary condition is formulated by taking the analytical condition given in equation (4 3) and applying finite difference approximations to the spatial and temporal differential terms. A single term of the boundary operator may be expressed thus·

$$B_m = \frac{I - D^{-1}}{\Delta z}[(1-a)I + aK^{-1}] + \frac{\cos\theta_m}{c}\left(\frac{I - K^{-1}}{\Delta t}\right)[(1-b)I + bD^{-1}] + \delta_m \quad (4\ 5)$$

where I, D and K are identity, spatial and temporal shift operators respectively, defined by

$$\begin{aligned} I\ {}_nE &= {}_nE(x,y,z) \\ D\ {}_nE &= {}_nE(x,y,z+1) \\ K\ {}_nE &= {}_{n+1}E(x,y,z) \end{aligned} \qquad (4\ 6)$$

and a, b are weighted time and space averages of time and space differences respectively After algebraic manipulation the boundary operator simplifies to

$$B_m = I - \alpha_m K^{-1} - \beta_m D^{-1} - \gamma_m D^{-1} K^{-1} \qquad (4\ 7)$$

where.

$$\alpha_m = \frac{a - g_m(1-b)}{a - 1 - g_m(1-b) - \delta_m \Delta z} \qquad (4\ 8)$$

$$\beta_m = \frac{a - 1 + g_m b}{a - 1 - g_m(1-b) - \delta_m \Delta z} \qquad (4\ 9)$$

$$\gamma_m = \frac{-a - bg_m}{a - 1 - g_m(1-b) - \delta_m \Delta z} \qquad (4\ 10)$$

$$g_m = \frac{\cos\theta_m \Delta z}{c\Delta t} \qquad (4\ 11)$$

Back substitution into equation (4.3) for a first order operator gives [4.11]

$${}_nE(x,y,z_{max}) = \alpha_1\ {}_{n-1}E(x,y,z_{max}) + \beta_1\ {}_nE(x,y,z_{max}-1) + \gamma_1\ {}_{n-1}E(x,y,z_{max}-1)$$

$$(4\ 12)$$

The method for applying the boundary operator to TLM is subject to choice One option is to strictly apply the condition to the electric field computed from the equivalent total voltage at the boundary nodes, and to use this to compute the reflected voltage pulse to be injected into

the mesh. A simpler alternative is to apply the boundary condition directly to voltage impulses travelling on the link-lines (see Figure 4.1). This method is valid since the boundary condition may be applied to either the electric or magnetic field, and a single voltage impulse may be viewed as a linear combination of field components. Thus for the first order condition the equation to be implemented is:

$$
{}^i_n V_{zpx}(x, y, z_{max}) = \alpha_1 \, {}^i_{n-1} V_{zpx}(x, y, z_{max}) + \beta_1 \, {}^i_n V_{zpx}(x, y, z_{max} - 1) +
$$
$$
\gamma_1 \, {}^i_{n-1} V_{zpx}(x, y, z_{max} - 1) \qquad (4\ 13)
$$

and a similar equation for ports polarised in y. For a second order condition, the boundary operator B may be evaluated by using equation (4.7) and calculating the product $B = B_1 B_2$ The equation to generate the pulses reflected by the boundary is therefore.

$$
{}^i_n V_{zpx}(x, y, z_{max}) = (\beta_1 + \beta_2) \, {}^i_n V_{zpx}(x, y, z_{max} - 1) - \beta_1 \beta_2 \, {}^i_n V_{zpx}(x, y, z_{max} - 2)
$$
$$
+ (\alpha_1 + \alpha_2) \, {}^i_{n-1} V_{zpx}(x, y, z_{max}) + (\gamma_1 + \gamma_2 - \alpha_1 \beta_2 - \beta_1 \alpha_2) \, {}^i_{n-1} V_{zpx}(x, y, z_{max} - 1)
$$
$$
- (\beta_1 \gamma_2 + \gamma_1 \beta_2) \, {}^i_{n-1} V_{zpx}(x, y, z_{max} - 2) - \alpha_1 \alpha_2 \, {}^i_{n-2} V_{zpx}(x, y, z_{max})
$$
$$
- (\alpha_1 \gamma_2 + \gamma_1 \alpha_2) \, {}^i_{n-2} V_{zpx}(x, y, z_{max} - 1) - \gamma_1 \gamma_2 \, {}^i_{n-2} V_{zpx}(x, y, z_{max} - 2) \qquad (4\ 14)
$$

It has been shown experimentally that applying the operator to impulses in this manner gives better results than applying to the electric field alone [4 12] The reflection errors generated by applying the boundary operator to the electric and magnetic field separately are in some circumstances opposite in sign [4.13], and this may explain why better results can be achieved by applying the operator to a linear combination of the two quantities. This property is more effectively exploited in a technique known as *Superabsorption* [4 14].

Another development of the one-way equation approach is the Variable Coefficient Boundary Condition (VCBC) [4.15] The VCBC is analogous to the the VIBC in the way that it exploits a wave angle prediction algorithm to improve the angular performance of the boundary A second order operator is used with $\theta_1 = \phi_e - \Delta\phi$ and $\theta_2 = \phi_e + \Delta\phi$, where $2\Delta\phi$ is a preselected angle between nulls in the second order reflection coefficient. During the simulation, the coefficients of the boundary condition given in equation (4.14) are modified by the predicted wave incident angle, and thus the direction of optimal absorption is effectively 'steered' towards the approaching wave. Using one-way equations to absorb from a wide range of angles is a considerable improvement when compared to the VIBC, however it suffers from similar problems and was not tested in detail for this reason.

4 2.4   Experimental study

A variety of numerical experiments were carried out to evaluate Higdon's method, including tests with the vehicle-like model described earlier. The purpose of the tests were to

- Compare accuracy of first and second order boundaries with the MTBC

- Examine the problems with stability reported in the literature.

- Assess the practical implications of using Higdon's method for complex vehicle models

Results

Overall, much more accurate results were obtained from Higdon's method than from the MTBC. Figure 4.9 shows the $f_c = 500$ MHz mesh result for a first order boundary The magnitudes of resonances are much closer to the reference solution, and this was found to hold for a variety of absorption angles (see Figure 4.10)

The result for $f_c = 400$ MHz shows good agreement with the reference solution (see Figure 4 11), however the $f_c = 600$ MHz model is unstable, and this made it necessary to truncate the time domain response after 2250 iterations prior to Fourier transforming

To further investigate the instability seen in the $f_c = 600$ MHz model the number of iterations was increased in the $f_c = 500$ MHz model. It was found that even in this model the time-domain response showed clear evidence of instability (Figure 4.12) It was found that the onset of instability occurred even earlier in the second order boundaries (Figure 4.13), and there were substantial difficulties in maintaining stability for the duration of the simulation in the fine-mesh benchmarks.
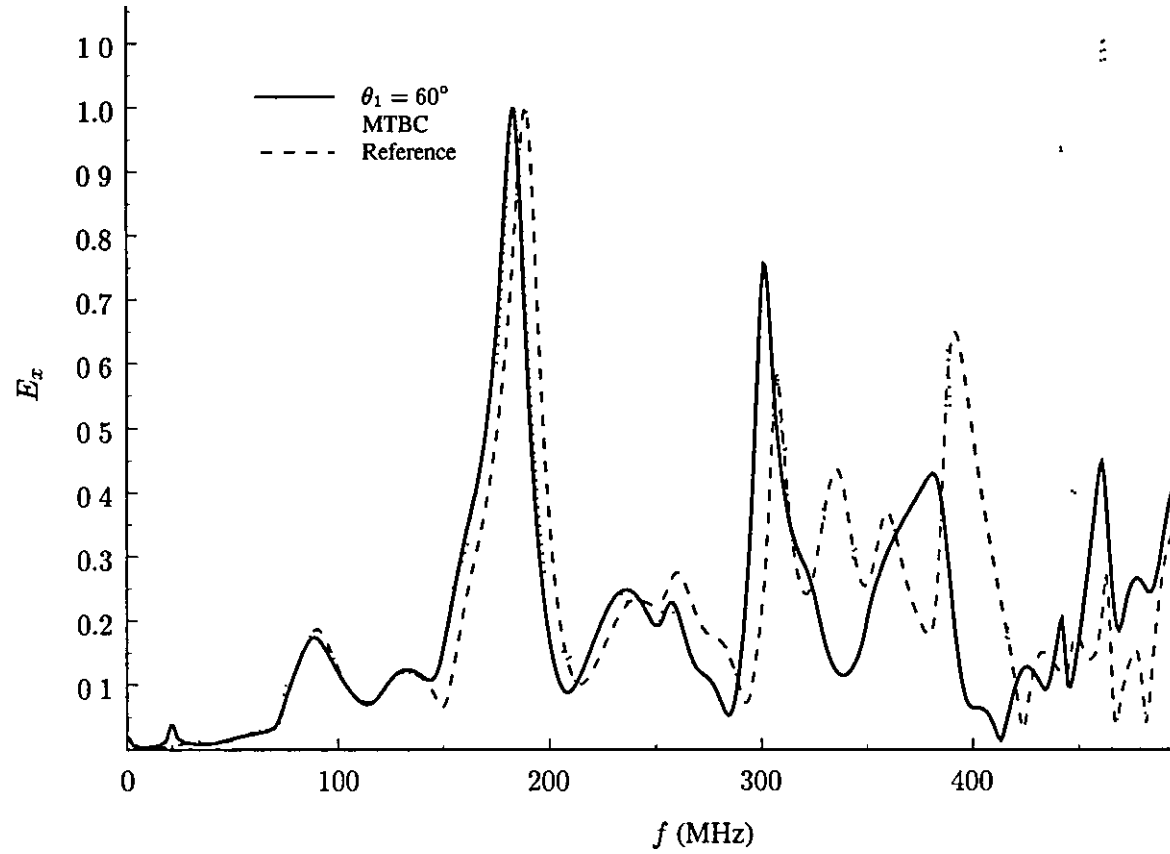
Figure 4 9 Normalised frequency response for $f_c = 500$ MHz model with first order Higdon method
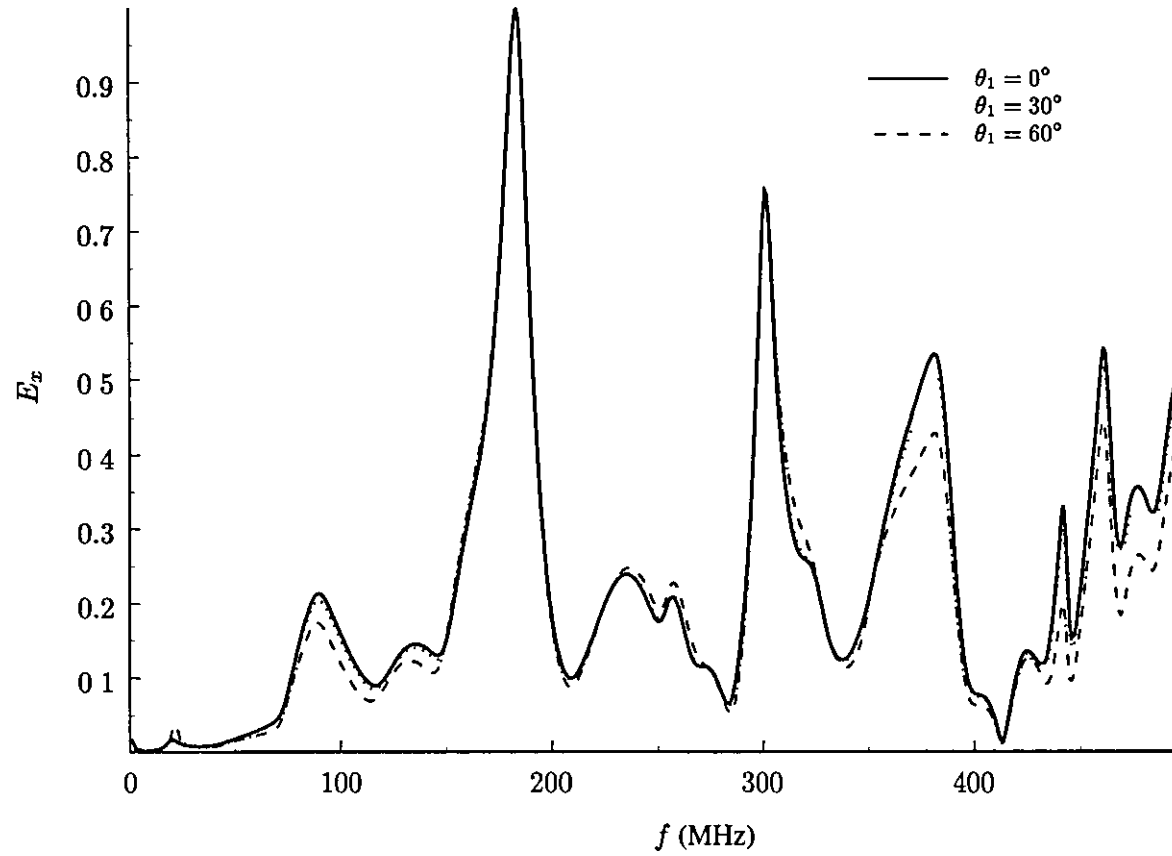
Figure 4 10 Effect of varying the absorption angle for first order Higdon method
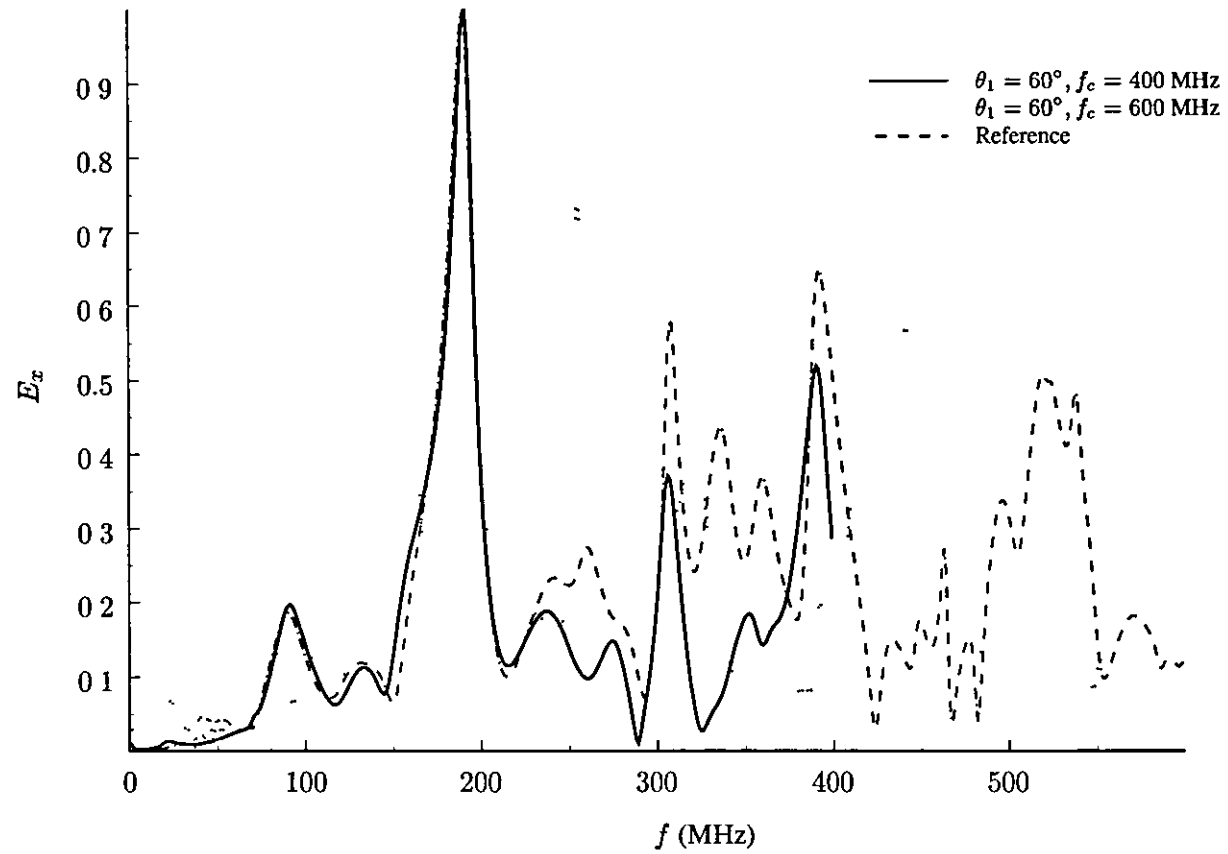
Figure 4 11 Absorption in other models
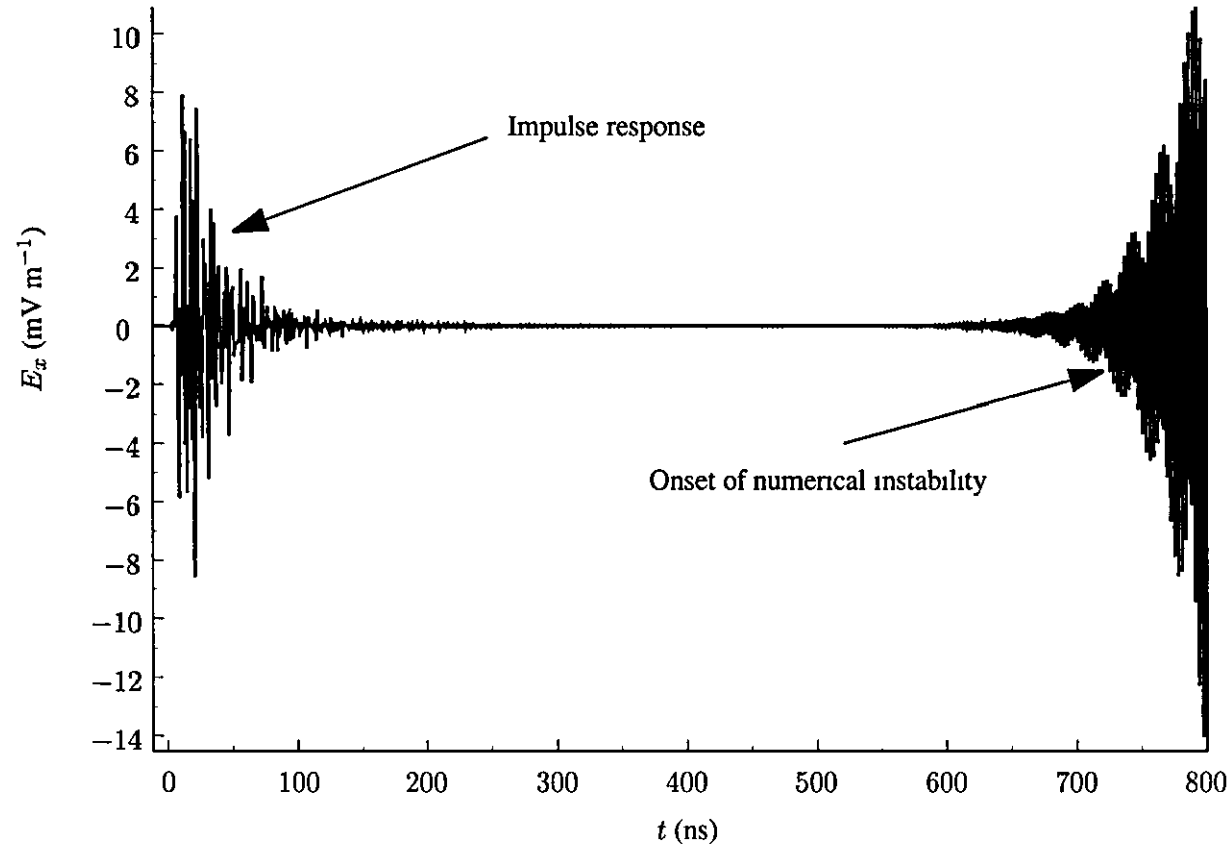
Figure 4 12 Instability in first order Higdon method, $\theta_1 = 0°$, $f_c = 500$ MHz
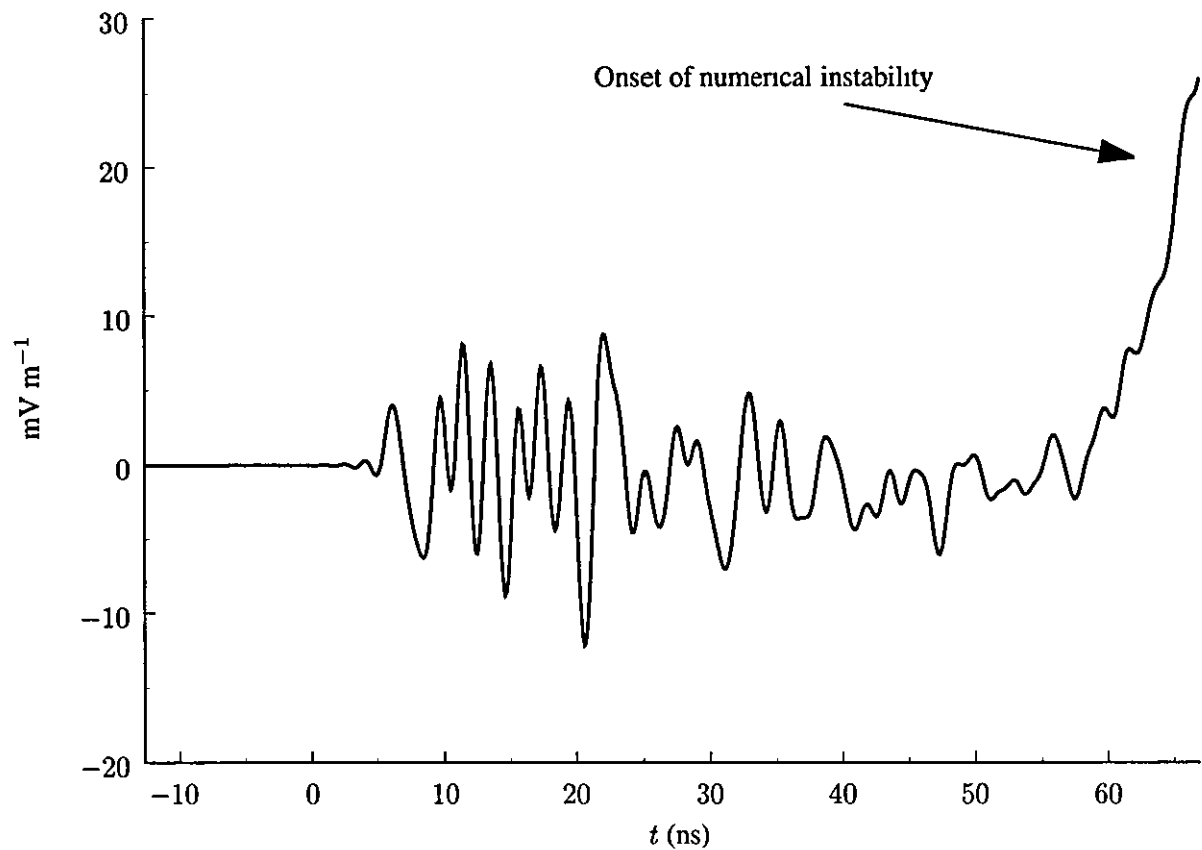
Figure 4 13 Instability in second order Higdon method, $\theta_1 = 30°$, $\theta_2 = 60°$, $f_c = 500\,\text{MHz}$

4 2 5   Discussion

The experiments highlighted one of the major limitations of Higdon's method— instability
There are numerous potential causes of instability, some of which are inherent in the analytical
formulation of the boundary operator and others which occur only in the discrete algorithm

Evanescent waves

The analytical condition described by equation (4.3) assumes that the waves striking the bound-
ary are propagating. Evanescent waves are unaccounted for in the formulation of the boundary
operator, and in general are not absorbed. In practice, this means that sources and objects must
be kept a reasonable distance from the boundary to allow evanescent fields to decay to a low
level   Chen *et al* have suggested that at least 10–15 nodes should be allowed for this to take
place [3 6]   In the test model at $f_c = 500$ MHz there were only 9 nodes, however, instability
was observed even in models where there were many more nodes available around the vehicle
It is therefore probable that evanescent waves were not the sole cause of instability in this study

Spurious modes

Another potential cause of instability is present because the wave propagation speed is a term in
the expression for the boundary operator As was explained in Section 2 5 2 (p 37ff), spurious
modes can be inadvertently excited in simulations Since their propagation speed is significantly
higher than that of other waves they are not automatically absorbed. In some cases the boundary
operator has a gain greater than unity at high frequency, and thus spurious modes are a potential
source of instability In order to improve stability preventative steps could be taken to minimise
the spurious modes in the model For example, the excitation could be band-limited However,
in the experiments a filtered impulsive excitation was tested and this failed to eliminate the
problem

Improved implementations of Higdon's method have been proposed which can extinguish the
spurious modes [3 6]. Other techniques reported have employed digital low-pass filters to re-
move high-frequency components [4 16]. However, studies into these techniques have only
reported limited success, with the onset of instability being delayed rather than prevented

Operator order and discretisation parameters

The discretisation process of the analytical operator, and selection of the operator order can also have a strong influence.

The choice of finite difference terms a and b has been shown to have an important effect on stability [4.11] It has been shown that to satisfy the analytical stability criterion $a = b \leq 0\,5$ [4.8] The popular choice for early studies of $a = b = 0\,5$ is to be avoided since it renders the algorithm susceptible to small numerical errors   The more reliable choice of $a = b = 0\,25$ is often adopted, as has been the case in this thesis, although Zhang has reported from experimental studies in 2-D TLM that $a = b = 0\,22$ delays the onset of instability the most effectively [4 17].

Corner region instability

The discrete algorithm is applied over the finite region of space represented by the margins of the TLM mesh It is important that objects or sources are not present in these regions as this breaches the conditions of the transform from analytical to discrete domains for the boundary operator A hidden consequence of this observation occurs in the 'corner regions' where two or three absorbing boundaries meet. Ramahi has observed that small errors occurring in the calculations for one boundary can act as a sources within the calculation region of an adjacent boundary [4.18]. This process amounts to an incompatibility at the corners and explains why instability often appears to originate from the corners in experiments. It has been further suggested that higher order operators are not inherently unstable, but are simply more susceptible to corner region instability. No solution to this problem has been found to date, and operator orders greater than $p = 3$ are generally regarded as impractical in open problems [3 6]

Damping factors

Low frequency components and D C. also present potential stability problems   Higdon has explained that the denominator of the analytical expression for the complex reflection coefficient approaches zero at low frequency [4.19]. The damping factors, δ_m, in equation (4.3) ensure that this situation does not occur, and thus the stability margin can be improved Unfortunately this makes the reflection coefficient frequency-dependent, and therefore the introduction of such a

term is to be avoided if a wide band response is required An attempt was made during testing to optimise the parameter δ_m, however, this appeared to make very little difference to stability

General comments

Implementation-related errors can be reduced by employing higher-precision arithmetic, for example by replacing the usual single-precision floating point numbers with double-precision numbers. This is a simple way of delaying instability, although the storage requirement is increased.

In general the problem of instability is a very difficult one to avoid or predict, and this makes the Higdon ABC undesirable. For example, it is common practice in very long computations to run a simulation until the user perceives that impulse response has died sufficiently for the analysis of results to begin Without prior knowledge, it is impossible to know whether numerical noise has contributed to the impulse response at that point, or indeed if numerical noise is about to dominate the response. This uncertainty raises important issues about the accuracy of the results

The chance that instability could occur affects the usefulness of the boundary If, for example, a simulation needs to run for two weeks to obtain useful results it would be a considerable waste of computation and time if instability occurred before the simulation had fully completed There seems to be no simple way of estimating when the instability will occur The experiments carried out suggest that a combination of factors are to blame, many of which are difficult quantify These problems are largely caused by an incompatibility between the TLM algorithm and the discrete operators applied at the boundary Thus stability problems are inherent in the method and this makes removing or controlling them extremely challenging

4.3   Global ABCs

In order to achieve proper absorption in three dimensions, it is necessary to handle the absorbing boundary as a feature of the whole computational domain, and not merely on a point-by-point basis. This type of approach is often known as a *Global ABC*

4.3.1   Time-domain diakoptics ABCs

Diakoptics is a well established method of partitioning large structures into smaller parts or *sub-structures* [4.20] The substructures are then solved individually and subsequently reassembled by convolution to form the solution

The fundamental principle of the method is based around a discrete form of the analytical Green's function The discrete time-domain Green's function (or *Johns Matrix* [4 21]) of a TLM substructure may be evaluated by measuring the time-domain outputs along a given reference plane for a unit impulse applied to each transmission-line through which the plane intersects The impulses returning through the reference plane are formed into matrix containing a time history of all possible unit impulse responses. The accuracy is determined by the number of time samples stored in the Johns matrix.

Hoefer has extended the concept to include the modelling of wide-band absorbing boundaries [4 21] It is necessary to evaluate the Johns matrix for a region of space which is large enough to ensure that no signals are reflected before the matrix is truncated in time The matrix obtained can then be applied to the boundary of a suitable computation domain and, through convolution with the outgoing boundary impulses, produce a highly accurate absorbing boundary.

The main disadvantage of the Johns Matrix approach is that the storage required is extremely large It is possible in some cases to reduce the storage and respective computational time by using homogeneity in the propagating waves to reduce the space dimensions in the Johns Matrix, however this is not normally possible in a generalised scattering problem For this reason, the majority of studies to date have focused on 2-D TLM and waveguide problems [4 11]. In 3-D, Krumpholz *et al.* have described a hybrid approach utilising both discrete and analytical Green's functions to reduce the computational overhead, however this suffers from stability problems [4.22]

Overall, the results reported for Johns Matrix ABCs are extremely good, however their storage requirement is prohibitive in the type of open field problem studied in this thesis

4 3 2   Perfectly Matched Layer boundaries

Probably the most promising ABC to be reported in recent years is the *perfectly matched layer* (PML) The PML technique operates by using a special type of absorbing material at the problem boundaries This lossy region is normally several cells thick. The properties of the perfectly matched medium ensure that (theoretically) it is reflectionless for incident waves originating from any direction, and of any frequency. The PML technique was originally described for FDTD by Bérenger [4.23, 4.24].

The principle behind the method is most clearly illustrated by examining the properties of the PML material itself. An ordinary matched layer is formed for a TM field distribution by examining the more general form of equation group (2 1) (given on p 15) with electric and magnetic conductivity terms:

$$\frac{\partial E_z}{\partial y} = -\mu \frac{\partial H_x}{\partial t} - \sigma_{my} H_x \tag{4 15}$$

$$-\frac{\partial E_z}{\partial x} = -\mu \frac{\partial H_y}{\partial t} - \sigma_{mx} H_y \tag{4 16}$$

$$\frac{\partial H_y}{\partial x} - \frac{\partial H_x}{\partial y} = \epsilon \frac{\partial E_z}{\partial t} + \sigma_{ez} E_z \tag{4 17}$$

If now the condition:

$$\frac{\sigma_{ei}}{\epsilon} = \frac{\sigma_{mi}}{\mu} \tag{4 18}$$

is enforced, then it is possible to show algebraically that the material has the same characteristic impedance as free space, and hence there would be no reflection between a medium-to-free space boundary. Such a material could be used as a matched (lossy) layer, but this arrangement will only absorb waves which strike the interface at normal incidence. The key to the PML's ability to absorb waves propagating at any arbitrary angle lies in the next stage of the analysis where Maxwell's equations are restated in terms of split field components   For example, if $E_z = E_{zx} + E_{zy}$, equations (4.15) and (4.16) may be rewritten thus:

$$\frac{\partial (E_{zx} + E_{zy})}{\partial y} = -\mu \frac{\partial H_x}{\partial t} - \sigma_{my} H_x \tag{4 19}$$

$$-\frac{\partial(E_{zx} + E_{zy})}{\partial x} = -\mu\frac{\partial H_y}{\partial t} - \sigma_{mx}H_y \tag{4 20}$$

Equation (4.17) is slit into two separate (non-physical) equations

$$\frac{\partial H_y}{\partial x} = \epsilon\frac{\partial E_{zx}}{\partial t} + \sigma_{ez}E_{zx} \tag{4 21}$$

$$-\frac{\partial H_x}{\partial y} = \epsilon\frac{\partial E_{zy}}{\partial t} + \sigma_{ez}E_{zy} \tag{4 22}$$

It can be shown that performing this splitting operation and reapplying the matching equation (4.18) to each of the newly created field subcomponents, that waves originating from any direction can be effectively dissipated. By duality, the same kind of expressions can be developed for TE waves The analysis is also possible for 3-D TEM waves by splitting both electric *and* magnetic fields into subcomponents.

In the discrete implementation, it just remains to select a suitable number of layers with differing conductivities to gradually absorb waves entering the PML material These layers normally begin with a small conductivity, and gradually increase to a higher value at the boundary. The function used to express this change in the material parameters is termed the *conductivity profile* Thus, outgoing waves are progressively absorbed, and any normal reflection due to the first layer's small but finite conductivity is minimised.

TLM implementations

There have been numerous attempts to produce a PML for use in TLM simulations Early attempts used an indirect approach where an FDTD region was provided to handle the PML, and this was interfaced to the TLM region by a special overlap region [4 25, 4 26]. The reflection coefficients which can be achieved by these methods are poorer than that achieved in a comparable all-FDTD simulation due to the limited accuracy of the interface layer Native-TLM approaches have been investigated by Pena and Ney [4 27, 4.28], Paul *et al* [4 29], and Dubard and Pompei [4 30] Of these approaches, the latter of the three appears to be most numerically efficient

Extension to evanescent waves

Because the PML can, due to its low reflection coefficient, be placed significantly closer than other boundaries to objects the presence of evanescent fields is a serious consideration It has been shown that in its basic form the PML fails to absorb these fields effectively [4 31] Fang and Wu have proposed a method of modifying the FDTD PML to absorb evanescent waves [4 32] This technique has subsequently been applied to TLM by Le Maguer and Ney [4 33, 4 34] by developing Dubard and Pompei's method [4.30]

The modified equations for this layer are (for example)·

$$\frac{1}{\xi_x}\frac{\partial H_y}{\partial x} = \epsilon\frac{\partial E_{zx}}{\partial t} + \sigma_{ez}E_{zx} \tag{4 23}$$

$$-\frac{1}{\xi_y}\frac{\partial H_x}{\partial y} = \epsilon\frac{\partial E_{zy}}{\partial t} + \sigma_{ez}E_{zy} \tag{4 24}$$

Where ξ_x, ξ_y are terms chosen to damp evanescent waves.

4 3 3   Method

Scattering in the PML SCN is achieved by a different method to the normal stub loaded SCN. The procedure must take account of the anisotropic loss terms and apply them to 12 separate field subcomponents, instead of the usual 6 field components during scattering Le Maguer and Ney have explained how the PML equations may be discretised [4 33, 4 34] The result of their analysis is a revised set of scattering equations:

$$\Delta_i E_{ij} = A_{ij}(V_{jni} + V_{jpi} + \hat{Y}_{sij}V_{oij} - 2V_{oik}) \tag{4 25}$$

$$\Delta_i E_{ik} = A_{ik}(V_{kni} + V_{kpi} + \hat{Y}_{sik}V_{oik} - 2V_{oij}) \tag{4 26}$$

$$Z_0\Delta_i H_{ij} = B_{ij}(V_{jnk} - V_{jpk} + \hat{Z}_{sij}V_{sij} - 2V_{sik}) \tag{4 27}$$

$$Z_0\Delta_i H_{ik} = B_{ik}(V_{kpj} - V_{knj} + \hat{Z}_{sik}V_{sik} - 2V_{sij}) \tag{4 28}$$

Where:

$$\hat{Y}_{sij} = 4\left(\frac{\epsilon_i\xi_i\Delta j\Delta k}{2c\Delta t\Delta i} - \frac{1}{2}\right)$$

$$\hat{Z}_{sij} = 4\left(\frac{\mu_i\xi_i\Delta j\Delta k}{2c\Delta t\Delta i} - \frac{1}{2}\right)$$

$$A_{ij} = \frac{2c\Delta t\Delta i}{\xi_j\Delta j\Delta k(2\epsilon_i + Z_0\sigma_{ej}c\Delta t)}$$

$$A_{ik} = \frac{2c\Delta t\Delta i}{\xi_k \Delta j \Delta k (2\epsilon_i + Z_0 \sigma_{ek} c\Delta t)}$$

$$B_{ij} = \frac{2c\Delta t\Delta i}{\xi_j \mu_i \Delta j \Delta k (2 + \frac{\sigma_{mj} c\Delta t}{\epsilon_i Z_0})}$$

$$B_{ik} = \frac{2c\Delta t\Delta i}{\xi_k \mu_i \Delta j \Delta k (2 + \frac{\sigma_{mk} c\Delta t}{\epsilon_i Z_0})}$$

These equations are used to compute the field components at the node by using their definitions, i e.

$$E_i = E_{ij} + E_{ik}$$

$$Z_0 \Delta i H_i = Z_0 \Delta i H_{ij} + Z_0 \Delta i H_{ik}$$

When this has been computed, the field components can be mapped to voltages and currents using similar equations to (2 33) and (2 34), and then the reflected voltages are calculated from equations (2 31) and (2 32)

This method uses 12 stubs to handle the PML medium properties instead of 6 (stub-loaded SCN) in normal medium. The incident voltage emerging from the stub at the next time step is calculated from field subcomponents as follows·

$$^iV_{oij} = \frac{\Delta i E_{ij}}{2} \tag{4 29}$$

$$^iV_{sij} = -\frac{Z_0 \Delta i H_{ij}}{2} \tag{4 30}$$

Similar terms are used for V_{oik} and V_{sik}.

The conductivity profile used in the experiments was a parabolic profile with conductivities defined [4.35]

$$\sigma_{ei}(L) = -\frac{\epsilon_0 c \ln(\rho_T)}{2\Delta i N^3}[(L+1)^3 + L^3] \tag{4 31}$$

Where N is the total number of layers and L is the layer index (where $L = 0, 1, 2, 3, \quad , N-1$). ρ_T is a chosen theoretical reflectivity corresponding to the first layer conductivity step, and this was set to -100 dB for numerical experiments. Magnetic conductivities, σ_{mi}, are chosen for the perfectly matched material by using equation (4 18)

This increasing conductivity profile is applied near to the problem boundary, with the conductivity applied in the coordinate direction or directions required for attenuation [4.23]. The extremities of the problem space are normally terminated with a matched boundary to extinguish any unattenuated wave components.

4 3 4   Experimental results

The result of applying various PML boundaries to the benchmark problem are shown in Figures 4.14 to 4 17. Figure 4.14 shows that the result for a 7-layer PML has basically the same features as the Higdon's method result shown in the previous section From this and Figure 4 15 it was concluded that the PML gave a result which was at least as good as Higdon's method, and much better than a matched termination boundary

Figure 4 16 shows the benchmark frequency response for 4-, 7-, and 10-layer PMLs The 10-layer PML had an evanescent wave absorbing term included, and this shows that merely applying a large number of layers and using a large value of ξ does not guarantee a good result The 7-layer PML is clearly better than the 4-layer PML, however, and this appeared to be the optimum for the normal reflection coefficient chosen.

It was found that the selection of the evanescent wave absorbing term was difficult, and a poor choice readily gave rise to added reflections at the interface. In Le Maguer and Ney, a profile was proposed which increased linearly close to the interface, and became uniform deep in the layer The study in this thesis used a uniform profile for simplicity, however this made it difficult to choose a high value for ξ. A value slightly greater than unity gave improved low frequency results, however increasing this to the value of 3 suggested by Le Maguer and Ney leads to the high frequency result being degraded (Figure 4 17).
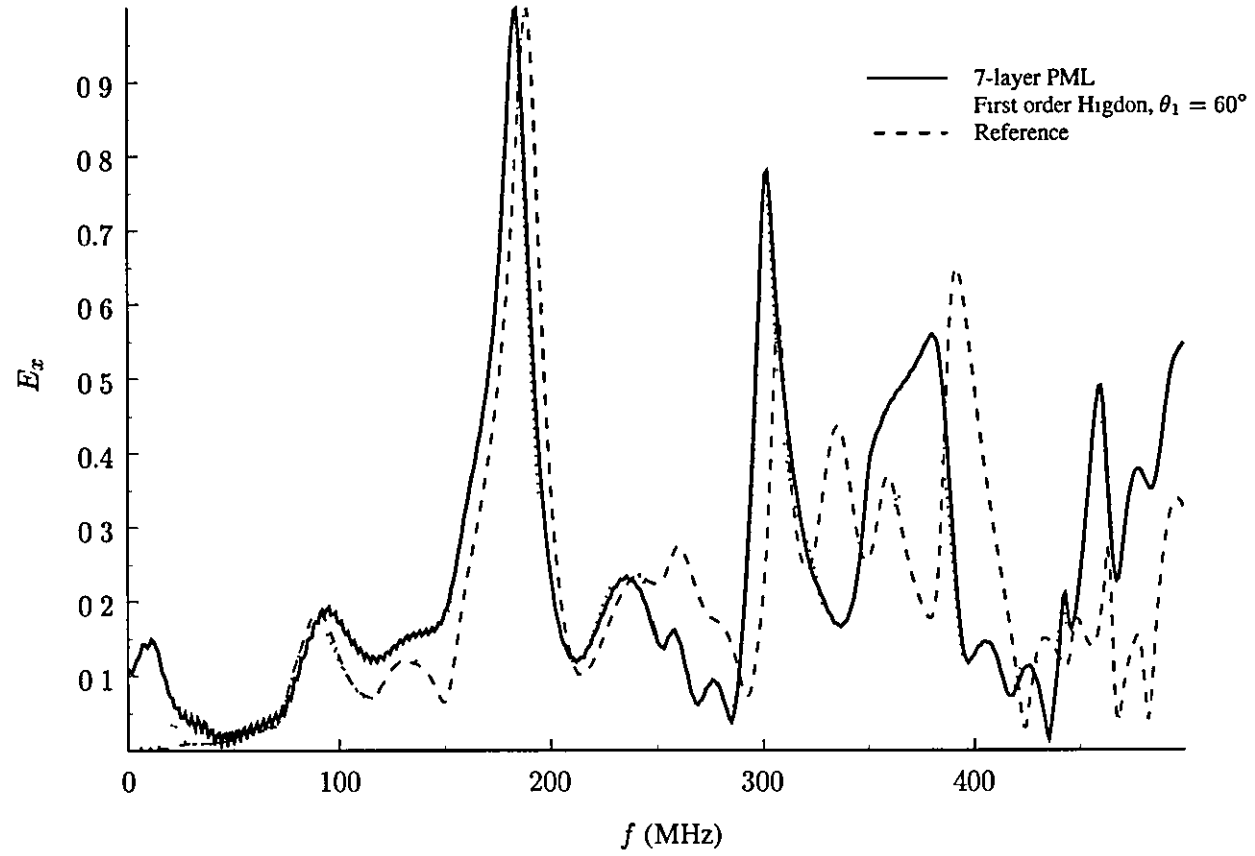
Figure 4 14 Comparison between 7-layer PML and first order Higdon's method for $f_c = 500$ MHz model
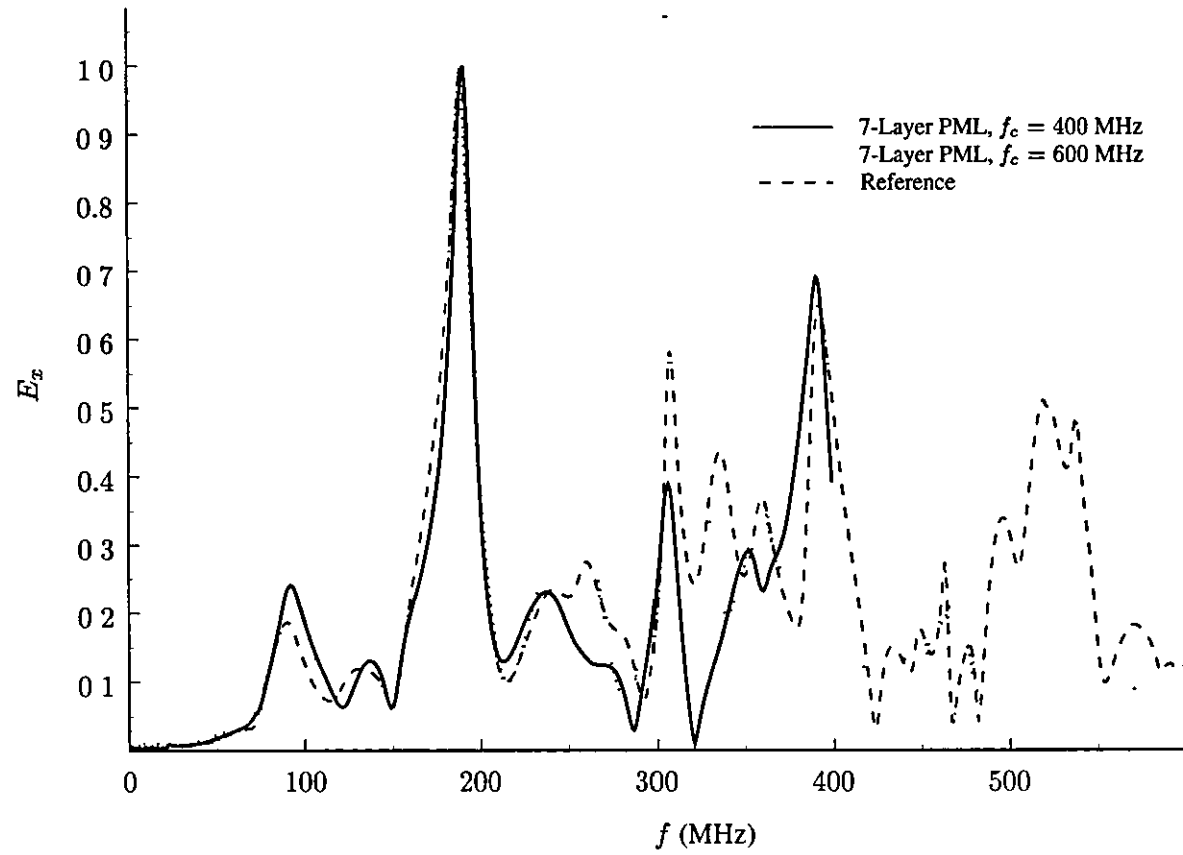
Figure 4 15 Differently discretised models computed with PML
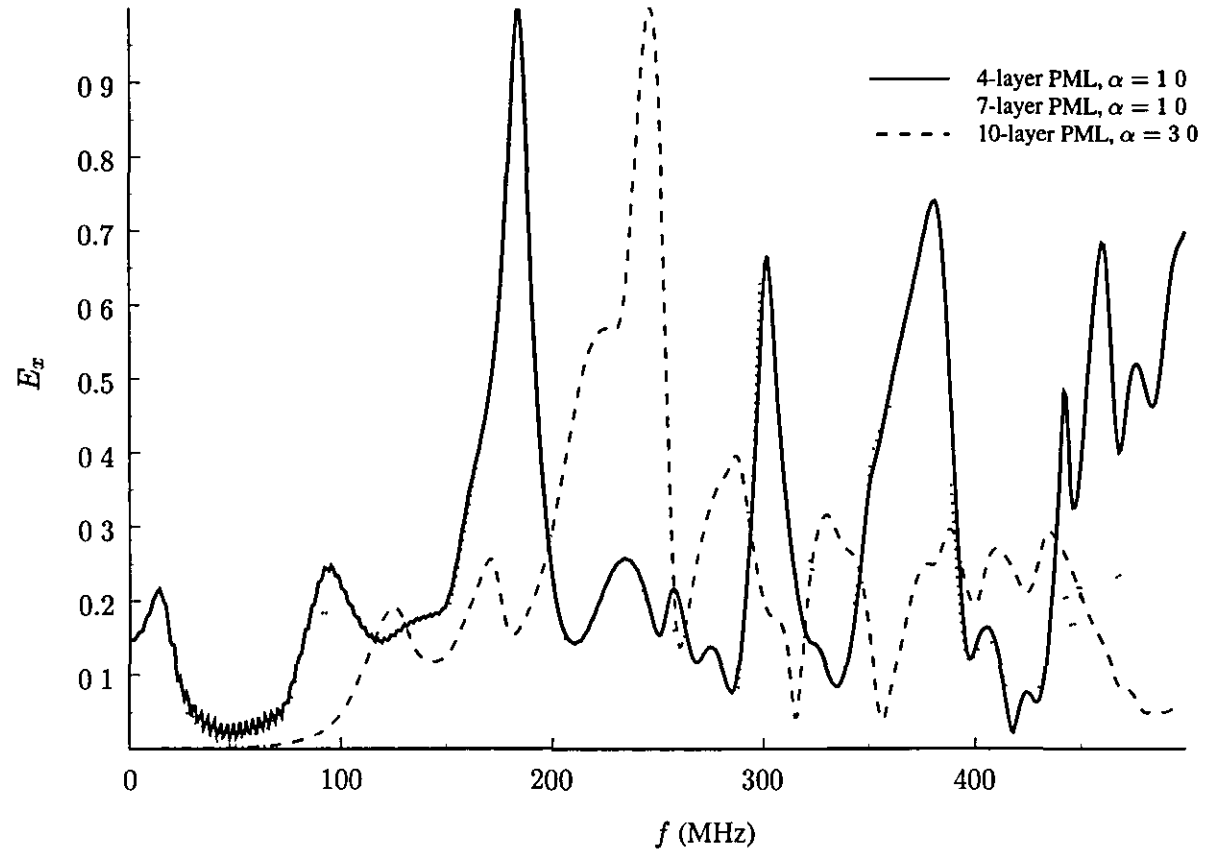
Figure 4 16 Effect of various layer thicknesses
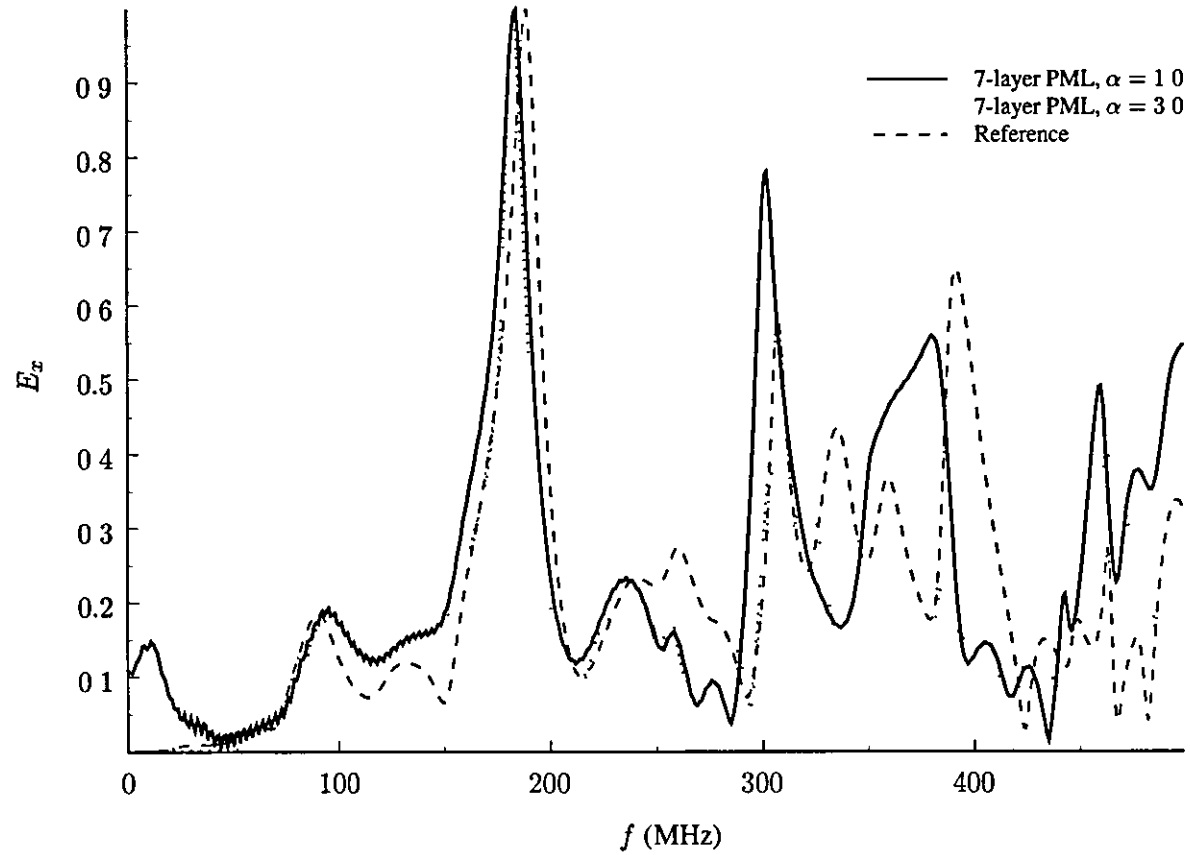
Figure 4 17 Effect of evanescent wave damping term on accuracy

4 3 5   Discussion

In these experiments it has been found that the PML is much more accurate than MTBC and at least as accurate as Higdon's method. It is not possible to conclude from this simple study that the PML is more accurate than Higdon's method, although the theory would seem to suggest this. The PML does absorb from all directions, and so this means that there should be less variability between the boundaries required for different problems.

In terms of stability, there were no problems observed in the configuration and simulation times selected Numerical errors are observed when the simulation is run for much longer, but the PML was generally found to be more robust than Higdon's method The literature already cited seems to suggest that instability occurs more readily in other applications, and this may require more investigation.

The results show that a certain amount of experimentation is required to determine how many layers are required and what profiles to choose for conductivity and evanescent wave absorbing terms. They also suggest that the relative boundary placement must be chosen carefully

One major problem with ABCs which require experimentation to produce the best result is that in very large models it is impractical to generate a reliable (even bigger) reference model with MTBC. Therefore there is some uncertainty about the exact performance of the ABC

It is also important to note that the PML cells use twice as much memory as standard unstubbed SCNs, and therefore the attempts to simulate a fixed memory availability in the experiments were, to an extent, unsuccessful For the $115 \times 46 \times 54$ mesh the 7-layer PML used a total of 35% more memory than the MTBC case. It would be fairer to compare MTBC results where the memory requirement was matched, but this would be very difficult to achieve.

4.4   Summary

A summary of the findings from the study are shown in Table 4 2.

ABC	Reflection coefficient	Angular response	Frequency independence	Memory usage	Stability
MTBC	Neglgible	Very poor, can only absorb from one direction	Yes	Neglgible, only one reflection coefficient required	Excellent, unconditional
VIBC	As for MTBC	Improved over MTBC, but incident angle must be accurately determined	Yes	Neglgible	Poor for complex field distributions
HIGDON	Relatively low, but depends on boundary order etc	Better than MTBC since several absorption angles may be selected	Yes, but only without damping factors	Moderate Voltages at previous time steps require storing	Moderate, high order operators are harder to stabilise
VCBC	As above	Better than VIBC since absorption can be achieved over a greater angle, and thus lower accuracy can be tolerated in the predicted incident angle	As above	As above	Poor for complex field distributions
JOHNS MATRIX	Potentially very low, but depends on duration of stored impulse response	Excellent	Yes	High	Excellent, unconditional
PML	Low, but depends on conductivity of first layer, number of layers and evanescent absorbing term ξ	Excellent	Yes	Moderate More per-node voltage storage required in PML region	Generally good, though some instability reported

Table 4 2 Properties of the ABC types studied

4.5   Conclusion

Whole vehicle simulations often involve long simulation runs (two-week computations are not uncommon), and often include varied features such as on- and off-vehicle antennae Given the long computation time, and the varied nature of the problem, it is debatable whether the more advanced techniques are appropriate

It has been shown that predicting the time where instability occurs can be extremely difficult, and performing exhaustive tests to test stability of all possible vehicles and configurations is impossible. Attempts to improve stability by means such as increasing the numerical accuracy are successful, but have an associated increase in the memory overhead. For these techniques to work effectively it would be necessary to carry out an extensive study of many vehicle models, and this was beyond the scope of this thesis.

Thus, the MTBC will probably remain the standard mesh truncation method for TLM due to

- Guaranteed stability in all circumstances

- Predictable accuracy, which can be maintained by a volume of free space

- Frequency-independent operation

- Simplicity to implement in software

It is worth remembering that most users of modelling are concerned with the device being modelled, and are not overly concerned with the operation of the TLM algorithm. In order to be useful to those users simple methods need to produced, or failing that methods where the decisions can be made mathematically by the TLM program itself. To date, that situation has not been reached by the one-way equation or the PML, and until then it is unlikely that advanced methods will be widely adopted.

References

[4 1] T G. Moore, J G. Blaschak, A. Taflove, and G. A Kriegsmann, "Theory and application of radiation boundary operators," *IEEE Trans. Antennas Propagat* , vol 36, no 12, pp 1797–1812, 1988

[4 2] D. Prescott and N. Shuley, "Reflection analysis of FDTD absorbing boundary conditions— Part I Time-space absorbing boundaries," *IEEE Trans Microwave Theory Tech.*, vol 45, no 8, pp 1162–1170, 1997.

[4 3] D. Prescott and N Shuley, "Reflection analysis of FDTD absorbing boundary conditions— Part II: Bérenger's PML absorbing layers," *IEEE Trans Microwave Theory Tech* , vol. 45, no. 8, pp 1171–1178, 1997.

[4 4] A. Ruddle, D. A. Topham, D D. Ward, and P. J. Page, "Theoretical investigation of automotive emissions measurements at 3 m and 10 m ranges," in *Digest of 13th Int Zurich Symposium on EMC*, (Zurich, Switzerland), pp. 285–289, February 16–18 1999

[4 5] N. R S. Simons and E. Bridges, "Method for modelling free space boundaries in TLM simulations," *Electron Lett* , vol 26, no 7, pp. 453–455, 1990

[4 6] G. Mur, "Absorbing boundary conditions for the finite-difference approximation of the time-domain electromagnetic-field equations," *IEEE Trans. Electromagn. Compat* , vol. 23, no. 4, pp. 377–382, 1981.

[4 7] B Engquist and A Majda, "Absorbing boundary conditions for the numerical simulation of waves," *Math Comp* , vol. 31, no 139, pp. 629–651, 1977

[4 8] R L. Higdon, "Absorbing boundary conditions for difference approximations to the multi-dimensional wave equation," *Math. Comp* , vol. 47, no. 176, pp. 437–459, 1986.

[4 9] R. L. Higdon, "Numerical absorbing boundary conditions for the wave equation," *Math Comp* , vol 49, no 179, pp. 65–90, 1987.

[4 10] J. A. Morente, J. A. Portí, and M Khalladi, "Absorbing boundary conditions for the TLM method," *IEEE Trans Microwave Theory Tech* , vol. 40, no. 11, pp 1095–2099, 1992.

[4 11] C Eswarappa and W J R Hoefer, "One-way equation absorbing boundary conditions for 3-D TLM analysis of planar and quasi-planar structures," *IEEE Trans Microwave Theory Tech*, vol. 42, no. 9, pp. 1669–1677, 1994.

[4.12] A. Giannopoulos and J. M. Tealby, "Comparison of the performance of absorbing boundary conditions in TLM and FDTD," *Electron. Lett*, vol 31, no 19, pp 1639–1640, 1995

[4.13] K. K. Mei and J. Fang, "Superabsorption— a method to improve absorbing boundary conditions," *IEEE Trans. Antennas Propagat*, vol. 40, no. 9, pp. 1001–1010, 1992

[4 14] N. Kukutsu and R Konno, "Super absorption boundary condition for guided waves in the 3-D TLM simulation," *IEEE Microw. and Guided Wave Lett*, vol 5, no 9, pp 299–301, 1995

[4 15] S C. Pomeroy, G. Zhang, and C. Wykes, "Variable coefficient boundary condition for TLM," *Electron Lett.*, vol. 29, no. 13, pp 1198–1200, 1993.

[4 16] C. Eswarappa and W. J. R. Hoefer, "Treatment of instabilities of one-way equation absorbing boundary conditions using digital filters," in *MTT Symposium Digest*, (Orlando, Florida, USA), pp 39–42, IEEE, 1995.

[4 17] G Zhang, *The application of transmission line matrix (TLM) method to the modelling of airbourne ultrasonics*. PhD thesis, University of Nottingham, Nottingham, U K, May 1993.

[4 18] O. M. Ramahi, "Stability of absorbing boundary conditions," *IEEE Trans. Antennas Propagat.*, vol. 47, no. 4, pp. 593–599, 1999.

[4 19] R. L. Higdon, "Radiation boundary conditions for elastic wave propagation," *SIAM J Numer Anal.*, vol. 27, no. 4, pp. 831–870, 1990.

[4 20] P B Johns and K. Akhtarzad, "The use of time domain diakoptics in time discrete models of fields," *Int. J. Numer Methods Eng.*, vol. 17, pp. 1–14, 1981

[4 21] W. J. R Hoefer, "The discrete time domain Green's function or Johns Matrix— a new powerful concept in transmission line modelling (TLM)," *Int J Numerical Modelling Electronic Networks, Devices and Fields*, vol. 2, pp. 215–225, 1989

[4 22] M. Krumpholz, B Bader, and P. Russer, "On the theory of discrete TLM Green's functions in three-dimensional TLM," *IEEE Trans Microwave Theory Tech*, vol 43, no 7, pp. 1472–1483, 1995.

[4 23] J.-P. Bérenger, "A perfectly matched layer for the absorption of electromagnetic waves," *J. Comp. Phys*, vol 114, pp. 185–200, 1994.

[4 24] J.-P. Bérenger, "Perfectly matched layer for the FDTD solution of wave-structure interaction problems," *IEEE Trans. Antennas Propagat.*, vol. 44, no 1, pp. 110–117, 1996

[4.25] C. Eswarappa and W. J. R Hoefer, "Implementation of Bérenger absorbing boundary conditions in TLM by interfacing FDTD perfectly matched layers," *Electron Lett*, vol. 31, no 15, pp 264–266, 1995.

[4 26] N. Peña and M. M. Ney, "Absorbing-boundary conditions using perfectly matched-layer (PML) technique for three-dimensional TLM simulations," *IEEE Trans. Microwave Theory Tech*, vol 45, no 10, pp 1749–1755, 1997.

[4.27] N. Peña and M. M. Ney, "A new TLM node for Bérenger's perfectly matched layer," *IEEE Microw. and Guided Wave Lett.*, vol. 6, no 11, pp 410–412, 1996

[4 28] M. M Ney, "Further notes on the hybrid PML node." Private communication, February 1998

[4 29] J. Paul, C. Christopoulos, and D. W. P. Thomas, "Perfectly matched layer for transmission line modelling (TLM) method," *Electron. Lett*, vol. 33, no 9, pp 729–730, 1997

[4 30] J. L. Dubard and D. Pompei, "Simulation of Bérenger's perfectly matched layer with a modified TLM node," *IEE Proc. Microw. Antennas Propag*, vol. 144, no 3, pp 205–207, 1997.

[4 31] J.-P. Bérenger, "Evanescent waves in PMLs: Origin of the numerical reflection in wave-structure interaction problems," *IEEE Trans. Antennas Propagat*, vol. 47, no 10, pp. 1497–1503, 1999.

[4.32] J. Fang and Z. Wu, "Generalized perfectly matched layer for the absorption of propagating and evanescent waves in lossless and lossy media," *IEEE Trans. Microwave Theory Tech*, vol. 44, no. 12, pp. 2216–2222, 1996.

[4 33] S. Le Maguer and M. M. Ney, "PML-TLM technique: Extension to evanescent waves and to advanced symmetrical condensed nodes," in *Digest of the Third International Workshop on TLM*, (Nice, France), pp. 93–102, IEEE, 27–29 October 1999

[4 34] S. Le Maguer, "Evanescent wave absorbing PML— errata " Private communication, July 2000.

[4 35] J. L. Dubard and D. Pompei, "Efficiency of the TLM-PML node." Lecture handout at 2nd Int. TLM Workshop, Munich, Germany, October 1997

CHAPTER 5:
IMPLEMENTATION

SOPHISTICATED models with a large number of nodes and many features place significant demands on the computational platform. It is crucial that the modelling process considers practical issues raised by the application of the algorithm on a digital computer Some of the specific challenges which present themselves when implementing TLM are

- The run time may be large.

- Specialised techniques may be required to model particular features of the problem

- There is an increasing interest in combining TLM with other numerical methods.

- There are issues related to the numerical accuracy.

- A large amount of memory may be required to store node voltages for the model

This chapter addresses these issues, and demonstrates the need to manage computational resources effectively in order to optimise the result of the modelling process

5 1   Run time

The amount of computational run time is an extremely important factor when assessing the practicality of any modelling task.

In TLM this run time will depend on the the number of time steps required, which in turn depends on·

- The required resolution in the transformed frequency response

- The duration of the time-domain impulse response of the physical system.

117

Precisely which of these is most significant depends on the characteristics of the system being modelled

Low Q-factor systems have a finite duration impulse response. In these this type of simulation, the energy in the system must be allowed to decay to a very low level to ensure that the observed resonances in the frequency domain are of the correct magnitude It follows that the lower the Q-factor, the shorter the duration of the impulse response and the sooner the simulation may be stopped It is therefore advantageous to incorporate losses in the model wherever they occur in the physical system in order to minimise the number of time steps and hence the computational run time

High Q-factor situations are less common in EMC, as they mainly occur in closed systems The energy decays extremely slowly, if at all, and so it is necessary to truncate the time domain response before the resonances have died away. When this truncation takes place depends on how accurately the data is required once it has been transformed into the frequency domain (using, for example, the Discrete Fourier Transform (DFT) [5.1]). An adequate number of samples are required in order to resolve close-together peaks in the spectrum and to obtain the magnitude of the resonances with suitable accuracy

The vast majority of situations encountered in EMC simulations of vehicles are low-Q, although there is interest in simulating reverberant (non-absorber-lined) rooms and these are in the high-Q category. For simulations where there is only moderate damping of the resonances, long computational runs are inevitable

5 1 1 Hardware

The TLM algorithm has been implemented on a wide range of computer hardware. Historically, powerful workstations have been the preferred computational platform, although there has been a recent trend towards using cheap, powerful, desktop Personal Computers (PCs) [5 2] The ever-increasing demands to produce more accurate models more quickly has raised the interest in using other hardware. These alternative implementations can be broadly categorised into

- Massively parallel SIMD (Single Instruction, Multiple Data) machines [5 3, 5.4, 5 5]

- Distributed parallel machines which use a network of workstations acting as a single parallel computer [5 6]

- Hardware accelerators, which may be added to a desktop PC to enhance performance [5 7]

The interest in implementing TLM on parallel platforms is understandable; particularly in the area of automotive EMC where complex, accurate geometry description and high model bandwidth is required

SIMD machines have been a popular choice of researchers because of the seemingly convenient manner that a 2-D TLM mesh maps onto a 2-D array of processing elements In practice there are considerable problems where the TLM mesh is larger than the number of processors. In these cases it is necessary to divide the problem into individual *tiles* for processing Often, the tiles are transferred from the host machine to the array for processing and returned once the TLM algorithm has been applied. The tiles are then connected in the host machine and so the algorithm continues

A technique like this was applied by Parsons *et al* [5.6] to a distributed parallel machine with many tiles being processed in parallel by different distributed workstations. The exchange of data between the host machine and the parallel array, or between workstations distributed over a computer network, is a relatively slow process when compared with the internal speed of the processor array, or of an individual workstation. As a result, the transfer of data can become the limiting factor in the overall performance, and this may outweigh any improvement in the calculation speed. Despite this potential problem, a number of investigators have reported an impressive speedup by applying parallel hardware to TLM.

Despite the interest in parallel computing and a number of successful implementations, no commercial parallel TLM code is readily available. The main reason for this is that parallel machines have a relatively short lifespan, are expensive and often require platform-specific code to be written. In addition, the implementation of the algorithm is more difficult since it may need careful optimisation for a particular architecture.

The future of parallel TLM may lie in distributed processing, because networks are common, data rates are improving, and powerful desktop PCs are relatively cheap Another strong advantage is that standards are beginning to emerge, such as Parallel Virtual Machine (PVM) and this allows a degree of platform independence for parallel computer codes [5.8].

5.2 Programming methodology

In order to implement the TLM algorithm with optimum efficiency, the computer code must be written carefully. Apart from accuracy, the performance, memory usage and complexity of the code are all important issues.

For example, scattering can be much more quickly achieved by using a special method, such as that described by Trenkić *et al.* [5.9] (based on the empirical form derived by Naylor and Ait-Sadi [2.19]), which minimises the number of mathematical operations. In addition the storage requirement can be minimised by selecting an appropriate node type, and by storing scattering coefficients only once per distinct node region.

A variety of specialised techniques are used to model the various features within a TLM model, and there is an increased interest in using hybrid methods where TLM is combined with other numerical techniques [5.10, 5.11]. These factors have contributed to the overall complexity of TLM codes, and this has increased the potential for programming errors. Object-oriented languages provide excellent facilities for managing complexity, and were investigated as an alternative to more traditional procedural approaches.

5 2 1   Object-oriented methods

A formal design methodology has been proposed by Rumbaugh *et al* [5 12] known as the *Object Modelling Technique* (OMT). A summary of the design process is shown in Figure 5 1 One important feature of the method is that the implementation is the last stage of the design. This ensures that all of the concepts, algorithms and architecture of the program are fully developed before any attempt is made to put the design into programming language. It also has the advantage that a degree of portability is maintained among the growing selection of object-oriented languages.

A simple TLM solver designed with OMT

In order to evaluate the method, OMT was applied to the design of a simple solver for SCN-based TLM without graded cells. One possible OMT diagram (following the notational scheme detailed in [5.12]) is shown in Figure 5.2.
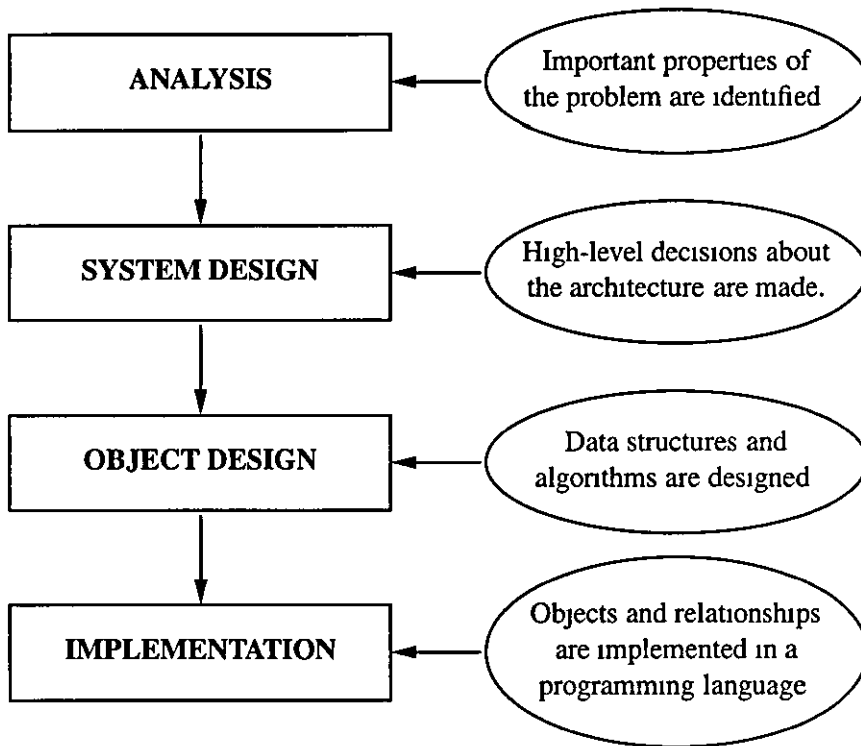
Figure 5 1 Object-oriented design methodology

A powerful feature of object-oriented languages is *polymorphism* This property allows different classes of object to have their own individual implementation of a given operation For example, three classes of transmission-line are defined in the model shown in Figure 5 2 Each class has an operation connect, and yet all are allowed to implement it differently For example, a normal Transmission-line object simply exchanges pulses during connect, however a Shunted-line object applies a transmission/reflection process when connect is invoked. Another useful facility in object-oriented code is *inheritance*, where new classes may be derived which are closely related to existing ones. For example, in the TLM model, there are three derived classes from the base class SCN, i e Source node, Short circuit node, and Stub-loaded SCN These nodes retain many of the properties of the base class, but may 'own' different variables and implement their operations differently. The ability to *encapsulate* objects is well developed in object-oriented languages. This allows for structured and readable source code which is suitably abstracted.

In practice, different types of SCN may be combined at will with different types of transmission line. This enables the different features of the physical problem to be incorporated into the model. At run time, calling scatter on nodes and connect on transmission lines invokes the

TLM mesh

time step
iteration number

Coordinates

SCN

$V_{xpy}, V_{xny}, V_{xpz}, V_{xnz}$
$V_{ypz}, V_{ynz}, V_{ypx}, V_{ynx}$
$V_{zpx}, V_{znx}, V_{zpy}, V_{zny}$

scatter
measure

Joined by
1,2   12

Transmission line

connect

Shunted line

$\Gamma_i, T_i, \Gamma_{i+1}, T_{i+1}$

connect

Terminated line

Γ_i

connect

Source node

E_x, E_y, E_z
H_x, H_y, H_z

scatter

Short circuit SCN

scatter
measure

Stub-loaded SCN

V_{ox}, V_{oy}, V_{oz}
V_{sx}, V_{sy}, V_{sz}

scatter
measure

Uses

Scattering coefficients

kv
ki

Figure 5 2 OMT model of a simple TLM program

correct routines for the specific object type in use It has been proved that object-oriented code is realisable and can produce highly readable and maintainable code, however several drawbacks have been highlighted by experiments.

5 2.2 Results and discussion

One of the main limitations of object-oriented code was found to be computational performance The execution speed of a simple object-oriented code was significantly poorer than that of a comparable non-object-oriented code. When more advanced programming techniques were employed in the object-oriented code (such as linked lists), the performance of the codes was similar. Employing these performance-enhancing measures tends to increase the complexity and degrades the simplicity of the code overall In addition, object-oriented techniques tend to reduce the ability of the programmer to control memory allocation In some circumstances, especially where a large number of nodes are to be processed, it is desirable to control the allocation of memory manually in order to obtain the best performance [5.13].

A slight storage increase was observed when using the object-oriented program This occurs due to the linking of objects through pointers and is unavoidable In some respects, the use of memory is more efficient since the complexity of an object used in a particular area of the problem can be chosen appropriately, e g. stubbed nodes need only be used where required and so fewer voltages are stored.

Object oriented techniques are a reliable and flexible way of producing a TLM program, however, applying object-oriented code at a node and transmission-line level was found to be awkward and offered no performance advantage over traditional approaches It was, however, found that applying the techniques to the user level routines significantly simplified the code The graphical user interface (GUI) was easily programmed using these methods, and has been successfully applied in this way by other investigators, such as So and Hoefer [5 14] It seems reasonable to adopt a mixture of techniques, using traditional methods to implement the TLM algorithm to satisfy performance considerations and using object-oriented methods to implement the input/output routines for convenience.

5 3   Numerical accuracy

Jin and Vahldieck have shown that the SCN and HSCN can be directly derived from Maxwell's equations through a process of centered differencing and averaging [2.12]. Furthermore, they observe that the connect process is intrinsically free from errors, and therefore the only source of localised error is that associated with the scatter process. Their analysis has shown that TLM has accuracy equivalent to a second order finite difference scheme both for graded and for ungraded meshes

In order to evaluate the practical effects of these observations, a popular canonical problem was employed A 1 m × 1 m × 1 m lossless cavity with PEC walls was modelled with an ungraded mesh of $\Delta l = 0.1$ m and 1000 iterations computed. Impulsive excitation was provided at a point within the cavity, and the resonant modes were examined in the manner described by Herring [5 15]

When the node voltages were stored as double precision real numbers, the frequency spectrum observed is that shown in Figure 5.3. In this problem it has been reported that the resonances calculated from the TLM model agree particularly well with the analytical solution for a cavity

resonator [5.16] and this was duly confirmed

|E|

(nV m^{-1} Hz^{-1})
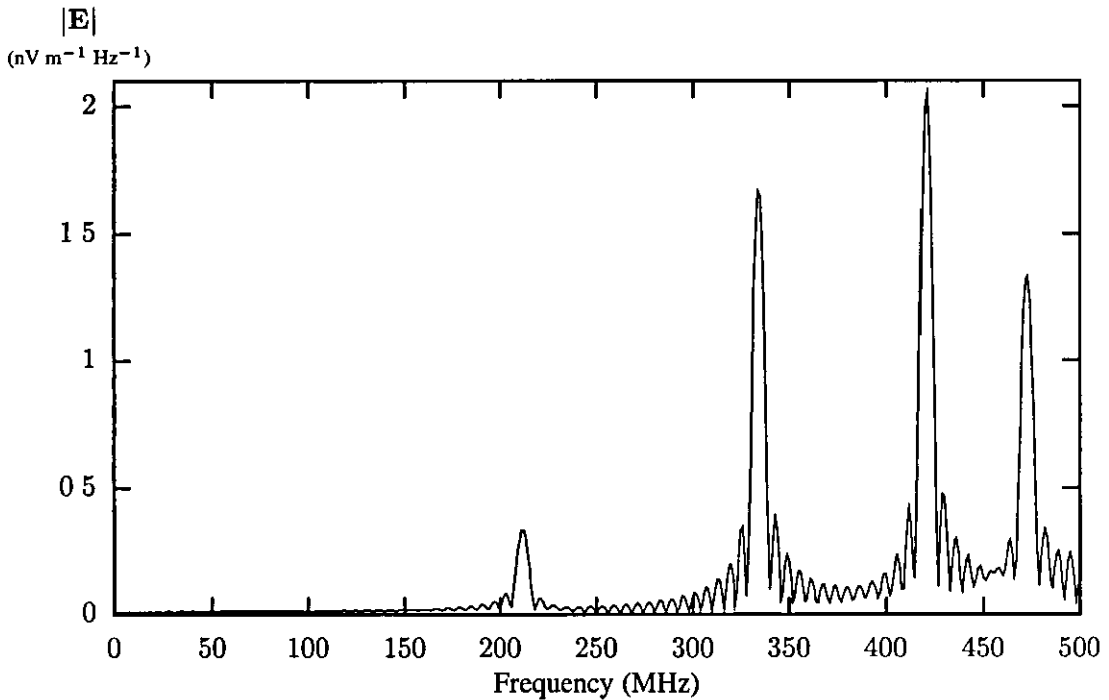
Figure 5 3: Simulated resonances in a 1 m^3 lossless cavity using double precision real numbers

In order to simulate the effect of lower precision arithmetic, a routine was built into the computer code to modify the floating point number during the scatter process. The routine emulated the effects of using lower precision arithmetic by rounding the mantissa of the node voltages to a fixed number of binary digits during calculations. The effect of this artificial rounding process on a sinusoid is shown in Figure 5.4 The machine in use observed the IEEE standard relating to floating point numbers [5 17], and simulations were conducted with different mantissa lengths in the range 1–24 bits The exponent length was also varied and the effects noted A further simulation was performed with double precision arithmetic in order to act as an accurate reference

Observations

The resultant amplitude of the resonant peaks observed in the frequency domain data for different mantissa lengths are plotted in Figure 5.5.

Where lower precision arithmetic was emulated in the code, significant rounding errors occurred and this effect manifests itself as artificial loss modelled in the system The main undesirable

Normalised
Amplitude
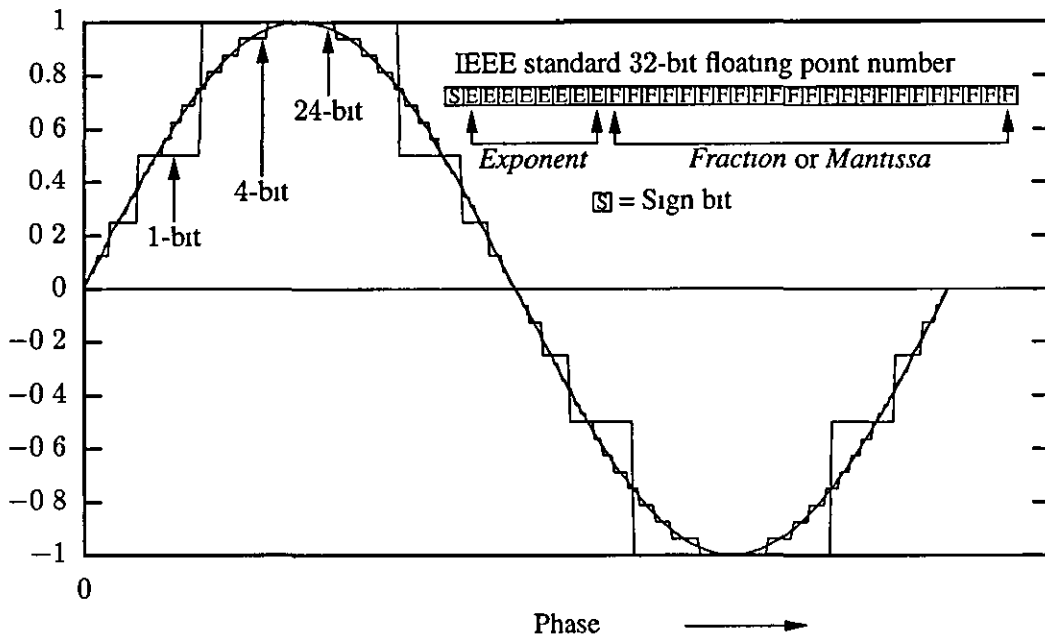
Figure 5 4: Effect of binary rounding the mantissa of a single precision number on a sinusoid

effect is that the Q-factor of the resonances is lowered (i e. the simulated resonances are leaky) which means that close-together resonances are harder to resolve Interestingly, the resonant frequencies in all of the simulations were reasonably accurate, even down to 4-bit precision

In terms of the amplitudes, the experiment indicates that good accuracy can be obtained with as few as 15 bits. This may be useful in a highly optimised hardware system, where the amount of stored data needs to be minimised On machines with IEEE standard floating point numbers it can be seen from the plot that using double precision arithmetic (53 bit mantissa, 64 bits overall) offers very little advantage over single precision (24 bit mantissa, 32 bits overall) in terms of accuracy in the observed electric field strength.

Altering the exponent bit length was found to only affect the dynamic range of the model, and with the excitation strength used there were no observable effects. With much larger or much smaller magnitude excitation there were problems with the signal going out of range Using appropriate scaling, it is possible to use a fixed point number, even an integer quantity, but this is inconvenient in practice and offers no computational advantage on most workstations

|E|
(nV m^{-1} Hz^{-1})

Figure graph showing curves.
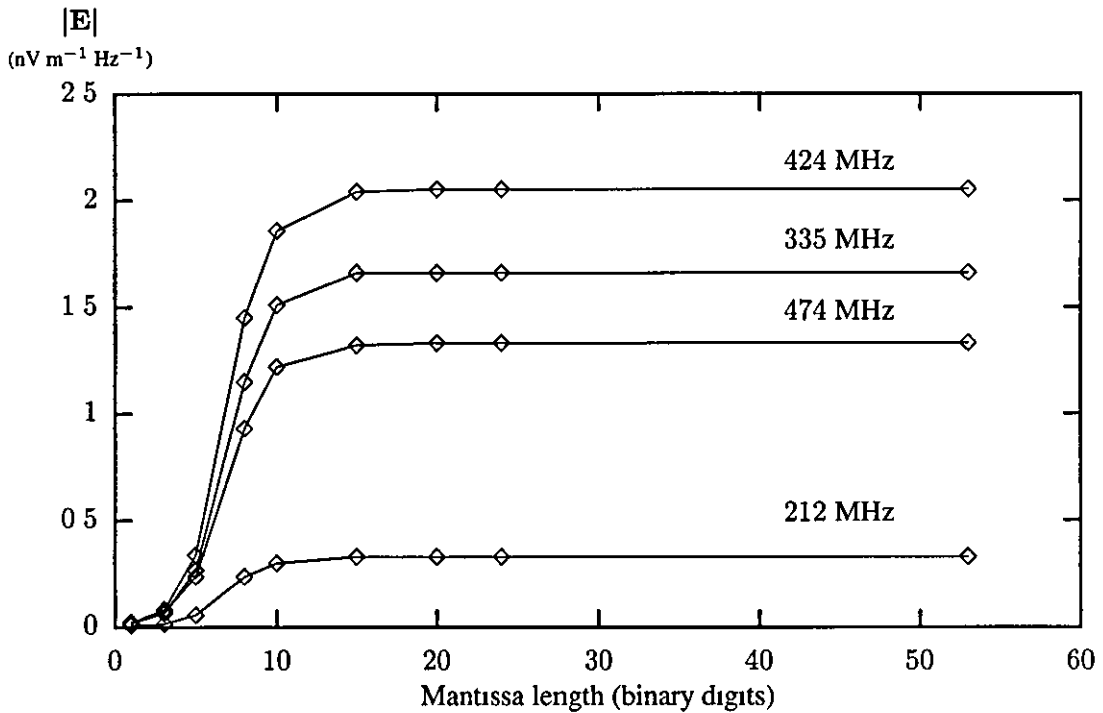
Figure 5 5 Resonant magnitudes for different mantissa lengths and an 8-bit exponent, except for 53-bit where exponent length = 11-bit (IEEE standard double precision number)

5 3 1   Roundoff errors in time step calculations

In some circumstances the rounding which occurs in floating point numbers is significant The actual process of rounding leads to *roundoff error*, and this is quite easily demonstrated by evaluating the expression X*(1/X) on a digital computer for different nonzero real numbers Different values for X produce a result which is not precisely equal to the (trivial) analytical solution of X=1.

Calculations of this type occur frequently in the evaluation of certain parameters within a TLM program   One particular example is the choice of stub values in the symmetrical condensed node. If the smallest value stub is the x-directed capacitive stub, then

$$\hat{Y}_{ox} = \frac{2\zeta}{\Delta t} - 4 \qquad (5\ 1)$$

where $\hat{Y}_{ox}$ is the normalised stub admittance and

$$\zeta = \frac{\epsilon_{rx}\ \Delta y\ \Delta z}{c\ \Delta x}$$

If this particular stub limits the maximum time step

$$\Delta t = \frac{\zeta}{2} \tag{5 2}$$

The analytical solution obtained by substitution is simply, $\hat{Y}_{ox} = 0$. However, experimentation shows that different values of ζ yield different values for this stub, some of which are negative. Even small valued negative stubs lead to instability in TLM simulations so this is a matter which needs to be addressed. It is helpful to examine how the errors introduced at each stage propagate by introducing the roundoff errors e_1 and e_2 into the analytical formulation, i e

$$\hat{Y}_{ox} = \frac{2\zeta}{\Delta t} + e_1 - 4 \tag{5 3}$$

$$\Delta t = \frac{\zeta}{2} + e_2 \tag{5 4}$$

Substituting as before·

$$\hat{Y}_{ox} = \frac{2\zeta}{\frac{\zeta}{2} + e_2} + e_1 - 4 \tag{5 5}$$

If now the inequality $\hat{Y}_{ox} \geq 0$ is applied, then the limit on the error terms may be expressed After a little manipulation, it is fairly straightforward to show that:

$$\frac{4}{e_1} - \frac{\zeta}{2e_2} \leq 1 \tag{5 6}$$

This inequality can be used to examine the rounding behaviour of the machine in use For example, if the divide operation rounds down the result this gives e_1 and e_2 a positive sign Examining equation (5 6), it can be seen that there are values for ζ where the inequality is not satisfied. In order to correct the problem, the time step may be reduced by a very small fraction to oppose the rounding error in the stub calculation A simpler method is to ensure that the program inspects all of the stub values, and sets any small negative stub values to zero.

5 3 2 Discussion

In general, the accuracy requirements of TLM are well within the capabilities of current computational platforms Floating point numbers are adequate for representing the node voltages

and stub values, although care must be taken to ensure that negative stub values generated by roundoff are eliminated.

Integer arithmetic is not suitable for most applications, since it degrades the dynamic range of the results and forces the use of appropriate scaling The microprocessors in most modern workstations and desktop PCs have high performance floating point operations built in, and so in terms of the run speed there is no particular advantage in using integer types.

5.4   Memory management

In vehicle EMC, the target has physical dimensions which may be many wavelengths at the highest frequencies of interest It is therefore inevitable that a very large number of TLM nodes will be required in order to produce a suitable model. In addition there are certain areas of the model where the wavelength of the incident radiation is much smaller than that in free space Much smaller cells are required in these areas in order to counteract the effects of dispersion, and thus the storage problem is exacerbated.

It is essential to ensure adequate memory is available for storing node voltages and other parameters within the model. Most operating systems employ the concept of *physical* memory which refers to the Random Access Memory available in the machine, and *virtual* memory which refers to additional memory emulated by means of dynamically exchanging blocks between physical memory and a storage device. This process is known as *memory paging* or *swapping*. The exchange of data between the device and memory is a relatively slow process, and the amount of swapping must be minimised in order to obtain the most efficient code.

In practice, individual machines have a memory limit for a given TLM code where the time taken to exchange memory blocks from the storage device becomes prohibitive [5 13] This is a qualitative measure, and may depend on an individual person's perception The limit may be significantly less than the total amount of memory available because of the temporary storage required for calculations etc , and by other programs consuming resources such as the operating system and the TLM program code itself which will be running concurrently. Approximate limitations for a range of workstations are shown in Table 5 1.

The amount of memory required is also affected by the number of stub voltages which need to be stored for each node. The storage requirements for each node are shown in Table 5 2

Iteration
time
(s)
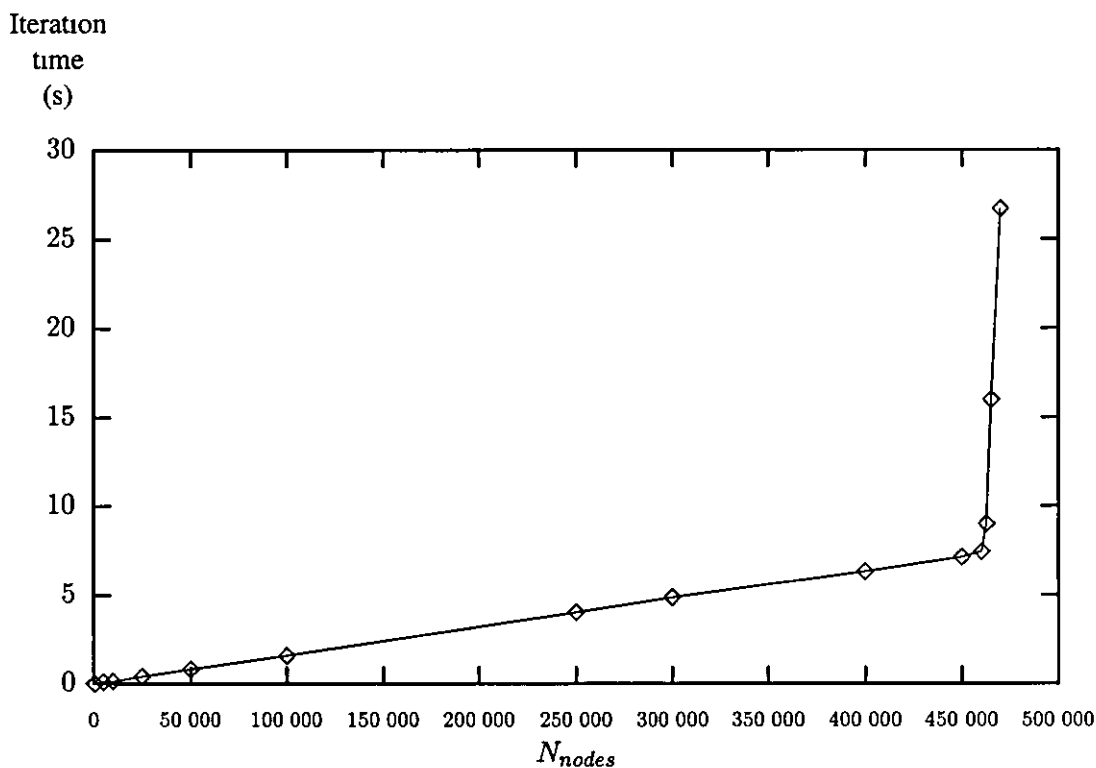
Figure 5 6 Run time on a Pentium 90 PC with 40 MB physical memory and 80 MB virtual memory
using the Linux operating system

Other factors, such as the number of materials in use can also significantly affect the storage
requirements in complex models. For example, for the machine used to generate Figure 5 6,
the plot demonstrates that the machine has a physical memory limit of approximately 450 000
nodes before the onset of swapping. This corresponds to approximately 31 MB of memory,
indicating that the TLM program code and operating system occupied approximately 9 MB of
physical memory

Machine	RAM	Number of nodes
Old 386/486	8 MB	$\sim 10^4$
Early Pentium	16 MB	$\sim 10^5$
Average Desktop PC	128 MB	$\sim 10^6$
Modern Workstation/Supercomputer [5.18]	2 GB upwards	$\sim 10^7$

Table 5 1. Approximate computational limits for SCNs

Node type	Variables	Storage requirement
SCN	12 float, single precision	48 bytes
Stub loaded SCN	18 float, single precision	72 bytes
HSCN (I)	15 float, single precision	60 bytes
HSCN (II)	15 float, single precision	60 bytes
SSCN	12 float, single precision	48 bytes

Table 5 2 Storage requirements for different 3-D node types

5.4 1 Assessing the storage requirement

In order to provide a quick assessment of how many nodes are required for a given physical system, a simple method was devised This method works on a 'best case' scenario, and assumes that cells of different sizes may be combined ideally.

Formulation

In order to satisfy dispersion constraints at least ten nodes are required per wavelength at the maximum frequency of interest This must be followed for all materials in the model, including those within materials of lower wave velocity such as dielectrics. Therefore materials with high relative permittivity and permeability require a correspondingly small cell size.

Given the ten nodes per wavelength limit and nonferrous material, it can be shown that the frequency normalised minimum node density required in region i of the TLM model, D_i, can be approximated by.

$$D_i = \left[\frac{10\sqrt{\epsilon_r}}{c}\right]^3 \quad (\text{node s}^3.\text{m}^{-3}) \tag{5 7}$$

The node density required for some typical materials used in motor vehicle manufacture are shown in Table 5.3. Note that in general the permittivity is both complex and frequency dependent, and although it is possible to include these properties in the TLM model they are often ignored for economy.

Once the volume of each material to model is known, the minimum number of nodes may be obtained from

$$N_{nodes} = f^3 \sum_{i=1}^{m} D_i \nu_i \tag{5 8}$$

Material	ϵ_r	D_i ($\times 10^{-24}$node $s^3.m^{-3}$)
Air	1.0006	37 0
Mineral Oil	2 2	121
PVC	2 7	164
Rubber	3	192
Glass	6	544
Water	80	26 500

Table 5 3. Frequency normalised minimum node densities for dielectric materials

Where ν_i is the volume of each distinct area of mesh, f is the maximum frequency of interest, and m is the number of distinct mesh volumes.

The number of nodes which can be realistically coped with depends on the computational platform, and can be determined experimentally. Given the maximum number of nodes which may be employed, and the material volumes in the physical system it is possible to estimate a practical frequency limit, f_{max} for the model by rearranging equation (5 8)

$$f_{max} = \sqrt[3]{\frac{N_{nodes,max}}{\sum_{i=1}^{m} D_i \nu_i}} \qquad (5\ 9)$$

Comments

In practice, this technique will often underestimate the number of nodes required and overestimate the practical frequency limit This is mainly due to the assumption that different sized cells can be combined arbitrarily which is not possible with current multigrid and grading techniques [5 19, 5 20, 5.21, 5 22] The amount of memory required for an individual problem is also increased by other specialised methods which may be in use (see Figure 2 13, p 40ff) Despite these limitations the method is useful for obtaining a first estimate, and has been found to be a valuable yardstick when determining the practicality of simulations

For example.

"What is the maximum frequency that can be expected from a TLM model of a screened room with dimensions 3.61 m × 3 05 m × 4.83 m when computed on a

desktop PC ?"

Assuming the PC available is the one tested in Figure 5 6, the maximum number of nodes before excessive swapping takes place is approximately $4\ 5 \times 10^5$.

The chamber volume is: $3\ 61 \times 3.05 \times 4\ 83 = 53.2\ m^3$.

The node density required in free space is approximately: 37×10^{-24} node $s^3\ m^{-3}$

Therefore $f_{max} = \sqrt[3]{\frac{4\ 5 \times 10^5}{37 \times 10^{-24} \times 53\ 2}} = \underline{611\ MHz}$

5 4 2   Dynamic node activation

At the very start of most TLM simulations a large number of nodes within the mesh are effectively redundant. Until voltage impulses are experienced on a particular node's ports, it is unnecessary to perform scattering, or to transfer pulses between inactive nodes Additionally, there are often nodes which are never involved in calculation such as those contained within volumes where, in the real world, fields do not penetrate From a computational viewpoint, it would be highly desirable to reduce the total number of calculations required in the simulation These observations were the motivation for producing the following algorithm

5 4 3   Algorithm development

The volume of nodes excited by a point source in a TLM mesh is shown in Figure 5 7   An algorithm can be devised to replicate this changing pattern in three dimensions in order to control the scattering and connecting processes during the simulation

The algorithm itself must not significantly increase the storage requirement nor must it be overly complex, since the TLM algorithm itself is very simple. If these specifications are not met then the overall performance is likely to be degraded rather than improved

As a first attempt, the possibility of examining all the port voltages at each time step and performing scattering accordingly was considered. This idea was quickly rejected by experiment In fact, the time taken to test each individual port voltage was found to be appreciable when compared with the calculation time of the TLM algorithm itself
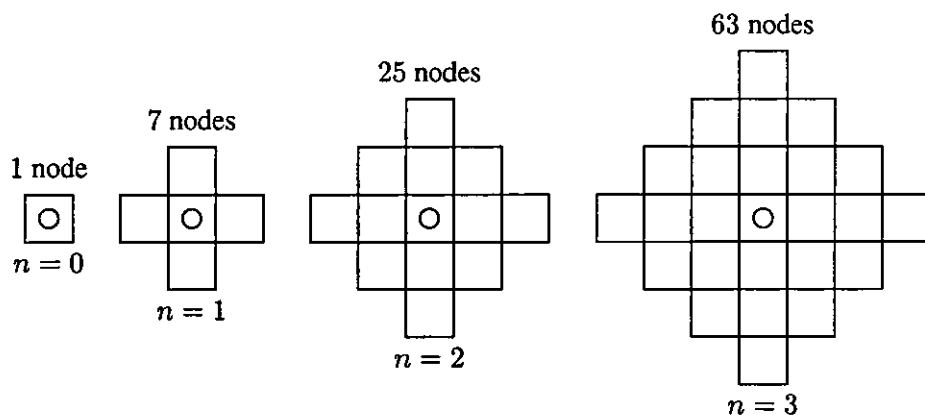
Figure 5 7 Nodes excited around a point source at time step n

The algorithm

In practice it was found that a small additional area of storage was necessary in order that the status of 'active' and 'inactive' was globally available to the scatter and connect routines in the program.

A system based on binary digits was devised with a single bit allocated for each node Logic '0' was stored for 'inactive' and '1' for active These bits were arranged in a 3-D array, denoted $a_n[x, y, z]$, with the contents of this array updated at each iteration This array was used as a control for the computation in the TLM algorithm

The update routine is an extremely simple process involving six logical OR operations per node as shown in equation (5.10).

$$
\begin{aligned}
a_{n+1}(x, y, z) \;=\;\; & a_n(x, y, z)+ \\
& a_n(x-1, y, z) + a_n(x+1, y, z)+ \\
& a_n(x, y-1, z) + a_n(x, y+1, z)+ \\
& a_n(x, y, z-1) + a_n(x, y, z+1)
\end{aligned}
\tag{5 10}
$$

At the start of the simulation, $a_0[x, y, z]$ was initialised to '0', and where nodes were excited in the TLM mesh a '1' was placed in a corresponding place in the bit array. Any bits outside the array were assumed to hold logic '0'.

By this process the spreading behaviour shown in Figure 5.7 could be emulated with a minimal

amount of additional storage and execution time

Incorporating 'dead' nodes

In some simulations there are permanently inactive nodes, such as those bounded by a perfect conductor The algorithm can be adapted to take account of these by including another binary array (see Figure 5 8). In this case the array, $K[x, y, z]$ is constant throughout, and contains a
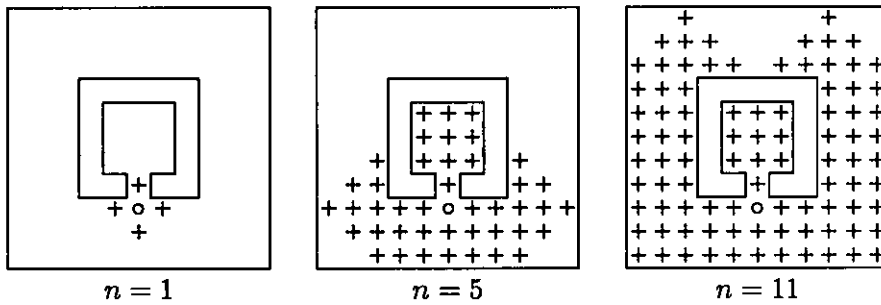

$n = 1$ $n = 5$ $n = 11$

Figure 5 8 Use of the algorithm with 'dead' nodes

mask for $a_n[x, y, z]$ i e. permanently inactive (dead) nodes are represented by '0' and all others by '1'. Each element of $K[x, y, z]$ is then logic 'ANDed' with its corresponding element in $a[x, y, z]$

$$
\begin{aligned}
a_{n+1}(x, y, z) &= K(x, y, z).[a_n(x, y, z) + \\
&\quad a_n(x - 1, y, z) + a_n(x + 1, y, z) + \\
&\quad a_n(x, y - 1, z) + a_n(x, y + 1, z) + \\
&\quad a_n(x, y, z - 1) + a_n(x, y, z + 1)]
\end{aligned}
\tag{5 11}
$$

This extension to the basic algorithm, has positive implications in terms of memory usage, since it is possible to avoid storing nodes which do not take part in the simulation.

5 4 4 Operation

The algorithm in its most basic form was applied to a $51 \times 51 \times 51$ node mesh of SCNs and differing types of excitation were applied. It can be seen from Figure 5.9 that reduced iteration times can be achieved by applying this method and the amount of improvement is dependent on the position of the excitation. The plot also shows that the algorithm has some overhead in

terms of computation time. It has been found that a better result can be achieved by stopping the update of $a_n[x, y, z]$ once it is full of '1's. Other tests were conducted with different mesh sizes,
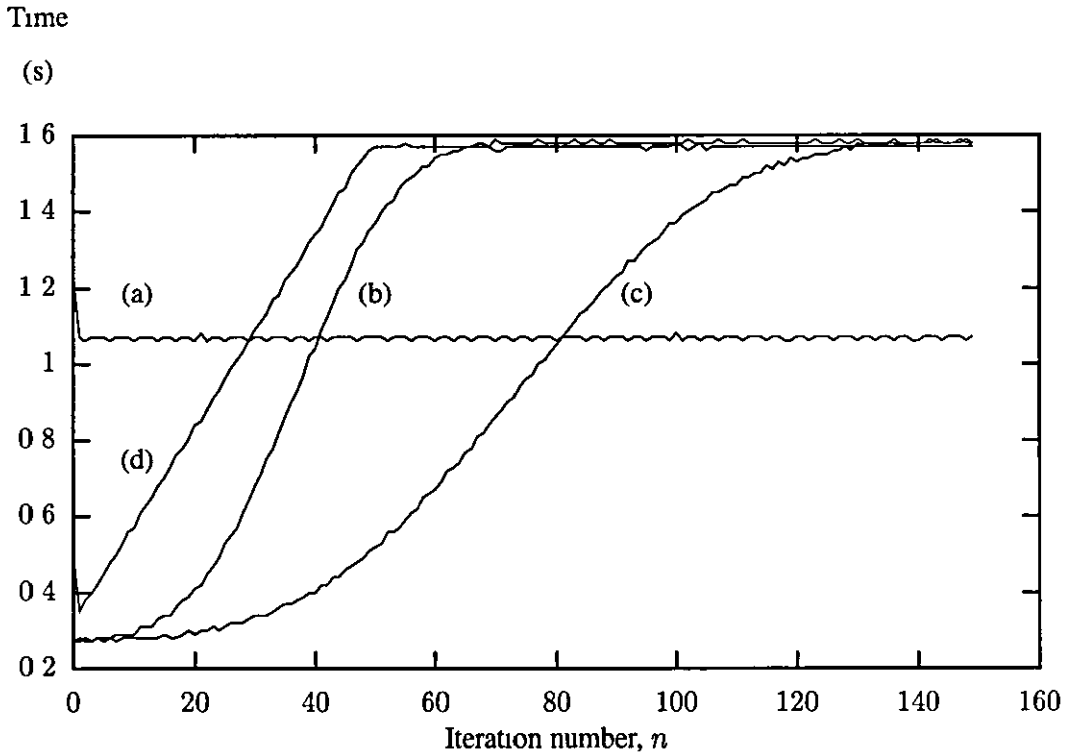

Figure 5 9 Iteration times in a 51 × 51 × 51 node TLM mesh for (a) normal simulation, (b) excitation at the mesh centre, (c) excitation near to a corner and (d) plane wave excitation at $z = 0$

and by using the algorithm in equation (5 11). Using 'dead' cells was found to be advantageous, producing significant savings in memory where large volumes bounded by PEC were present in the model

5 4 5   Discussion

It is possible to produce an expression for the number of nodes involved in the calculation at time step n by considering the way that the pattern shown in Figure 5.7 evolves in three dimensions:

$$N_{live} = \frac{1}{3}(4n^3 + 6n^2 + 8n + 3) \tag{5.12}$$

The excited volume for an ungraded mesh of SCNs at time step n is therefore

$$\nu_{live} = N_{live} \, \Delta l^3 = \frac{\Delta l^3}{3}(4n^3 + 6n^2 + 8n + 3) \tag{5 13}$$

It is useful to compare this volume to the volume which would be excited in the real world by a point source radiating in free space. A point source spreading spherically with the wavefront propagating at c ms^{-1} would excite a volume of:

$$\nu_{live(real)} = \frac{4}{3}\pi r^3 = \frac{4}{3}\pi(ct)^3 \tag{5.14}$$

If it is assumed that $t = 0$ when $n = 0$ and the maximum time step in the TLM mesh is $\Delta l/2$, so

$$t = n\frac{\Delta l}{2c} \tag{5 15}$$

Therefore, the volume of excitation is.

$$\nu_{live(real)} = \frac{4}{3}\pi c^3 \left(\frac{\Delta l}{2c}\right)^3 n^3 = \frac{\pi}{6}\Delta l^3 n^3 \tag{5 16}$$

The volume of nodes which have voltage impulses travelling on them is larger than the volume produced from the spreading wavefront This is to be expected as voltage impulses travel considerably faster on the TLM mesh than waves below the cutoff frequency (see Figure 5 10) By
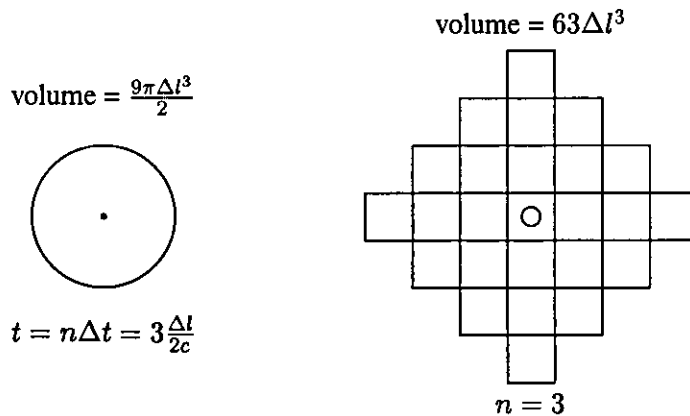
Figure 5 10 Volume of space and equivalent volume of nodes excited around a point source

dividing equation (5.13) by equation (5 16) it can be shown that for large values of n the volume of nodes involved in the computation is $\frac{8}{\pi}$ times the physical volume bounded by the wavefront

As this result demonstrates, the TLM mesh is filled with individual impulses much earlier than it is filled with waves. Even in very low-Q simulations the total simulation time should permit the wave to traverse the workspace several times. Taking this into account, it is debatable whether

there is any benefit in applying an algorithm However, the advantage of using 'dead' nodes is considerable since the computational time and memory requirement scales linearly with the number of nodes

Overall, the algorithm is simple to implement in software, and offers some advantages. It is most likely to find application in highly optimised systems, such as hardware accelerators for TLM (e g that described by Stothard and Pomeroy [5.7]). In these systems it may be possible to implement the algorithm directly in high-speed logic and thus the overhead may be negligible There may also be scope for application in distributed processing, by using the array to represent tiles of nodes instead of individual nodes. The time stepping in the algorithm could be a multiple of the TLM time step appropriate to the tile size This could then form the basis of a 'fast start' routine

5.5   Conclusion

In this chapter some of the issues facing the efficient implementation of TLM have been addressed. Object-oriented programming techniques have been considered, and an OML model for 3-D TLM has been presented and evaluated It has been demonstrated that acceptable accuracy can be obtained by using floating point numbers with a mantissa length as low as 15 bits, although this may only be applicable to specialised TLM processors since most current platforms adhere to the IEEE standard for floating point numbers. Strategies have been proposed for assessing and reducing the total memory requirement An algorithm has been demonstrated which activates nodes when required in the calculation and by doing so reduces computation times in some circumstances.

References

[5.1] J G. Proakis and D. G. Manolakis, *Digital signal processing· Principles, algorithms and applications*, ch. 9, pp. 684–760. New York Macmillan, 2nd ed , 1992

[5 2] Anon., "Three-dimensional EM software for PCs," *Microwave J*, vol 40, no. 5, pp 354–357, 1997

[5 3] J L Dubard, O. Benevello, D. Pompei, J Le Roux, P. P. M. So, and W. J. R Hoefer, "Acceleration of TLM through signal processing and parallel computing," in *Computation in Electromagnetics*, pp. 71–74, IEE, 25–27 November 1991.

[5 4] C C Tan and V. F Fusco, "TLM modelling using an SIMD computer," *Int J Numerical Modelling Electronic Networks, Devices and Fields*, vol 6, pp 299–304, 1993

[5 5] P. P. M So, C. Eswarappa, and W. J. R. Hoefer, "Parallel and distributed TLM computation with signal processing for electromagnetic field modelling," *Int J. Numerical Modelling Electronic Networks, Devices and Fields*, vol. 8, pp. 169–185, 1995

[5 6] P J Parsons, S. R. Jaques, S. H. Pulko, and F A. Rabhi, "TLM modeling using distributed computing," *IEEE Microw. and Guided Wave Lett*, vol. 6, no. 3, pp 141–142, 1996.

[5 7] D Stothard and S C. Pomeroy, "Dedicated TLM array processor," *Applied Computational Electromagn. Soc. J.*, vol. 13, no 2, pp 188–196, 1998

[5 8] V S. Sunderam, "PVM: A framework for parallel distributed computing," *Concurrency Practice and Experience*, pp. 315–339, December 1990.

[5 9] V Trenkić, C Christopoulos, and T. M. Benson, "Efficient computation algorithms for TLM," in *Digest of the First International Workshop on TLM Modeling*, (Victoria, BC, Canada), pp. 77–80, IEEE, 1–3 August 1995.

[5.10] S. Lawton, D. D. Ward, S. R. Cloude, and J. F. Dawson, "Hybrid time domain modelling for automotive EMC," in *Proc. 2nd Int. Conf. on Computation in Electromagnetics*, (Nottingham, UK), pp 275–278, IEE, 12–14 April 1994.

[5 11] C Eswarappa and W J R. Hoefer, "Real time interface between TLM and FDTD modules and applications," in *Digest of the First International Workshop on TLM Modeling*, (Victoria, BC, Canada), pp. 59–62, IEEE, 1–3 August 1995.

[5.12] J Rumbaugh, M Blaha, W. Premerlani, F. Eddy, and W. Lorensen, *Object-oriented modeling and design* New York: Prentice-Hall, 1991.

[5 13] J. L. Herring, *Developments in the Transmission-Line Modelling Method for Electromagnetic Compatibility*. PhD thesis, University of Nottingham, May 1993 pp 104–109, pp. 207–208.

[5.14] P. P. M. So and W. J. R. Hoefer, "Recent advances in transmission line matrix method electromagnetic wave modelling and visualization," in *Digest of the First International Workshop on TLM Modeling*, (Victoria, BC, Canada), pp. 183–186, IEEE, 1–3 August 1995.

[5 15] J. L. Herring, *Developments in the Transmission-Line Modelling Method for Electromagnetic Compatibility* PhD thesis, University of Nottingham, May 1993. ch 3

[5 16] R E. Collin, *Foundations for Microwave Engineering*, ch. 7, pp. 500–504 Electrical Engineering Series, New York· McGraw Hill, 2nd ed , 1992.

[5.17] ANSI/IEEE Standard for binary floating point arithmetic. 754–1985

[5.18] D D Ward and A. R. Ruddle, "Developments in automotive electromagnetic modelling," *SAE Special Publications*, vol. 1336, pp 17–27, February 1998.

[5 19] J L Herring and C. Christopoulos, "The use of graded and multigrid techniques in transmission-line modelling," in *Computation in Electromagnetics*, pp 142–145, IEE, 12–14 April 1994

[5.20] J. L Herring and C. Christopoulos, "Solving electromagnetic field problems using a multiple grid transmission-line modeling method," *IEEE Trans Antennas Propagat* , vol. 42, no. 12, pp 1654–1658, 1994

[5 21] M I Sohby, M H. Abd El-Azeem, and K W Royer, "A new multi-grid 3-D TLM algorithm for simulation of microwave FSS," in *MTT Symposium Digest*, vol. 2, (San Franscisco, CA, USA), pp. 439–442, IEEE, 17–21 June 1996.

[5 22] J. Wlodarczyk, "New multigrid interface for the TLM method," *Electron Lett* , vol. 32, no 12, pp. 1111–1112, 1996

CHAPTER 6:
CONCLUSIONS

THE aim of this thesis was to identify and develop efficient techniques for the electromagnetic modelling of motor vehicles. The objectives have been achieved by targeting two key areas: the use of efficient numerical techniques, and the algorithm implementation. This chapter outlines the contribution of this thesis, and suggests areas for future research

6.1   Contribution of this thesis

The TLM technique was chosen as a starting point for this thesis as it is multi-featured and well established as a numerical technique for EMC simulation. Whole-vehicle simulations are a particularly challenging class of EM model, due to their high level of geometrical complexity and the high frequencies involved in tests It is essential to conserve computational resources in order to obtain accurate simulations in a realistic time frame

The development of the TLM method has been critically reviewed, focusing on the strengths and weaknesses encountered when applied to automotive EMC problems. A wide range of techniques are available which can be used to improve the accuracy and efficiency in particular areas of the model.

Symmetry boundary conditions can be useful for reducing the memory requirement in models A new partial implementation of a Huygens' surface has been developed which uses a symmetry condition to produce plane waves for simulation of EM immunity. This method improves over an earlier method by allowing plane wave generation with arbitrary polarisation

The absorbing boundary performance in TLM simulations has a significant impact on the overall efficiency. The traditional matched termination boundary performs poorly when placed in close proximity to objects. High-performance techniques, which have been reported in recent years, such as the one-way equation method and perfectly matched layer can be effective in certain cir-

cumstances This allows the boundary to be placed closer to the object and thus preserves computational resources. Due to the limited and often unpredictable stability of high-performance absorbing boundaries, they may in some cases prove unsuitable for use in automotive models.

The manner in which the TLM algorithm is implemented can have adverse effects on the efficiency, particularly in terms of the numerical accuracy and memory usage Object oriented programming methods have been employed in this thesis to construct a TLM program There are some conceptual advantages in using object oriented methods, however these are largely offset by the latent increase in memory usage and degradation of the execution speed.

Memory usage overall is a pivotal factor since the per-node computational time climbs very steeply once a certain threshold is reached. A simple calculation technique has been described which can quickly assess the practicality of modelling a particular physical system, or can alternatively indicate the upper frequency limit for a given level of computational resources

A new method has been presented which reduces the total number of calculations by dynamically activating nodes This method can reduce computation time in low-Q simulations There is particular merit in avoiding the storage of nodes in volumes where there is no significant field penetration.

6.2   Suggestions for further research

The work in this thesis has suggested a number of avenues for further research

6 2.1   Computational performance

It is debatable which type of computer offers the most effective and efficient platform for TLM There is much interest in using parallel computers, and in some cases these have proved very successful. It is however unclear whether their high complexity and cost justifies their use, especially when many of the studies reported to date have indicated that the computer used was not operating at full capacity. It would be worthwhile to assess the cost per performance unit for these machines. In addition, it would be useful to conduct a survey of the relative suitability and performance of each for a benchmark TLM program.

It has been speculated that the future of parallel computing lies in using multiple desktop com-

puters with high-performance network connections. A study is needed to examine the implications of this type of computer hardware, focusing on the specific difficulties referred to in Chapter 5 of slow data transfer rate when compared to computation time.

6.2.2 Programming techniques

Another area of research highlighted by this thesis is that of code architecture It has been shown that even relatively minor changes in software can alter the performance dramatically This fact has often been ignored, although in practical terms it can affect the maximum frequency of the model in a manner comparable to the numerical algorithm itself More research effort into program architecture and wider dissemination amongst the TLM community is needed to produce better, faster TLM implementations, and to reduce the amount of repeated research in institutions.

6 2 3 Accuracy of TLM simulations

Improving the representation of curved and sloped boundaries is of importance to both the TLM and FDTD communities. These methods are of particular interest, because they have the potential to significantly improve model accuracy. Although a number of smooth surface techniques have been proposed, no comparative study has been reported for TLM, and test cases have been limited. Further research is required to determine whether these methods are effective in complex-geometry problems.

In simple situations and on an individual basis many of the errors observed in simulations are well understood. In general, however, it is not clear how the cumulative effects influence the overall model error. A study to formalise and predict the magnitude of errors from different sources would be desirable. The concept of an 'error budget' could be introduced, which operates in a manner analogous to noise analysis in electronic circuits For example, if results are required within a 6 dB accuracy it may be possible to budget for the errors due to sharp edges, wires, and other factors. This would permit the user to quantify the expected errors from a variety of sources, and allow the engineer to alter the model to meet a particular accuracy requirement.

6 2 4   Developing numerical techniques for EMC

On the wider subject of modelling in EMC, there are a number of areas which have potential to improve simulation efficiency.   Research has been ongoing for several years into hybrid methods   The purpose of hybridisation is to capitalise on the best features of a number of techniques by combining them in a single model. Research has been fairly sparse in this area, although some studies have reported very promising results. Further study is required in order to establish which numerical methods can be efficiently and effectively combined

At a practical level, hybrid methods may introduce additional problems, such as in pre-processing, and this needs to be more fully investigated. For instance, if a vehicle body shell was modelled using a combination of TLM and TDFEM a tetrahedral mesh might be required on the shell (to make use of TDFEM's conformal meshing) and a cubic mesh elsewhere (to make use of TLM's efficient modelling of space).

6 2 5   Validation

Although outside the scope of this thesis, experimental validation of modelling results is an important activity So far the TLM method has been demonstrated to give good agreement with measured results for a wide variety of systems (see Chapter 1 references for more details) It would be valuable to disseminate the results from a more systematic study, comparing modelling results to experimental results for a variety of typical vehicle EMC situations The evidence from such a study would encourage the acceptance of modelling among the wider EMC community. It would also help non-expert users of modelling to understand which problems can be tackled and to gain realistic expectations of the outcome of the modelling process

6.3   Overall conclusion

To produce efficient whole-vehicle simulations for EMC purposes, various techniques and strategies are necessary. The particular importance of applying symmetry wherever possible, using reliable absorbing boundaries, and producing an efficient implementation of the TLM algorithm itself have been described in this thesis.

The TLM method is a powerful, mature technique with many features which can assist the

user to make the best use of computing resources. Historically, the evolution of the method and the increase in computing power have enabled higher model frequencies and greater model complexity. However, legislative requirements for EMC and the demands of engineers have increased at an even greater rate. There is no reason to assume that this trend will change in the future. Regardless of the improvements in computational performance, better models will always be sought. Therefore, the need to manage resources will remain paramount, particularly in challenging situations such as the whole-vehicle problems addressed by this thesis.

AUTHOR'S PUBLICATIONS

A number of publications have resulted from the work in this thesis These are as follows

[1] J A Flint, M D. Melton, S. C. Pomeroy, and D. D. Ward, "TLM algorithm development using object oriented methods," in *TLM Applications Beyond Electromagnetics*, (Hull, UK), pp 4.1–4.3, University of East Anglia, 24 June 1997.

[2] J. A. Flint, M D. Melton, S. C. Pomeroy, and D. D Ward, "Programming techniques for TLM," in *Digest of the Second International Workshop on TLM*, (Munich, Germany), pp 119–125, IEEE, 29–31 October 1997.

[3] J A Flint, A. D. Goodson, and S C Pomeroy, "Visualising wave propagation in bio-acoustic lens structures using the transmission line modelling method," *Proceedings of the Institute of Acoustics*, vol. 19, no. 9, pp. 29–37, 1997.

[4] J. A. Flint, "Echolocation— sound transmission." An illustration displayed in the National Science Museum of Japan, Tokyo as part of an exhibition to mark the International Year of the Ocean, 7 March – 10 May 1998.

[5] J A Flint, A. D. Goodson, and S. C Pomeroy, "Visualising wave propagation in bio-acoustic lens structures using the transmission line modelling method," *Bioacoustics*, vol. 9, pp. 213–235, 1998. Abstract from the IoA underwater biosonar and bioacoustics symposium

[6] J A. Flint, S. C. Pomeroy, and D. D. Ward, "Challenges facing automotive electromagnetic immunity simulations with TLM," in *Proceedings of Prep'99*, (Manchester, UK), pp 5–8, IoP, 5–7 January 1999.

[7] J A Flint, S C. Pomeroy, and D D Ward, "Compact partial Huygens' surface for TLM," *Electron Lett.*, vol. 35, no. 2, pp. 132–133, 1999.

146

[8] J. A. Flint, S. C. Pomeroy, and D D. Ward, "Simple and efficient plane-wave excitation in 3-D TLM," in *Proceedings of York EMC '99*, (York, UK), pp 1–5, IEE, 12–13 July 1999

[9] M. D. Melton, J. A Flint, S C Pomeroy, and D D. Ward, "Numerical results of a precise placement algorithm for TLM," in *Digest of the Third International Workshop on TLM*, (Nice, France), pp. 215–222, IEEE, 27–29 October 1999.

[10] A. D Goodson, J. A. Flint, S C. Pomeroy, and T. W. Cranford, "Bio-sonar characteristics of the harbour porpoise (Phocoena phocoena)," in *Proceedings of the 5th European Conf on Underwater Acoustics (ECUA 2000)*, (Lyon, France), pp 479–484, Office for official publications of the European communities, 10 July 2000. P. Chevret, M. E Zakharia and P. Dubail (editors)

[11] A D. Goodson, J A Flint, and T. W. Cranford, *The Harbor Porpoise (Phocoena phocoena)— Modeling the sonar transmission mechanism*. Chicago, USA University of Chicago. Part of a chapter on current research in the book *Advances in the study of echolocation in bats and dolphins*. J A. Thomas, C. F. Moss and M. M Vater (editors) Accepted, awaiting publication.